Volatility and Correlation in Financial Markets: theoretical developments and numerical analysis

By Camilla Pisani

A PhD thesis submitted to School of
Business and Social Sciences, Aarhus University,
in partial fulfilment of the PhD degree in
Economics and Business Economics

December 2015

Supervisor: Elisa Nicolato
Co-supervisor: Peter Løchte Jørgensen

Funded by the European Union

Preface

This thesis is the result of my PhD studies at the Department of Economics and Business Economics (previously Economics and Business) at Aarhus University, during the period from January 2013 to December 2015. The research leading to these results has received funding from the People Programme (Marie Curie Actions) of the European Union's Seventh Framework Programme FP7/2007-2013/ under REA grant agreement n° 289032. The thesis solely reflects the author's personal opinion and the Union is not liable for any use that may be made of the information contained therein.

First of all, I am truly grateful for the financial support received from the European Union, giving me in the first place the possibility to carry out the PhD but also to attend various conferences and courses around the world and spend time in really stimulating working environments. I would like to thank all the HPC-Finance network for interesting discussions during our meetings and in particular prof. Juho Kanniainen, prof. Antoon Pelsser, and prof. Eduardo Trigo Martínez and prof. Rafael Moreno Ruiz for having hosted me at Tampere University of Technology, Maastricht University and Malaga University.

I would like to thank my supervisor prof. Elisa Nicolato and my co-supervisor prof. Peter Løchte Jørgensen, without them I would not even be in Denmark. Thank you Elisa for your energy and enthusiasm, for encouraging me and inciting me at all moments. The time we spent together whether was at the department or some conference around the world has been really inspiring, instructive and fun.

During my PhD studies I had the pleasure to spend one semester at the department of Mathematics at Imperial College, in London. I am really grateful to prof. Damiano Brigo for hosting me, inspiring me through numerous discussions and provide me with interesting research topics.

Moreover, I would like to thank all my coauthors: prof. Paolo Baldi, prof. Elisa Nicolato, David Sloth, prof. Damiano Brigo and Francesco Rapisarda.

I am really lucky for having so many friends and PhD colleagues who morally supported me during these three years: from the people of the IC dorm when I first arrived in Denmark, to all the friends I left in Italy and those I met in and outside the department.

Finally, all my gratitude to my family who encouraged me before moving to Denmark and supported me all the way long: to my parents Sabrina and Vittor Carlo who transmitted me curiosity and passion and taught me to be strong and never give up, to my little sister Ludovica who despite being so far is and always will be my best friend, to my cousins Alessia and Andrea, my aunts, uncles and grandmothers. Vi voglio bene.

I could not conclude without thanking my boyfriend. Thank you Sergi for supporting me, be ready to help me and consulate me at any time, from any part of the world you were or I was. I have been so lucky to meet you.

Camilla Pisani
Aarhus, December 2015

Updated Preface

The pre-defence meeting was held on March 4th, 2016, at Aarhus University. The assessment committee consisted of Thomas Kokholm from Aarhus University, Rolf Poulsen from University of Copenhagen and Antoine Jacquier from Imperial College, London.

I would like to thank the committee for carefully reviewing my thesis and for the useful comments and suggestions they made.

Camilla Pisani
Aarhus, March 2016

Summary

Below we provide a short summary of each chapter in the thesis.

In **Chapter 1**, we develop some simple simulation algorithms for CIR and Wishart processes, the main idea being to split the corresponding infinitesimal generator and thus reduce the problem to the simulation of the square of a matrix valued Ornstein-Uhlenbeck process to be added to a deterministic process. In this way, we provide a weak second order scheme requiring only the simulation of i.i.d. Gaussian r.v.'s and simple matrix manipulations. The procedure is therefore really easy to implement and it also presents good performance. However, convergence results are provided only under some restrictions on the parameters.

This chapter is based on the paper *"Simple Simulation schemes for CIR and Wishart processes"* published on the *International Journal of Theoretical and Applied Finance*.

In **Chapter 2**, we study the impact of jumps distributions on the implied volatility skew from realized variance options and VIX options. We consider a generalization of the Heston model allowing for jumps in the instantaneous variance dynamics, also called SVJ-v model, which encompasses non Gaussian Ornstein Uhlenbeck type processes (Barndorff-Nielsen and Shepard [14]). Under this framework we show that by selecting alternative jump distributions, one can obtain significantly different shapes of the implied volatility of variance, some clearly at odds with the upward-sloping volatility skew observed in variance markets.

In **Chapter 3**, we recapitulate some of the most popular algorithms for the inversion of Laplace transform and we analyse how they perform when applied to the computation of prices of realized variance options, under the SVJ-v model with

Inverse Gamma jump-sizes. In particular, we show how different formulations of the Laplace transform can lead to numerically different prices. Therefore, careful attention must be paid when applying this pricing method.

In **Chapter 4**, we generalize the MVMD model suggested in Brigo et al. [28] by introducing shifted dynamics. In this framework, we propose a definition of implied correlation and we investigate whether the model is able to consistently reproduce the implied volatility of cross rates, once the single components are calibrated to univariate shifted lognormal mixture dynamics models. In other words, we study whether the shifted MVMD model is able to consistently reproduce triangular relationships among FX cross rates. Finally, we introduce a shifted model with uncertain volatilities and correlation which features greater flexibility and allow to capture the correlation skew better. The Markovian projection of this model is a generalization of the shifted MVMD model.

Dansk Resumé

Nedenfor giver vi et kort resumé af hvert kapitel i afhandlingen.

I **kapitel 1** udvikler vi nogle simple simulationsalgoritmer til CIR og Wishart processer, hvor den fundamentale idé er at splitte generatoren og derved reducere problemet til simuleringen af kvadratet af en matrix Ornstein-Uhlenbeck process, som adderes med en deterministisk process. På denne måde fremsætter vi en *weak second order* algoritme, som kun kræver simulering af i.i.d. Gaussiske s.v.'s og nemme matrix operationer. Derfor er proceduren meget nem at implementeres og virker godt. Dog er konvergensresultater kun givet under nogle restriktioner på parametrene.

Dette kapitel er baseret på forskningsartiklen *"Simple Simulation schemes for CIR and Wishart processes"* publiceret i *International Journal of Theoretical and Applied Finance*.

I **kapitel 2** undersøger vi effekten af springfordelingen på det implicitte volatilitetssmil for realiseret variansoptioner og VIX optioner. Vi anvender en generalisering af Heston (1993) modellen kaldet SVJ-v modellen, som tillader springene i variansen og omfatter ikke-Gaussiske Ornstein Uhlenbeck procestyper (Barndorff-Nielsen and Shepard [14]). Under denne modelstruktur viser vi at forskellige springfordelinger kan føre til fundamentalt forskellige former af implicit volatilitet, hvoraf nogle er tydeligt inkonsistente med den positive hældning på volatilitetssmilet, som man observerer i variansmarkeder.

I **kapitel 3** opsummerer vi nogle af de mest populære algoritmer for inversionen af Laplace transformation og vi undersøger præstationen af algoritmerne, når de anvendes til udregning af priser på realiseret variansoptioner, under SVJ-v mod-

ellen med Inverse Gamma springstørrelser. I særdeleshed viser vi at ækvivalente formuleringer af Laplace transformationen kan føre til numerisk forskellige priser. Derfor er opmærksomhed nødvendigt, når man anvender den prissætningsmetoden.

I **kapitel 4** generaliser vi MVMD modellen foreslået i Brigo et al. [28] ved at introducere forskudte dynamikker. Under denne model foreslår vi en definition på *implicit korrelation* og vi undersøger om modellen kan reproducere den implicitte volatilitet på cross rater på en konsistent måde, når de enkelte komponenter er kalibreret til univariate forskudte lognormale mixture dynamik modeller. Med andre ord undersøger vi om den forskudt MVMD model kan reproducere de triangulære forbindelser mellem FX cross rater. Endelig introducerer vi en forskudt model med usikre volatiliteter og usikker korrelation, som medfører øget fleksibilitet og reproducerer bedre korrelationens skævhed. Markoviansk projektionen af modellen er en generalisering af den forskudt MVMD model.

Contents

Introduction

After the financial crisis in 2008 and the following economic developments, the need for reliable financial models has notably increased, especially for portfolio and risk management purposes. In addition to reflect features of true market prices, financial models should also enjoy some property of analytical tractability. In particular, prices of common derivatives such as call and put options should be computable, at least numerically. Reliability of numerical pricing methods is also extremely important, in particular when calibrating a model, that is when looking for the parameters in the model which better reproduce true market prices.

This introduction is meant to provide a brief but concise description on a few basic concepts for a better understanding of the thesis. Definitions of *implied volatility* and *implied correlation* will be briefly described below.

Volatility and Correlation

At the beginning of the seventies the introduction of futures contracts in financial markets called for the construction of adequate models for the description of the evolution of financial assets (stocks, bonds, etc.). The first very simple but enlightening model was introduced by F. Black and M. Scholes [22] in 1973. Under this model, the price of the underlying asset S_t is solution of the SDE

$$\frac{dS(t)}{S(t)} = rdt + \sigma dW_t$$

where W_t is a Brownian motion (which may be considered as the source of uncertainty of S_t), $r \geq 0$ is the instantaneous interest rate and $\sigma \geq 0$ represents the volatility. The latter gives a measure of the variation (oscillations) of the price S_t over time. This dynamics allows for an explicit formulation for the computation

of European call and put option prices. A call option is a financial contract between two parties, giving the buyer the right, but not the obligation, to buy an agreed quantity of a particular commodity or financial instrument (the underlying) from the seller of the option, at a certain time (the expiration date or maturity of the option) and for a prefixed price (the strike price). On the other hand, a put option gives the buyer the right to sell the underlying to the seller of the option, at the prefixed maturity and for a certain strike price.

Due to the availability of closed-form formulae for these types of contracts, the Black and Scholes model gained great popularity. However, when comparing prices under this model with real market prices, it is observed that the volatility σ is not a constant, but depends on both the maturity of the option and the strike price. The curve $K \to \sigma(T, K)$ is called *implied volatility* (Björk [21], Hull [78]).

Failure of the constant volatility assumption indicates some inadequacy of the Black and Scholes model. In the attempt to amend the Black and Scholes model, different suggestions have been made and nowadays modelling of the implied volatility has become an active area of research. Among the various proposed models, we distinguish *stochastic volatility* models where the volatility is modelled as a stochastic process and *local volatility* models where the volatility is defined as a deterministic function of the time and the underlying. We refer to Gatheral [62] for an overview on the topic. Recently, *stochastic local volatility* models combining features of both, have also been introduced (Alexander and Nogueira [7]).

Together with a good understanding of the dynamics of single assets, it is also important to adequately model the joint dynamics of multiple assets. Indeed, multi-assets options whose value depend on more than one asset are also available in financial markets. These are popular for example for portfolio diversification purposes, as investments in many assets can potentially reduce risk, with respect to the case where one single asset is hold.

Let us consider two assets (S_1, S_2). A simple attempt in order to describe the joint dynamics of (S_1, S_2) could be to consider a bi-dimensional Black and Scholes model, where the relationship between changes in the two assets is modelled

through a correlation parameter ρ between the corresponding Brownian motions

$$\begin{aligned}
\frac{dS_1(t)}{S_1(t)} &= rdt + \sigma_1 dW_1(t) \\
\frac{dS_2(t)}{S_2(t)} &= rdt + \sigma_2 dW_2(t) \\
d\langle W_1, W_2 \rangle &= \rho dt.
\end{aligned}$$

However, as for the volatility σ, also the correlation $\rho(T, K)$ shows some dependence on both the maturity and the strike price. The curve $K \to \rho(T, K)$ is called *implied correlation* (see e.g. Austing [10]).

In order to better describe the joint dynamics of groups of assets and to reproduce the fact that correlation is random rather than a constant parameter, multidimensional stochastic and local volatility/correlation models have been proposed (Da Fonseca et al. [46], Langnau [87]).

Motivation and structure of the thesis

This thesis comprises four self-contained chapters. The aim is the analysis, both from a theoretical and a numerical perspective, of some financial models with attention to the implied volatility/implied correlation curve they reproduce.

We start with Chapter 1, which is based on the paper *"Simple Simulation schemes for CIR and Wishart processes"*. Here we focus on the numerical simulation of the square root or CIR process and of the Wishart process, generalization of the CIR to the multidimensional framework. Both processes have many possible applications in finance, among others as instantaneous volatility in the benchmark Heston [77] stochastic volatility model and as variance-covariance matrix of a group of assets in the WASC model (Da Fonseca et al. [46]). The Wishart process can also be used to include more factors into the volatility of one single asset, as in the WMSV model of Da Fonseca et al. [47]. Our simulation scheme has therefore many possible applications e.g., for pricing under stochastic volatility/stochastic correlation models. Other applications include interest rate models, as in Cox et al. [43] and Gnoatto [68].

In the first Chapter of the thesis, we focus on the analysis of the Heston model and the Wishart model, mainly from a simulation point of view. On the other hand,

it is also interesting and useful to check whether a model is theoretically able to reproduce some features of financial market data, such as the implied volatility curve, before actually using it in practice.

This is the aim of the paper *"The impact of jump distributions on the implied volatility of variance"* (Chapter 2). Here, we consider a class of models which extend the Heston stochastic volatility model by including jumps into the dynamics of the instantaneous variance and we analyze the asymptotic behaviour of the implied volatility from realized variance options and VIX options. Specifically, we provide some mathematical conditions relating the distribution of the jumps with the wings of the implied volatility of variance. Besides showing theoretical results, we also provide numerical illustrations, both in the case of realized variance options and VIX options. In particular, in order to compute prices of call options on the realized variance, we adopt the approach in Carr et al. [34]. According to this procedure, the Laplace transform of the call-price function can be expressed in terms of the Laplace transform of the realized variance itself. As a consequence, whenever an explicit expression for the Laplace transform of the realized variance is available, call prices can be recovered by Laplace inversion techniques. While this approach seems to be effective and easy to implement from a theoretical point of view, numerical difficulties may appear when actually implementing the code, for example in Matlab. Indeed, this is what we experienced when providing the numerical illustrations for Chapter 2.

In the paper *"Pricing Realized Variance Options using Laplace transforms: a comparison of inversion methods"* (Chapter 3) we illustrate some of these issues when considering the Heston model augmented with Inverse Gamma jumps in the instantaneous variance.

Finally, Chapter 4 is based on the paper *"The MVMD model: shifted dynamics and correlation skew"*, which I started during my staying abroad at Imperial College, in London. Here we move from stochastic volatility models and applications to volatility derivatives to consider a multidimensional local volatility/local correlation model denominated MVMD model, of which we investigate some uses in the FX market. This model was introduced in Brigo et al. [28] as a multidimensional extension of the LMD model in in Brigo and Mercurio, [24] and [25]. In this thesis, we generalize it by introducing shifted dynamics, which allow to better reproduce the implied volatility curve of the single assets. We analyze the implied correlation

under this model, focussing on triangular relationships among FX exchange rates. Finally, we propose a shifted model with uncertain volatility and correlation which reproduces the correlation skew better.

Chapter 1

Simple Simulation schemes for CIR and Wishart processes

Simple Simulation schemes for CIR and Wishart processes [1]

Paolo Baldi
Dept. of Mathematics, Tor Vergata University, Rome

Camilla Pisani
Dept. of Economics and Business Economics, Aarhus University

Abstract

We develop some simple simulation algorithms for CIR and Wishart processes. We investigate rigorously the square of a matrix valued Ornstein-Uhlenbeck process, the main idea being to split the generator and to reduce the problem to the simulation of the square of a matrix valued Ornstein-Uhlenbeck process to be added to a deterministic process. In this way we provide a weak second order scheme that requires only the simulation of i.i.d. Gaussian r.v.'s and simple matrix manipulations.

1.1 Introduction

This paper introduces some simple algorithms to simulate a Wishart process. They work only under some assumptions on the parameters, but they are quite simple to implement and work well. The Wishart process was introduced in Bru [32] as the matrix valued process that is the solution of

$$X_t^x = x + \alpha I_d t + \int_0^t \left(\sqrt{X_s^x}\, dW_s + dW_s^T \sqrt{X_s^x}\right) \tag{1.1}$$

[1]Original article published as IJTAF,16,8,2013,15 Pages DOI:10.1142/S0219024913500453

where $(W_t)_{t\geq 0}$ denotes a $d \times d$ square matrix of independent standard Brownian motions, $\alpha \in \mathbb{R}^+$ and x is symmetric positive semidefinite. We shall consider under the name of Wishart the following more general process

$$X_t^x = x + \int_0^t (\alpha\, a^T a + bX_s^x + X_s^x b^T)ds + \int_0^t \sqrt{X_s^x}dW_s a + a^T dW_s^T \sqrt{X_s^x} \quad (1.2)$$

where $(W_t)_{t\geq 0}$, α, a and x are as above and b is another $d \times d$ matrix. Under the assumption $\alpha \geq d-1$, that we will assume hereafter, existence of a unique weak solution of the previous equation has been proved (see Bru [33], Cuchiero, Filipović, Mayerhofer and Teichmann [45] e.g.). We shall denote $W_d(x, \alpha, b, a; t)$ the solution of (1.2). This process is the natural multidimensional generalization of the one-dimensional CIR process, i.e. the solution of

$$dX_t = (a - \kappa X_t)dt + \sigma\sqrt{X_t}dB_t \quad (1.3)$$

with $x_0, \sigma, a \geq 0, \kappa \in \mathbb{R}$, $(B_t)_t$ being a standard Brownian motion.

The Wishart process has appeared recently in stochastic volatility models in finance as in Gourieroux and Sufana [70] or Da Fonseca, Grasselli and Tebaldi [47] where a generalization of the model of Heston [77] is developed. Indeed it appears that a one-dimensional process such as the CIR is not sufficient to explain the various sources of volatility and that a multidimensional process is more suitable to this task. Also a single Wishart can be used in order to model the volatilities of many assets.

Finally, Wishart processes can be used as models for interest rates (see e.g. Gnoatto [68]).

The main problem when dealing with processes on cones (Wishart processes take values on the cone of positive semidefinite matrices) is that they may reach the boundary of the cone where the coefficients are not Lipschitz continuous so that strong existence of the solution is not granted by the usual existence theorems. Moreover classical simulation methods such as the Euler-Maruyama scheme are not applicable: for instance, applying the Euler scheme to the CIR process,

$$\widehat{X}_{t_i} = \widehat{X}_{t_{i-1}} + \frac{T}{N}(a - k\widehat{X}_{t_{i-1}}) + \sigma\sqrt{\widehat{X}_{t_{i-1}}}\big(W_{t_i} - W_{t_{i-1}}\big) \quad (1.4)$$

X_{t_i} may become negative for some t_i so that the approximation $X_{t_{i+1}}$ at the following time is not defined. For this reason, it is important to find alternative

simulation schemes. The main reference for the simulation of Wishart processes is Ahdida and Alfonsi [5] where a simulation method working for every value of $\alpha > d-1$ is developed. The methods we propose here are much simpler but work only under the more restrictive assumption $\alpha \geq d$.

Let $[0,T]$ a time interval and let us fix a regular grid $0 = t_0 < t_1 = h < t_2 = 2h < \cdots < t_N = T$ on this interval, where $h = \frac{T}{N}$. We can define the subsequent values $(\widehat{X}_{t_i}, 0 \leq i \leq N)$ of the approximation as soon as we have a family of probability laws $(\widehat{p}_x(t), t > 0)$ (the transition probabilities) representing the conditional distribution of $X_{t_{i+1}}$ given $X_{t_i} = x$. More precisely, for every measurable bounded function f

$$\mathbb{E}\big[f\big(\widehat{X}_{t_{i+1}}\big)|\mathscr{F}_{t_i}^N\big] = \int_R f(z)\widehat{p}_{\widehat{X}_{t_i}}(h)(dz)\ , \tag{1.5}$$

where $\mathscr{F}_{t_i}^N = \sigma(X_{t_1}, \ldots, X_{t_i})$. In other words, once the value $\widehat{X}_{t_i}$, at time t_i is determined, the value $\widehat{X}_{t_{i+1}}$, at time t_{i+1} is obtained by sampling the law $p_{\widehat{X}_{t_i}}(h)$.

We shall produce some simple simulation schemes for the Wishart process of the second order, according to the following definition.

Definition 1.1.1. *Let $\mathbb{D} \subset \mathbb{R}^d$ a domain and $(X_t^x)_t$, $x \in \mathbb{D}$ a $\mathbb{D}$-valued process. We say that*

$$\big(\widehat{X}_{t_i}, 0 \leq i \leq N\big) \tag{1.6}$$

is a weak ν-th order scheme for this process if there exists $K > 0$ such that

$$\big|\mathbb{E}(f(X_T^x)) - \mathbb{E}(f(\widehat{X}_{t_N}))\big| \leq \frac{K}{N^\nu} \tag{1.7}$$

for every $f \in C_K^\infty(\mathbb{D}, \mathbb{R})$. The quantity $|\mathbb{E}(f(X_T^x)) - \mathbb{E}(f(\widehat{X}_{t_N}))|$ is the weak error *associated to f.*

In Section 1.2 we prove that the square of a matrix valued Ornstein-Uhlenbeck process is a Wishart process. In Section 1.3 we recall the composition of schemes rule of Ninomiya and Victoir [95] and derive simulation schemes for CIR processes. In Section 1.4 the results of the previous sections are put together in order to devise a simulation scheme for Wishart processes. Finally in Section 1.5 we report the results of numerical simulations.

Notation

- $\mathscr{M}_d(\mathbb{R}) = d \times d$ real matrices
- $\mathscr{S}_d^+(\mathbb{R}) =$ symmetric $d \times d$ positive definite matrices
- I_d, $0_d =$ identity $d \times d$ matrix, null $d \times d$ matrix
- $(I_d^n)_{h,k} = 1_{\{1 \le h = k \le n\}}, n \le d$
- $A^T, tr(A), det(A) =$ transpose, trace, determinant of matrix A
- $W_d(x_0, \alpha, b, a) =$ Wishart process (i.e. solution of (1.2)) with parameters α, b, a starting at $x_0 \in \mathscr{S}_d^+(\mathbb{R})$

1.2 Squared matrix valued Ornstein-Uhlenbeck processes

In this section we show that the square of an Ornstein-Uhlenbeck matrix process is actually a particular case of a Wishart process which is the starting idea of our procedure. Similar properties were mentioned already in Bru [33] §3.

Proposition 1.2.1. *Let $a,\ b \in \mathscr{M}_d(\mathbb{R})$ and B_t a $n \times d$ Brownian motion. Let $(Y_t)_t$ the $n \times d$-dimensional Ornstein-Uhlenbeck process solution of*

$$dY_t = Y_t b\, dt + dB_t\, a, \quad Y_0 = y\ . \tag{1.8}$$

Then, $X_t = Y_t^T Y_t \sim W_d(x, n, b^T, a)$, $x = y^T y$.

Proof. Keeping in mind that $X_{ij}(t) = \sum_{h=1}^d Y_{hi}(t) Y_{hj}(t)$, it is simple to compute the increasing process associated to X_t. Indeed

$$\begin{aligned} d\langle X_{ij}, X_{ij}\rangle_t &= \sum_{h=1}^n d\langle Y_{hi}, Y_{hj}\rangle_t = \sum_{h=1}^n d\langle (Ba)_{hi}, (Ba)_{hj}\rangle_t = \\ &= \sum_{h=1}^n \sum_{m,l=1}^d d\langle B_{hl} a_{li}, B_{hm} a_{mj}\rangle_t = \sum_{h=1}^n \sum_{m,l=1}^d a_{li} a_{mj} \delta_{lm} dt = \\ &= \sum_{h=1}^n \sum_{l=1}^d a_{li} a_{lj} dt = n(a^T a)_{ij} dt \end{aligned} \tag{1.9}$$

and therefore $d\langle X, X\rangle_t = n(a^T a)dt$. Hence, by Ito's formula,

$$\begin{aligned} dX_t = dY_t^T\, Y_t + Y_t^T\, dY_t + n\, a^T a\, dt = \\ = (n\, a^T a + b^T Y_t^T Y_t + Y_t^T Y_t b)\, dt + a^T\, dB_t^T Y_t + Y_t^T\, dB_t\, a. \end{aligned} \tag{1.10}$$

We prove now that

$$dX_t = (n\, a^T a + b^T X_t + X_t b)\, dt + a^T\, dW_t^T\, \sqrt{X_t} + \sqrt{X_t}\, dW_t\, a \tag{1.11}$$

for an appropriate $d \times d$ Brownian motion $(W_t)_{t\geq 0}$ and this will conclude the proof.

Let $V_t = ker(X_t) = ker(Y_t^T Y_t)$ and p_{V_t}, $p_{V_t^\perp}$ the matrices of the projections $\mathbb{R}^d \to V_t$ and $\mathbb{R}^d \to V_t^\perp$ respectively. Let $p_{V_t}^*$, $p_{V_t^\perp}^*$ their respective adjoints, i.e. the embeddings $V_t \to \mathbb{R}^d$ and $V_t^\perp \to \mathbb{R}^d$ respectively. Let $A_1(t) = p_{V_t^\perp}^*(Y_t^T Y_t)^{-1/2} p_{V_t^\perp} Y_t^T$ and $A_2(t) = p_{V_t}^* p_{V_t}$, so that $A_1(t)A_1(t)^* = p_{V_t^\perp}^* p_{V_t^\perp}$ and $A_1(t)A_1(t)^* + A_2(t)A_2(t)^* = I_d$ (recall however that $A_1(t)$ is $d \times n$ whereas $A_2(t)$ is $d \times d$). Let now B' a $d \times d$ Brownian motion independent of B and let

$$W_t = \int_0^t A_1(t)\, dB_t + \int_0^t A_2(t)\, dB_t' \tag{1.12}$$

then it is immediate that W is a $d \times d$ Brownian motion. As $\sqrt{X_t}\, p_{V_t}^* p_{V_t} = p_{V_t}^* p_{V_t} \sqrt{X_t} = 0$, we have $\sqrt{X_t}\, dW_t = (Y_t^T Y_t)^{1/2}\, dW_t = Y_t^T\, dB_t$ and $dW_t^T \sqrt{X_t} = dB_t^T Y_t$. Replacing these quantities in (1.10) we obtain (1.11). □

Proposition 1.2.1 extends to the matrix valued case the well known fact that the square of a linear Ornstein-Uhlenbeck process associated to the SDE $dY_t = -\frac{\kappa}{2}\, Y_t\, dt + \frac{\sigma}{2}\, dB_t$ is a CIR process as in (1.3) with $a = \frac{\sigma^2}{4}$.

1.3 The rule of composition of schemes

If $p^{(1)}$, $p^{(2)}$ are second order transition probabilities of simulation schemes for diffusion processes with generators L_1 and L_2 respectively, then the schemes

$$q(t) = p^{(1)}(\tfrac{t}{2}) \circ p^{(2)}(t) \circ p^{(1)}(\tfrac{t}{2}) \tag{1.13}$$

and

$$q(t) = \tfrac{1}{2}\left(p^{(1)}(t) \circ p^{(2)}(t) + p^{(2)}(t) \circ p^{(1)}(t)\right) \tag{1.14}$$

are both second order schemes for the diffusion with generator L_1+L_2 (see Theorem 1.17 in Alfonsi [8] which extends ideas of Ninomiya and Victoir [95]).

Let us apply this composition rule to the case of a CIR process that is solution of

$$dX_t = \big(a - \kappa X_t\big)dt + \sigma\sqrt{X_t}\, dW_t, \quad X_0 = x \geq 0 \ . \tag{1.15}$$

Its generator can be decomposed

$$L = \big(a-\kappa x\big)\frac{d}{dx}+\frac{1}{2}\,\sigma^2 x\,\frac{d^2}{dx^2} = \underbrace{\Big(\frac{\sigma^2}{4} - \kappa x\Big)\frac{d}{dx} + \frac{1}{2}\,\sigma^2 x\,\frac{d^2}{dx^2}}_{:=L_2} + \underbrace{\Big(a - \frac{\sigma^2}{4}\Big)\frac{d}{dx}}_{:=L_1} \cdot \tag{1.16}$$

A second order transition probability for L_1 (which is the generator of a deterministic motion) is simply the translation $x \to x + (a - \frac{\sigma^2}{4})t$. As for L_2, being the generator of the square of the Ornstein-Uhlenbeck process

$$dY_t = -\frac{\kappa}{2}\, Y_t\, dt + \frac{\sigma}{2}\, dB_t \ , \tag{1.17}$$

one may just recall that, with the initial condition $Y_0 = y$, Y_t is $N(e^{-\frac{\kappa}{2}t}y, (1 - e^{-\kappa t})\frac{\sigma^2}{4k})$-distributed. Therefore a second order (actually exact) transition probability for L_2 can be realized as

$$X_{t_i} \to \Big(e^{-\frac{\kappa}{2}\,h}\sqrt{x} + \frac{\sigma}{2}\,\sqrt{\psi_k(h)}\, W\Big)^2 \tag{1.18}$$

where $\psi_\kappa(t) = \frac{1}{\kappa}(1 - e^{-\kappa t})$ and W denotes a $N(0,1)$ distributed r.v. (here $h = t_{i+1} - t_i$ is the amplitude of the time discretization).

Therefore, thanks to the composition rule all the following are second order schemes for the process (1.3):

$$q_1(t) = p^{(1)}(\tfrac{t}{2}) \circ p^{(2)}(t) \circ p^{(1)}(\tfrac{t}{2}) \tag{1.19}$$

$$q_2(t) = p^{(2)}(\tfrac{t}{2}) \circ p^{(1)}(t) \circ p^{(2)}(\tfrac{t}{2}) \tag{1.20}$$

$$q_3(t) = \tfrac{1}{2}\,\big(p^{(1)}(t) \circ p^{(2)}(t) + p^{(2)}(t) \circ p^{(1)}(t)\big) \tag{1.21}$$

and also

$$q_4(t) = p^{(1)}(\tfrac{t}{4}) \circ p^{(2)}(\tfrac{t}{2}) \circ p^{(1)}(\tfrac{t}{2}) \circ p^{(2)}(\tfrac{t}{2}) \circ p^{(1)}(\tfrac{t}{4}) \tag{1.22}$$

which turns out to be a second order scheme by application of the composition rule twice.

We have therefore

Proposition 1.3.1. *Assume $a \geq \frac{\sigma^2}{4}$. Then q_1, q_2, q_3 and q_4 are discretization schemes of order 2 for the CIR process (1.15).*

The condition $a \geq \frac{\sigma^2}{4}$ is necessary in order to ensure that the iteration $p^{(1)}$ produces a value in $\mathbb{R}^+$.

The numerical results of Section 1.5 will allow to compare the performances of these four schemes, q_2 and q_4 appearing to be the most promising.

Note also that if $a = \frac{\sigma^2}{4}$, then all four schemes reduce to $p^{(2)}$ and therefore have zero bias. We shall see in the next section that actually also for other values of a it is possible to obtain an exact simulation scheme.

1.4 The simulation of Wishart processes

The arguments of the previous paragraph are easily extended to a matrix valued framework thus obtaining a simulation scheme for the Wishart process. Consider the generator of a $W_d(x, \alpha, b, a)$

$$L = tr[(\alpha a^T a + bx + xb^T)D] + 2tr(xDa^T aD) \ . \tag{1.23}$$

Let us assume $\alpha \geq d$ and write it as the sum $L = L_1 + L_2$ where, denoting $n = \lfloor \alpha \rfloor$ the integer part of α,

$$L_2 = tr[(na^T a + bx + xb^T)D] + 2tr(xDa^T aD) \tag{1.24}$$

is the generator of a $W_d(x, n, b, a)$ which is a squared Ornstein-Uhlenbeck process, whereas

$$L_1 = tr[(\alpha - n)a^T aD] \tag{1.25}$$

is again the generator of a deterministic process associated to an ordinary differential equation and

$$X_{t_{i+1}} = X_{t_i} + (\alpha - n)a^T a\, t \tag{1.26}$$

is a second order scheme for L_1. Therefore, thanks to Proposition 1.2.1, given a second order scheme for a $n \times d$ dimensional Ornstein-Uhlenbeck process, we can obtain a second order discretization scheme for a generic Wishart process using the scheme composition rule. Actually it is possible to simulate exactly such a matrix valued Ornstein-Uhlenbeck process as follows

Let Y be the matrix valued solution of the equation

$$dY_t = Y_t b^T dt + dB_t a, \quad Y_0 = y. \tag{1.27}$$

Let us recall how it is possible to write its solution explicitly. First of all $Y_t = ye^{tb^T}$ is solution of

$$\dot{Y}_t = Y_t b^T, \quad Y_0 = y \ . \tag{1.28}$$

If we look for a solution of (1.27) of the type $Y_t = C_t e^{tb^T}$, Ito's lemma gives

$$dY_t = dC_t \, e^{tb^T} + C_t e^{tb^T} b^T \, dt \tag{1.29}$$

and, comparing with (1.27), we obtain that C_t must satisfy

$$dC_t \, e^{tb^T} = dB_t a \ . \tag{1.30}$$

Therefore

$$C_t = \int_0^t dB_s a e^{-sb^T} \tag{1.31}$$

and we obtain that the solution of (1.27) is given by

$$Y_t = ye^{tb^T} + \int_0^t dB_s a e^{(t-s)b^T} \ . \tag{1.32}$$

This is a matrix valued Gaussian r.v. with mean ye^{tb^T} and whose covariances are

$$\begin{aligned} &\mathbb{E}\Big(\Big(\int_0^t dB_s a e^{(t-s)b^T}\Big)_{ij}\Big(\int_0^t dB_s a e^{(t-s)b^T}\Big)_{hk}\Big) = \\ &= \sum_{r,\ell} \mathbb{E}\Big(\int_0^t dB_{ir}(s)(ae^{(t-s)b^T})_{rj} \int_0^t dB_{h\ell}(s)(ae^{(t-s)b^T})_{\ell k}\Big) = \\ &= \delta_{ih} \int_0^t \sum_r (ae^{(t-s)b^T})_{rj}(ae^{(t-s)b^T})_{rk} \, ds = \\ &= \delta_{ih}\Big(\int_0^t (ae^{(t-s)b^T})^T(ae^{(t-s)b^T}) \, ds\Big)_{jk} = \delta_{ih}\Big(\int_0^t e^{ub} a^T a e^{ub^T} \, du\Big)_{jk} \ . \end{aligned} \tag{1.33}$$

Remark that, given a matrix W whose coefficients are independent and $N(0,1)$ distributed and a matrix A, then the matrix-valued r.v. WA has covariances

$$\mathbb{E}((WA)_{ij}(WA)_{hk}) = \sum_{r,\ell} \mathbb{E}(W_{ir}A_{rj}W_{h\ell}A_{\ell k}) = \delta_{ih}(A^T A)_{jk} \ . \tag{1.34}$$

So an exact second order scheme for the Ornstein-Uhlenbeck process Y is, again denoting $h = t_{i+1} - t_i$,

$$\widehat{Y}_{t_{i+1}} = \widehat{Y}_{t_i} e^{hb^T} + WC^{1/2} \tag{1.35}$$

where $W \sim N(0_d, I_d)$ and C is the matrix

$$C = \int_0^h e^{ub} a^T a e^{ub^T} \, ds. \tag{1.36}$$

Therefore we can derive a second order (actually exact) scheme for L_2 in the following way (recall that Y is $n \times d$-valued, whereas the process with generator L_2 is $d \times d$-valued):

$$X_{t_{i+1}} = \left(Y_{t_i} e^{hb^T} + WC^{1/2}\right)^T \left(Y_{t_i} e^{hb^T} + WC^{1/2}\right) \tag{1.37}$$

where Y_{t_i} is any $n \times d$ matrix such that $Y_{t_i}^T Y_{t_i} = X_{t_i}$ possibly obtained by taking the square root of the positive defined $d \times d$ matrix X_{t_i} and then adding $n - d$ rows of zeros. If we denote $p^{(2)}$ this scheme and $p^{(1)}$ the scheme in (1.26), by the composition rule the schemes defined in (1.19), (1.20), (1.21) and (1.22) are second order for a $W_d(x, \alpha, b, a)$ process. Remark that in this construction the condition $\alpha \geq d$ appears again, similarly to what happens for the CIR process, in order to ensure that each iterations produces a positive definite matrix.

Proposition 1.4.1. *Assume $\alpha \geq d$ and denote $p^{(1)}$ and $p^{(2)}$ the transition probabilities defined in (1.26) and (1.37) respectively. Then the schemes defined in (1.19), (1.20), (1.21) and (1.22) are of order 2 for the Wishart process (1.1).*

These schemes require only the simulation of Gaussian r.v.'s and the computation, at every iteration, of the square root of a matrix. They require also, but only once, the computation of the matrices e^{hb^T} and C and of its square root. This task is easily performed when using a high-level language environment as, for instance, Matlab or Scilab. When programming in C one may consider of performing the computation of e^{hb^T} and C with Scilab or any other high level language and then give them as arguments to the C code.

Remark 1.4.2. *The schemes produced in Proposition 1.4.1 are exact if α is an integer larger that d and are therefore expected to have a very small bias when $\alpha - \lfloor \alpha \rfloor$ is small. This fact is confirmed by the numerical experiments of the next section.*

Remark 1.4.3. *The previous remark suggests how to produce a possibly more accurate scheme also for the CIR process. Actually just remark that a CIR process is a Wishart process with* $d = 1$.

More explicitly, if $n := \lfloor \frac{4a}{\sigma^2} \rfloor$, *an exact scheme for the generator*

$$\widetilde{L}_2 = \Big(n \, \frac{\sigma^2}{4} - \kappa x \Big) \frac{d}{dx} + \frac{1}{2} \, \sigma^2 x \, \frac{d^2}{dx^2} \tag{1.38}$$

is obtained through the simulation of a $n \times 1$ *dimensional Ornstein-Uhlenbeck process. An exact scheme for it with step* h *is therefore*

$$X_{t_{i+1}} = \Big(Y_{t_i} e^{-\frac{\kappa}{2} h} + \frac{\sigma}{2} \, \sqrt{\psi_k(h)} \, W \Big)^T \Big(Y_{t_i} e^{-\frac{\kappa}{2} h} + \frac{\sigma}{2} \, \sqrt{\psi_k(h)} \, W \Big) \tag{1.39}$$

where W *is now a* $n \times 1$ *matrix whose entries are independent and* $N(0,1)$*-distributed and* Y_{t_i} *denotes any* $n \times 1$ *matrix such that* $Y_{t_i}^T Y_{t_i} = X_{t_i}$. *Denoting* $\widetilde{p}^{(2)}$ *this scheme and* $\widetilde{p}^{(1)}$ *the scheme*

$$X_{t_{i+1}} = X_{t_i} + \Big(a - n \, \frac{\sigma^2}{4} \Big) h \tag{1.40}$$

one obtains a second order scheme for L *as in (1.16) by composing them according to one of the rules (1.19)–(1.22). The schemes obtained in this way are exact if* $\lfloor \frac{4a}{\sigma^2} \rfloor$ *is an integer number and can be expected to perform better than the schemes described in 1.3 if* $\lfloor \frac{4a}{\sigma^2} \rfloor$ *is large.*

1.5 Numerical results

CIR processes

First of all we have performed 1000 runs of 1000 simulated paths each, and collected the values of the paths at time 1. For every run we have computed the chisquare discrepancy between the empirical distribution obtained at time 1 with the known exact distribution at time 1 duly discretized (into 32 subintervals). We have thus obtained 1000 random numbers that, if the empirical distribution were drawn from the exact distribution would be each $\chi^2(31)$-distributed. In Figure 1.1 we report the histograms of these numbers against the density of the $\chi^2(31)$ distribution. We have computed, for two different values of a, an approximation of the characteristic function at 1, $\mathbb{E}[e^{iX_T^x}]$, for $T = 1$, whose exact value can be derived from the

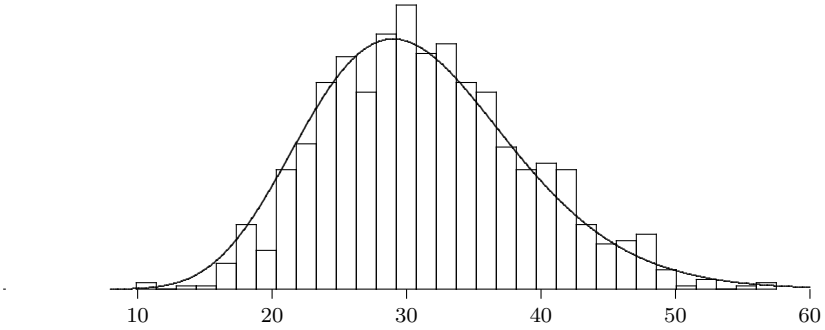

Figure 1.1: The chisquare comparison. Here the parameters were: $\kappa = 0.5$, $\sigma = 0.8$, $a = 5$ with $x_0 = 0.01$. We used the scheme q_2 of (1.20).

estimator	bias $\times 10^4$
q_1	2.42
q_2	0.64
q_3	1.12
q_4	0.99
$A - A$ 2^{nd} order	0.72
$A - A$ 3^{rd} order	0.56

Table 1.1: Bias of the estimators of $\mathbb{E}[e^{iX_1}]$ for the values $\kappa = 0.5$, $\sigma = 0.8$, $a = 0.4$ and starting at $x_0 = 0.01$. The true value is $0.9139167 + i\,0.2968570$, $6.4 \cdot 10^6$ simulated paths, time step $h = \frac{1}{10}$.

known explicit expression of the Laplace transform of the distribution at time 1 (see Lamberton and Lapeyre [86] p. 131 e.g.).

Tables 1.1 and 1.2 give a comparison of the biases of the different estimators, whereas Figures 1.2 and 1.3 gives the corresponding graphical information.

Wishart processes

We have tested the simulation scheme of 1.4 computing numerically the value of the characteristic function and comparing with the exact value. Actually (see e.g. Proposition 5 in Ahdida and Alfonsi [5]) the characteristic function of a $W_d(x, \alpha, b, a)$ at time t at $v \in \mathscr{M}_d(\mathbb{R})$ is given by

$$L(v) = \mathbb{E}[\exp(itr(vX_t^x))] = \frac{\exp(tr[iv(I_d - 2iq_tv)^{-1}m_txm_t^T])}{det(I_d - 2iq_tv)^{\frac{\alpha}{2}}} \cdot \tag{1.41}$$

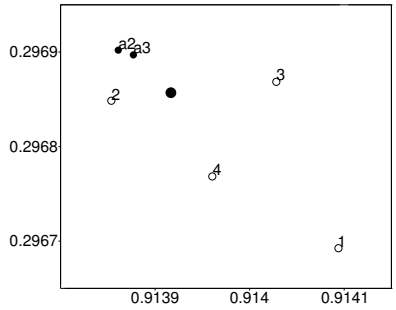

Figure 1.2: Graphic of the simulations of Table 1.1: the true value (the large •), the estimators q_1, q_2, q_3 and q_4 (∘), and the Ahdida-Alfonsi procedures (•) of order 2 (a2) and 3 (a3).

estimator	bias $\times 10^4$
q_2	2.49
q_2, $W15 \times 1$	0.88
q_4	4.02
q_4 $W15 \times 1$	3.40
$A - A$ 2^{nd} order	2.32
$A - A$ 3^{rd} order	1.49

Table 1.2: Bias of the estimators of $\mathbb{E}[e^{iX_1}]$ for $a = 2.5$ starting at $x_0 = 0.01$, with $\kappa = 0.5$, $\sigma = 0.8$ as above. The true value is $-0.2782669 + i\,0.7344139$, $6.4 \cdot 10^6$ simulated paths, the time step $h = \frac{1}{10}$. $W15 \times 1$ indicates that the simulation has been performed taking the square of a 15×1 dimensional Ornstein-Uhlenbeck process, as explained in Remark 1.4.3 (here $\lfloor \frac{4a}{\sigma^2} \rfloor = 15$).

where

$$m_t = e^{tb}, \quad q_t = \int_0^t e^{sb} a^T a e^{sb^T}\, ds\ . \tag{1.42}$$

We performed simulations with two different values of α and

$$a = \begin{pmatrix} 2 & 1 & 0 \\ 0 & 1 & 0 \\ 0 & 0 & 1 \end{pmatrix} \qquad b = -\begin{pmatrix} 4 & 1 & 1 \\ 0 & 1 & 1 \\ 0 & 0 & \frac{1}{10} \end{pmatrix} \tag{1.43}$$

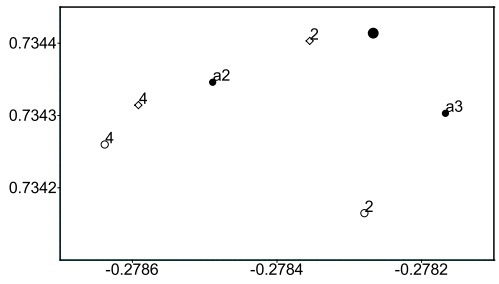

Figure 1.3: Graphic of the outcomes of Table 1.2: the true value (the large •), the estimators q_2 and q_4 taking the square of a linear Ornstein-Uhlenbeck process (∘) the estimators q_2 and q_4 taking the square of a 15×1 Ornstein-Uhlenbeck process (⋄) and the Ahdida-Alfonsi procedures of order 2 (a2) and 3 (a3).

and initial distribution

$$x_0 = \begin{pmatrix} 1 & 0 & 0 \\ 0 & 4 & 0 \\ 0 & 0 & 1 \end{pmatrix} \tag{1.44}$$

and computed the characteristic function $\mathbb{E}(e^{tr(ivX_1^x)})$ with

$$v = \begin{pmatrix} 0.24 & 0.12 & -0.01 \\ 0.12 & 0.16 & 0.08 \\ -0.01 & 0.08 & 0.08 \end{pmatrix} \tag{1.45}$$

We performed 400 runs of 16 000 simulated paths each with the four schemes q_1–q_4 and the Ahdida-Alfonsi procedures of order 2 and 3. The values of the corresponding overall estimators (over $400 \times 16000 = 6.4 \cdot 10^6$ paths) for the value $\alpha = 3.7$ is plotted in Figure 1.5 and the corresponding biases are given in Table 1.3. The outcome is plotted in Figure 1.4. Table 1.4 and Figures 1.6 and 1.7 provide the same information for the value $\alpha = 5.1$. In this case, α being close to its integer part it is to be expected that q_1, q_2, q_3 and q_4 should perform particularly well.

In conclusion the simulation schemes proposed above in this paper are very simple to implement and appear to perform satisfactorily. The Ahdida-Alfonsi procedures remain however the only ones to our knowledge to confront with the case $d - 1 \leq \alpha < d$, which is important in financial applications.

scheme	bias $\times 10^3$
q_1	5.68
q_2	2.60
q_3	5.89
q_4	1.51
$A - A\ 2^{nd}$	2.42
$A - A\ 3^{rd}$	1.97

Table 1.3: By (1.41), the value of the characteristic function at v, with the given a, b, x_0 and $\alpha = 3.7$ is $1.653838 + i7.120555$.

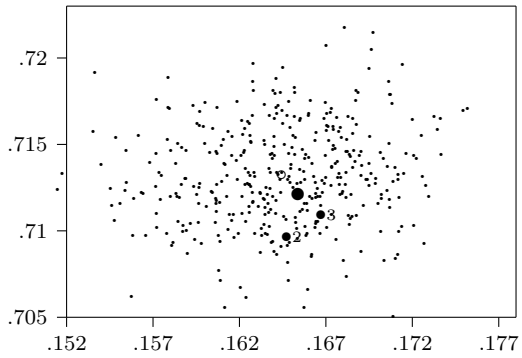

Figure 1.4: 400 estimated values with 16 000 paths each (with scheme q_4) compared with the true value (the large •). We used the scheme (1.22) and the time interval $[0, 1]$ split into 10 subdivisions. ∘ denotes the overall estimated value. Marked are also the estimators obtained using the Ahdida-Alfonsi procedure of order 2, •2, and of order 3, •3.

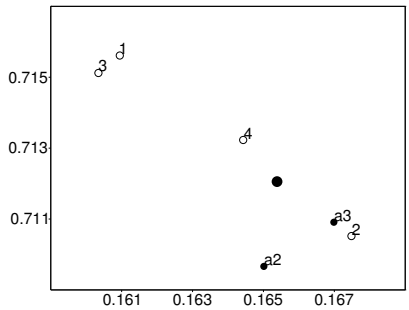

Figure 1.5: The outcomes of our four algorithms based on the square Ornstein-Uhlenbeck (∘), the true value (the large •) and the Ahdida-Alfonsi procedures of order 2 (a2) and 3 (a3). Here $\alpha = 3.7$.

scheme	bias $\times 10^4$
q_1	8.73
q_2	5.05
q_3	9.40
q_4	3.42
$A - A\ 2^{nd}$	32.91
$A - A\ 3^{rd}$	16.08

Table 1.4: The exact value of the characteristic function at v, with the given a, b and $\alpha = 5.1$ is $-0.1576554 + i0.6380182$. Remark that the given values of the bias have to be multiplied by 10^4 (instead of 10^3 in Table 1.3). Of course the good performance of the schemes q_1–q_4 is due to the fact that this value of alpha is close to its integer part.

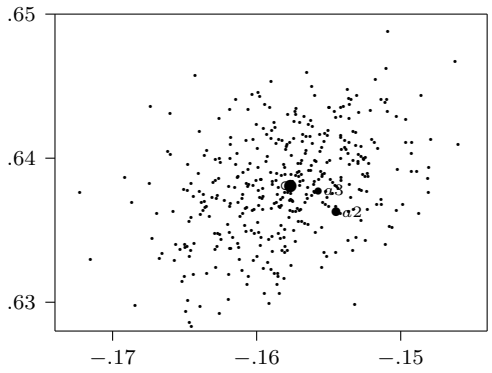

Figure 1.6: Again 400 estimated values with 16 000 paths each compared with the true value (large •). Now $\alpha = 5.1$ and we simulated the square of a 5×3 Ornstein-Uhlenbeck process. We used the scheme (1.22) and the time interval $[0, 1]$ split into 10 subdivisions. ∘ denotes the overall estimated value (almost invisible, very near the true value). Marked are also the estimators obtained using the Ahdida-Alfonsi procedure of order 2, •2, and of order 3, •3.

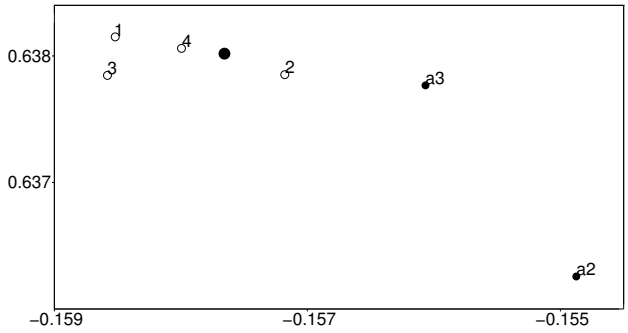

Figure 1.7: The outcomes of the four estimators based on the squared Ornstein-Uhlenbeck (∘), the true value (the large •) and the Ahdida-Alfonsi procedures of order 2 (a2) and 3 (a3). Here $\alpha = 5.1$ and the underlying Ornstein-Uhlenbeck process was 5×3-dimensional.

Chapter 2

The Impact of Jump Distributions on the Implied Volatility of Variance

The Impact of Jump Distributions on the Implied Volatility of Variance

Elisa Nicolato
Dept. of Economics and Business Economics, Aarhus University

Camilla Pisani
Dept. of Economics and Business Economics, Aarhus University

David Sloth
Danske Bank

Abstract

We consider a tractable affine stochastic volatility model that generalizes the seminal Heston [77] model by augmenting it with jumps in the instantaneous variance process. In this framework, we consider both realized variance options and VIX options, and we examine the impact of the distribution of jumps on the associated implied volatility smile. We provide sufficient conditions for the asymptotic behavior of the implied volatility of variance for small and large strikes. In particular, by selecting alternative jump distributions, we show that one can obtain fundamentally different shapes of the implied volatility of variance smile – some clearly at odds with the upward-sloping volatility skew observed in variance markets.

2.1 Introduction

There is a vast and lively literature investigating the presence of jumps in the evolution of financial assets. In a seminal paper, Duffie et al. [53] proposed the class of affine jump-diffusion processes, a flexible and tractable modelling framework allowing for jumps both in asset prices and in their stochastic variances. Since then, affine models have been applied empirically in a number of studies, including

Broadie et al. [30], Chernov et al. [39], Eraker et al. [56], and Eraker [55] among others. These studies generally find evidence for discontinuities both in the price level and its volatility. In particular, the consensus appears to be that jumps are needed to capture the steep and negative skew observed in the short end of the volatility surface implied by equity options. We refer to Duffie et al. [53] and Gatheral [62] for a detailed analysis of the effect of jumps when calibrating affine models to S&P500 option prices.

A substantial body of literature considers the pricing of derivatives written on the volatility or variance of an asset such as CBOE's VIX index. In contrast to the case of equity markets, the volatility surface implied by volatility options is characterized by an upward sloping smile. As indicated by Sepp [101], this stylized feature reflects the fact that out-of-the-money call options on volatility provide protection against market crashes. To compensate for the insurance risk, the writer of a call on volatility will charge a premium accordingly, very much like the writer of put on the stock or index itself. Several authors suggest that the inclusion of jumps in the volatility process provides a parsimonious and empirically justifiable way to capture the positive skew associated with volatility derivatives. Among them, Sepp [100], [101], and Lian and Zhu [90] propose augmenting the popular square-root dynamics of Heston [77] to include exponential jumps in the instantaneous variance process.

Despite the common notion that jumps are a necessary modelling ingredient, the question of how to model the distribution of jumps and its financial implications seems to be a matter of lesser relevance. A number of different jump specifications has been examined within the literature concerning equity derivatives. For example, Nicolato and Venardos [94] and Carr et al. [35] compare the performances of alternative affine models when calibrated to S&P500 option prices. These studies indicate that, ceteris paribus, the specific choice of jump distribution has a minor effect on the qualitative behavior of the skew and the term structure of the implied volatility surface of equity options.

This might be the reason why a similar analysis is basically absent from the literature on volatility derivatives. To the best of our knowledge, the above-mentioned exponential distribution appears to be the only candidate proposed to model jump sizes in the instantaneous variance process.

As a matter of fact, several authors have looked at a number of alternative

dynamics based on diffusive or more general continuous-paths processes. To name a few, Drimus [52] considers Log-OU stochastic volatility models, Gatheral [63] proposes a double mean reverting process while Drimus [51] and Baldeaux and Badran [13] examine the performance of the 3/2 model. Also fractional dynamics have been recently examined by Bayer et al. [15] as an alternative to the diffusive forward variance model proposed by Bergomi [19].

Finally, among the related literature we mention the work of Papanicolau [96] where the relationship between VIX options and the negative moments of the SPX is analyzed in a model-free way.

In this paper we fix the dynamics of the underlying asset within the affine jump-diffusion framework and we focus uniquely on the effect of changing the law of the jump component. We show that, in contrast to the case of SPX options, the particular distribution of jumps does have a profound impact on the pricing of volatility derivatives, predicting completely different shapes and characteristics of the associated implied volatility surface.

To keep matters simple, we consider the class of SVJ-v models, a particular case of affine stochastic volatility models which accounts for jumps in the dynamics of the variance process. The SVJ-v framework allows for an enormous variety of jump distributions, and it includes variance specifications of the Ornstein-Uhlenbeck type introduced by Barndorff-Nielsen and Shepard [14]. This subclass is particularly neat, as the instantaneous variance evolves solely by jumps, which allows us to isolate the unique impact of the jump distribution on volatility derivatives.

We start our analysis by considering options written on the variance realized by the returns of an underlying asset over the life-time of the contract. Existing studies on pricing of realized variance options include Carr et al. [34], Drimus [51], and Sepp [100], while Cont and Kokholm [42] develop a flexible market model for consistent valuation of realized variance derivatives, index options, and VIX derivatives. The main advantage of dealing with this kind of contracts in the SVJ-v framework is that the realized variance can be identified with the integrated variance and its Laplace transform is available in closed-form. This enables us to combine classical Tauberian theorems with the more recent results of Lee [89] and Gulisashvili [73] on implied volatility asymptotics, and investigate the intimate link between the distribution of jumps, the distribution of realized variance, and ultimately the impact on the implied volatility of realized variance options.

More specifically, we provide simple and easy-to-check sufficient conditions relating the tail-distribution of the variance jumps with the asymptotic behavior of the implied volatility for small as well as large strikes. Rather than deriving precise asymptotic estimates, we are interested in the qualitative behavior of the wings, i.e., whether they are upward or downward sloping, as this gives an indication of the overall smile shape. We provide numerical illustrations for a variety of positive distributions for jump specifications, showing how the commonly used exponential law might not be the optimal choice as it inherently leads to a downward-sloping volatility skew. Finally, we extend the analysis to the case of VIX options and we obtain similar results.

The rest of the paper is organized as follows: In Section 2.2 we present the necessary background on wing asymptotics and we provide some preliminary results on wing asymptotics for a general distribution of the underlying. In Section 2.3 we specialize the analysis to the case of realized variance options in the SVJ-v modelling framework and we derive sufficient conditions based on the jump component for the asymptotic behavior of the smile. In Section 2.4 we describe a number of alternative jump distributions and present numerical illustrations for the selected cases. In Section 2.5 we extend the analysis to the wing asymptotics of VIX options and in Section 2.6 we summarize and conclude the paper. In the Appendix we provide the details of some lengthy proofs.

2.2 Preliminary Results on Wing Asymptotics

In this section we provide a few preliminary results relating the asymptotic behavior of the implied volatility at small or large strikes to the distribution of the underlying random quantity. To be more precise, fix a maturity T and denote by H_T the risk-neutral value of the underlying asset at maturity. Assuming a simplified economy with zero interest rates and dividend payments, the price of a European call with strike K is given by $C(K) = \mathbb{E}\,(H_T - K)^+$. The corresponding put price $P(K)$ can be obtained by the put-call parity relation

$$C(K) - P(K) = \mathbb{E}[H_T] - K\,.$$

At this stage, we do not specify the nature of the underlying. We only require that H_T is a positive random variable with finite first moment which, without loss of generality, we normalize to one, $\mathbb{E}[H_T] = 1$. The distribution function, the tail function and the Laplace transform of H_T are denoted by

$$F_H(x) = \mathbb{Q}(H_T \leq x), \qquad \overline{F}_H(x) = 1 - F_H(x), \qquad \mathscr{L}_H(x) = \mathbb{E}[e^{-xH_T}]\,.$$

The implied volatility $I(K)$ associated with $C(K)$ is defined as the solution of the equation

$$C(K) = \Phi\left(\frac{\log(1/K)}{I(K)\sqrt{T}} + \frac{I(K)\sqrt{T}}{2}\right) - K\Phi\left(\frac{\log(1/K)}{I(K)\sqrt{T}} - \frac{I(K)\sqrt{T}}{2}\right),$$

where $\Phi(\cdot)$ denotes the cumulative distribution function of a standard normal law. We assume $0 < F_H(x) < 1$ thus excluding cases for which the impled volatility is trivially defined as zero.

The analysis of $I(K)$ at extreme strikes, referred to as *smile wings*, has attracted considerable attention during the last decade. In a ground-breaking paper, Lee [89] relates the smile wings to the number of moments of the underlying distribution H_T. Since then, a large part of the literature has been devoted to providing refinements and extensions of Lee's moment formulas. See, for example, the work of Benaim and Friz [17], [18], Gulisashvili [71], [73] and the monograph by Gulisashvili [72]. The results relevant to this work are summarized in Theorems 2.2.1 and 2.2.3 below. The function ψ appearing in the formulations is given by

$$\psi(x) = 2 - 4(\sqrt{x^2 + x} - x),$$

and $g(x) \sim h(x)$ means that $g(x)/h(x) \to 1$ as either $x \to 0$ or $x \to \infty$ depending on the context. Also, recall that a positive, measurable function f on $\mathbb{R}_+$ is said to be *regularly varying* at ∞ with index $\rho \in \mathbb{R}$ if the following holds

$$\lim_{x\to\infty} \frac{f(\xi x)}{f(x)} = \xi^\rho\,, \tag{2.1}$$

for all $\xi > 0$. In this case we write $f \in R_\rho$. When $f \in R_0$, then we say that f is *slowly varying* at ∞. It can be shown that $f \in R_\rho$ if and only if it takes the following form

$$f(x) = x^\rho \ell(x) \tag{2.2}$$

where $\ell \in R_0$.

Let us start by considering the behavior of $I(K)$ at large strikes.

Theorem 2.2.1. *The following statements hold for the implied volatility $I(K)$ at large strikes.*

(i) Let $p_H = \sup\ \big\{p : \mathbb{E}[H_T^{p+1}] < \infty\big\}$, then

$$\limsup \frac{I^2(K)T}{\log(K)} = \psi(p_H) \quad as \quad K \to \infty. \tag{2.3}$$

(ii) If $p_H < \infty$, then we can replace lim sup *with the limit and write*

$$I^2(K) \sim \psi(p_H)\frac{\log(K)}{T} \quad as \quad K \to \infty\,, \tag{2.4}$$

if and only if we can find $f_1, f_2 \in R_{-\rho}$ with $\rho = p_H$, such that $f_1(K) \leq C(K) \leq f_2(K)$ for all $K > K_0$, with K_0 large enough.

(iii) If $p_H = \infty$, then

$$I(K) \sim \frac{1}{\sqrt{2T}} \log(K) \left(\log \frac{1}{C(K)}\right)^{-1/2} \quad as \quad K \to \infty. \tag{2.5}$$

The large strike formula (2.3) is derived in Lee [89], while statements (2.4) and (2.5) can be found in Gulisashvili [73]. Simple applications of Theorem 2.2.1 yield the following results which will be pivotal to the analysis we carry out in Sections 2.3 and 2.5.

Proposition 2.2.2. *The following holds:*

(a) Suppose that the tail function $\overline{F}_H \in R_{-\rho-1}$ for $\rho > 0$. Then the asymptotic equivalence (2.4) *at large strikes holds with $p_H = \rho$.*

(b) Suppose that the tail function $\overline{F}_H$ is dominated by a Weibull-type function, i.e. there exist positive constants α, β, $\gamma > 0$ and a $x_0 > 0$ such that

$$\overline{F}_H(x) \leq \gamma e^{-\alpha\, x^\beta} \quad for\ all \quad x > x_0\,. \tag{2.6}$$

Then $p_H = \infty$ and $I(K) \to 0$ as $K \to \infty$.

Proof. Recall that

$$\mathbb{E}[H_T^{p+1}] = \int_0^\infty u^{p+1} dF_H(u) = (p+1) \int_0^\infty u^p \overline{F}_H(u) du \,, \tag{2.7}$$

and

$$C(K) = \int_K^\infty \overline{F}_H(u) du \,. \tag{2.8}$$

(a) Well known results from regular variation theory, see e.g. Feller [58], VIII.9, state that for a bounded $\ell \in R_0$ and for $x \to \infty$ the following holds:

$$\text{If } q < -1 \,, \text{ then } \int_0^x u^q \ell(u) du \text{ converges, while it diverges if } q > -1 \,. \tag{2.9}$$

$$\text{If } q < -1 \,, \text{ then } \frac{x^{q+1}\ell(x)}{\int_x^\infty u^\rho \ell(u) du} \to -(q+1) \,. \tag{2.10}$$

Hence, by virtue of (2.2) and (2.7), the first statement implies that $p_H = \rho$. The second statement applied to (2.8) shows that $C(K) \in R_{-\rho}$ and the conclusion follows immediately from (ii) in Theorem 2.2.1.
(b) Still from (2.7) we see that condition (2.6) implies that $p_H = \infty$. Furthermore, notice that for $q \in \mathbb{R}$ the following holds

$$\lim_{x\to\infty} \frac{x^{q+1} e^{-\alpha x^\beta}}{\int_x^\infty u^q e^{-\alpha u^\beta} du} = \infty \,. \tag{2.11}$$

Hence, for K large enough, it holds that

$$C(K) \le \int_K^\infty \gamma e^{-\alpha u^\beta} du \le AK e^{-\alpha K^\beta}$$

where A is a positive constant, and the result now follows from Gulisashivili's criterion (2.5) for large strikes. □

Direct application of Proposition 2.2.2 may be difficult as in many models the tail function of the underlying distribution is not known, while the Laplace transform is available in closed form. In some cases, conditions based on $\mathscr{L}_H$ can be obtained via Tauberian theory, which offers a number of results relating the behavior of F_H near infinity/zero to that of $\mathscr{L}_H$ near zero/infinity. In particular, from Theorem 8.1.6 in Bingham et al. [20] it follows that if n is a strictly positive integer and $n = \rho + r$ with $\rho > 0$ and $0 < r < 1$, then

$$\overline{F}_H(x) \in R_{-\rho} \quad \text{if and only if} \quad (-1)^n \mathscr{L}_H^{(n)}(1/x) \in R_r \,, \tag{2.12}$$

where we have used the notation $f^{(n)} = \frac{d^n f}{dx^n}$. So, for non integer ρ, the regular variation condition required in part (a) of Proposition 2.2.2 may be assessed via (2.12). In contrast, we cannot find an equivalent formulation of the tail condition (2.6) in terms of $\mathscr{L}_H$ unless $\beta = 1$. In this case, the domain $\mathscr{D}_H = \{x \in \mathbb{R} : \mathscr{L}_H(x) < \infty\}$ determines whether $\overline{F}_H(x)$ is exponentially dominated, since

$$\overline{F}_H(x) \leq \gamma e^{-\alpha x} \quad \text{for all } x \geq x_0 \quad \text{ if and only if } \quad 0 \in \mathring{\mathscr{D}}_H\,, \tag{2.13}$$

as one may show via Markov's inequality.

Let us consider the behavior of $I(K)$ at small strikes. Once again, we start by listing the relevant results from Lee [89] and Gulisashvili [73].

Theorem 2.2.3. *The following statements hold for the implied volatility $I(K)$ at small strikes.*

(i) Let $q_H = \sup\ \big\{q : \mathbb{E}[H_T^{-q}] < \infty\big\}$, then

$$\limsup \frac{I^2(K)T}{\log(1/K)} = \psi(q_H) \quad \textit{as} \quad K \to 0. \tag{2.14}$$

(ii) If $q_H < \infty$, then we can replace lim sup *with the limit and write*

$$I^2(K) \sim \psi(q_H)\frac{\log(K)}{T} \quad \textit{as} \quad K \to 0\,, \tag{2.15}$$

if and only if we can find $f_1, f_2 \in R_{-\rho}$ with $\rho = q_H + 1$ such that $f_1(1/K) \leq P(K) \leq f_2(1/K)$ for all $K < K_0$, with K_0 small enough.

(iii) If $q_H = \infty$, then

$$I(K) \sim \frac{1}{\sqrt{2T}}\left(\log\frac{1}{K}\right)\left(\log\frac{K}{P(K)}\right)^{-1/2} \quad \textit{as} \quad K \to 0. \tag{2.16}$$

The small strikes analogous of Proposition 2.2.2 reads as follows.

Proposition 2.2.4. *Assume F_H is continuous. The following holds:*

(a) Suppose that for a $\rho \geq 0$, $F_H(1/x) \in R_{-\rho}$. Then the asymptotic equivalence (2.15) *holds with index $q_H = \rho$.*

(b) Suppose that there exist positive constants α, β, $\gamma > 0$ and $x_0 > 0$ such that F_H satisfies

$$F_H(x) \leq \gamma e^{-\alpha\, x^{-\beta}} \quad \text{for all} \quad x < x_0. \tag{2.17}$$

Then the left-wing index $q_H = \infty$ and $I(K) \to 0$ as $K \to 0$.

Proof. Since F_H is continuous, the moment $E[H_T^{-q}]$, $q > 0$ can be expressed as

$$\mathbb{E}[H_T^{-q}] = q \int_0^\infty u^{q-1} F_H(1/u) du\,,$$

while the price of a put is given by

$$P(K) = \int_0^K F_H(u) du = \int_{1/K}^\infty u^{-2} F_H(1/u) du\,.$$

The results now follow from Theorem 2.2.3, proceeding in complete analogy with proof of Proposition 2.2.2. □

Similar to the large strikes case, part (a) of Proposition 2.2.4 can be reformulated in terms of the Laplace transform as a result of Karamata's Tauberian theorem. In fact, by Feller [58], XIII.5 Theorem 3, we have that for $\rho > 0$, the following holds

$$F_H(1/x) \in R_{-\rho} \quad \text{if and only if} \quad \mathscr{L}_H(x) \in R_{-\rho}, \tag{2.18}$$

and in this case $\mathscr{L}_H(x) \sim \Gamma(1+\rho) F_H(1/x)$ as $x \to \infty$. As for condition (2.17) in part (b), one may use a Tauberian result of the exponential type to verify the stronger requirement that $\log F_H(x) \sim -\alpha x^{-\beta}$. More precisely, from de Bruijn's Tauberian Theorem it follows that if $r \in (0,1)$ and $\beta > 0$ satisfy $\frac{1}{r} - \frac{1}{\beta} = 1$, and $\alpha\,, s > 0$, then

$$\lim_{x\to 0} x^\beta \log F_H(x) = -\alpha \quad \text{if and only if} \quad \lim_{x\to\infty} \frac{\log \mathscr{L}_H(x)}{x^r} = -s\,, \tag{2.19}$$

and in this case $(r\,s)^{1/r} = (\alpha\,\beta)^{1/\beta}$. See, e.g., Bingham et al. [20], Theorem 4.12.9.

2.3 Realized Variance Options in the SVJ-v model

In this section, we specialize the analysis carried out above, to the case of options written on the realized variance of an asset. Recall that the continuously sampled

realized variance, hereafter denoted by V_T, is defined as the annualized quadratic variation of the log-price process over the time interval $[0, T]$. More precisely, we set

$$V_T = \frac{1}{T}[X]_T \,, \tag{2.20}$$

where $X_t = \log S_t$ denotes the log-price and

$$[X]_T = \lim_{\Delta \to 0} \sum_{n=1}^{N} (X_{t_n} - X_{t_{n-1}})^2 \,,$$

where $\Delta = t_{i+1} - t_i$ is the step size of the partition $0 < t_1 < \cdots < t_N = T$.

In this work, we assume that the underlying price process evolves according to an affine stochastic volatility model known in the literature as the SVJ-v model. Specifically, we maintain the assumption of zero dividends and interest rates, and we model the log-price X and its instantaneous variance v via the following risk-neutral dynamics

$$\begin{aligned} dX_t &= -\tfrac{1}{2} v_t \, dt + \sqrt{v_t} dW_t \\ dv_t &= \lambda(\theta - v_t) dt + \sigma \sqrt{v_t} dB_t + dJ_t \end{aligned} \tag{2.21}$$

where λ, θ and σ are positive constants, the processes W and B are – possibly correlated – Brownian motions while J is an increasing and driftless Lévy process which is independent of (W, B). Thus, the unit-time Laplace transform $\mathscr{L}_J(u) = \mathbb{E}[e^{-uJ_1}]$, takes the form

$$\mathscr{L}_J(u) = e^{\kappa_J(u)} \quad \text{with} \quad \kappa_J(u) = \int_0^\infty (e^{-ux} - 1) \nu_J(dx), \quad u \geq 0 \,, \tag{2.22}$$

where the Lévy measure ν_J is a measure on the positive real line such that $\int_0^1 x \nu_J(dx) < \infty$. Finally, the parameters λ, θ and σ are non-negative constants.

The stochastic volatility model (2.21) generalizes the seminal Heston [77] model by augmenting the square root process describing v to allow for jumps. Furthermore, by setting $\theta = \sigma = 0$ in (2.21), we obtain the *non-Gaussian Ornstein-Uhlenbeck* (OU for short) model class proposed by Barndorff-Nielsen and Shepard [14]

$$v_t = e^{-\lambda t} v_0 + \int_0^t e^{-\lambda(t-s)} dJ_s \,, \tag{2.23}$$

where the instantaneous variance moves uniquely by jumps.

The name SVJ-v refers to the fact that in (2.21), jumps are allowed only at the variance level, in contrast to more general affine specifications such as the SVJJ model of Duffie et al. [53], where both v and X are affected by jumps. The main advantage of the SVJ-v framework is that the quadratic variation coincides with the integrated variance, and therefore the realized variance (2.20) is given by

$$V_T = \frac{1}{T}\int_0^T v_t dt.$$

In affine models, such a quantity is easy to handle as its Laplace transform is known in closed form. Duffie et al. [53] show that $\mathscr{L}_V(u,T) = \mathbb{E}[e^{-uV_T}]$ is given by

$$\mathscr{L}_V(u,T) = e^{\kappa_V(u,T)} \quad \text{with} \quad \kappa_V(u,T) = \alpha(u,T) + v_0\beta(u,T) + \delta(u,T)\,, \tag{2.24}$$

where the functions α, β and δ satisfy the ODEs

$$\frac{\partial}{\partial t}\alpha = \theta\lambda\beta \tag{2.25}$$

$$\frac{\partial}{\partial t}\beta = -\lambda\beta + \frac{1}{2}\sigma^2\beta^2 - \frac{u}{T}\,, \tag{2.26}$$

$$\frac{\partial}{\partial t}\delta = \kappa_J(-\beta)\,, \tag{2.27}$$

with initial conditions $\alpha(u,0) = \beta(u,0) = \delta(u,0) = 0$. For the full SVJ-v model with $\theta, \sigma > 0$, the explicit solutions read as follows

$$\alpha(u,t) = -\frac{2\lambda\theta}{\sigma^2}\log\left(\frac{\gamma(u)+\lambda+(\gamma(u)-\lambda)e^{-\gamma(u)t}}{2\gamma(u)}\right) - \frac{\lambda\theta}{\gamma(u)+\lambda}t \tag{2.28}$$

$$\beta(u,t) = -\frac{u}{T}\frac{2(1-e^{-\gamma(u)t})}{\gamma(u)+\lambda+(\gamma(u)-\lambda)e^{-\gamma(u)t}} \tag{2.29}$$

$$\delta(u,t) = \int_0^t \kappa_J(-\beta(u,s))ds\,, \tag{2.30}$$

where $\gamma(u) = \sqrt{\lambda^2 + 2\sigma^2\frac{u}{T}}$. In the OU specification (2.23), the realized variance V_T can be explicitly written as

$$V_T = v_0\epsilon(T) + \int_0^T \epsilon(T-t)dJ_t\,, \tag{2.31}$$

where

$$\epsilon(t) = \frac{1-e^{-\lambda t}}{\lambda T}\,, \tag{2.32}$$

and the expression for κ_V simplifies to

$$\kappa_V(u,T) = -u\,\epsilon(T)v_0 + \int_0^T \kappa_J(u\,\epsilon(t))dt\,. \tag{2.33}$$

Based on the explicit form of $\mathscr{L}_V$, the Tauberian theory allows for a comfortable analysis of the distributional properties of the realized variance. In particular, we are interested in analyzing how alternative selections of the jump law J_1 affect V_T and, in turn, the asymptotic behavior of the volatility curve $I(K)$ implied by realized variance options. Consistent with the notation adopted so far, we write F_J, F_V for the distribution functions of J_1, V_T, and $\overline{F}_J$, $\overline{F}_V$ for the corresponding tail functions.

We start with a preliminary lemma stating that moment finiteness and regularly varying tail are properties which J_1 passes on to V_T basically unchanged. The proof is based on a careful examination of the ODEs (2.28)–(2.30), and makes use of the Tauberian equivalence (2.12). Although quite simple, the derivation is somewhat lengthy and therefore the details are reported in the Appendix.

Lemma 1. *In the SVJ-v model* (2.21) *the following holds:*

(i) If $p \geq 0$, *then* $\mathbb{E}\,[J_1^p] < \infty$ *if and only if* $\mathbb{E}\big[V_T^p\big] < \infty$.

(ii) If $\overline{F}_J \in R_{-\rho}$ *with* $\rho > 0$ *non integer, then* $\overline{F}_V \in R_{-\rho}$. *In the OU subclass* (2.23), *the statement holds for arbitrary* $\rho > 0$.

Statement (i) shows that to guarantee $\mathbb{E}\,[V_T] < \infty$ and enable a meaningful analysis of options written on V_T, we need to assume

$$\mathbb{E}[J_1] < \infty \quad \text{or, equivalently,} \quad \int_0^\infty x\nu_J(dx) < \infty\,. \tag{2.34}$$

In addition, we see that denoting by

$$p_J = \sup\,\big\{p : \mathbb{E}[J_1^{p+1}] < \infty\big\}\,, \tag{2.35}$$

Lee's formula (2.3) at large strikes holds with index $p_V = p_J$. Proposition 2.3.1 below illustrates further how the tail properties of the jump distribution determine the behavior of the implied volatility $I(K)$ at large strikes.

Proposition 2.3.1. *In the SVJ-v model* (2.21) *the following holds:*

(a) *Suppose that* $\overline{F}_J \in R_{-\rho-1}$ *with* $\rho > 0$ *non integer. Then the large strikes asymptotic equivalence* (2.4) *holds with* $p_V = \rho$. *In the OU subclass* (2.23), *the statement holds for arbitrary* $\rho > 0$.

(b) *Suppose that* $\overline{F}_J$ *is exponentially dominated*

$$\overline{F}_J(x) \leq \gamma e^{-\alpha\, x} \quad \textit{for all} \quad x \geq x_0$$

with α, $\gamma > 0$ *and* x_0 *large enough. Then* $p_V = \infty$ *and* $I(K) \to 0$ *as* $K \to \infty$.

Proof. Statement (a) follows directly from Proposition 2.2.2-(a), and Lemma 1-(ii). As for statement (b), (2.13) implies that $\kappa_J(u_0) < \infty$ for a $u_0 < 0$. A simple inspection of (2.28) – (2.30) shows that there exists $u_1 < 0$ such that $\kappa_V(u_1) < \infty$, and the conclusion follows from Proposition 2.2.2-(b). □

Let us now examine the impact of the jump distribution on the implied volatility at small strikes. It turns out that in SVJ-v specifications which comprises a diffusion component, jumps have no effect on the asymptotic behaviour of the left wing of $I(K)$, which always vanishes to zero.

Proposition 2.3.2. *Consider the SVJ-v model* (2.21) *with* $\sigma > 0$. *Then, for any choice of jump distribution* J_1, *it holds that* $q_V = \infty$ *and* $I(K) \to 0$ *as* $K \to 0$.

Proof. Let $s = \sqrt{\frac{2}{T\sigma^2}}$. From (2.28), (2.29), we see that $\lim_{u\to\infty} \frac{\alpha(u,T)+\beta(u,T)}{u^{1/2}} = -s$. Furthermore, $\beta(u,t) \geq -s\, u^{1/2}$ for all $u\,, t \geq 0$ and from (2.30) it follows that

$$T\kappa_J(s\, u^{1/2}) \leq \delta(u,T) \leq 0 \quad \text{for all } u \geq 0\,.$$

Since $\frac{1-e^{-u^{1/2}sx}}{u^{1/2}} \leq \min(sx, 1)$, for all $u \geq 1$, we can use a dominated convergence argument to show that $\lim_{u\to\infty} \frac{\kappa_J(su^{1/2})}{u^{1/2}} = 0$, so that $\lim_{u\to\infty} \frac{\delta(u,T)}{u^{1/2}} = 0$. All in all, it holds that $\lim_{u\to\infty} \frac{\log \mathscr{L}_V(u)}{u^{1/2}} = -s$ and the result follows from de Bruijn's Tauberian equivalence (2.19), and Proposition 2.2.4-(b). □

To obtain a more flexible behavior of $I(K)$ at small strikes, we need to keep within the OU model subclass. However, from expression (2.31) we see that V_T is bounded from below by $v_0\epsilon(T)$, and therefore the asymptotic analysis as $K \to 0$ is meaningful only if $v_0 = 0$.

Proposition 2.3.3. *Consider the OU model* (2.23) *with* $v_0 = 0$*, and assume* F_J *is continuous. Then, the following holds:*

(a) Suppose that $F_J(1/x) \in R_{-\rho}$*, with* $\rho > 0$*. Then the asymptotic equivalence* (2.15) *holds with small strikes index* $q_V = \rho T$*.*

(b) Suppose that $\log F_J(x) \sim -\alpha x^{-\beta}$ *as* $x \to 0$*, with* $\alpha\,, \beta > 0$*. Then* $q_V = \infty$ *and* $I(K) \to 0$ *as* $K \to 0$*.*

Proof. Part (a). By Karamata's equivalence (2.18), it holds that $\mathscr{L}_J(x) = x^{-\rho}\ell(x)$, with $\ell \in R_0$. Also, recall a result from Korevaar [84], IV.2, stating that if $\ell \in R_0$ then for any $\delta > 0$, there are positive constants b and B such that

$$b\left(\frac{u+1}{v+1}\right)^{-\delta} \leq \frac{\ell(u)}{\ell(v)} \leq B\left(\frac{u+1}{v+1}\right)^{\delta} \qquad \text{whenever } 0 \leq v \leq u < \infty\,. \tag{2.36}$$

Then, from (2.33) we obtain that for a $\xi > 0$, the following holds

$$\lim_{x\to\infty} \frac{\mathscr{L}_V(\xi x)}{\mathscr{L}_V(x)} = \exp\int_0^T \log\left(\lim_{x\to\infty} \frac{\mathscr{L}_J\left(\xi\epsilon(t)x\right)}{\mathscr{L}_J\left(\epsilon(t)x\right)}\right) dt = \xi^{-\rho T}\,,$$

where, to interchange limit and integral, we have applied a dominated convergence argument based on (2.36). Therefore, $\mathscr{L}_V \in R_{-\rho T}$ and the statement follows from Proposition 2.2.4-(a). As for assertion (b), set r and s as in (2.19) and use (2.33) to obtain

$$\lim_{x\to\infty} \frac{\log \mathscr{L}_V(x)}{x^r} = \int_0^T \lim_{x\to\infty} \frac{\kappa_J(x\epsilon(t))}{x^r} dt = -s\int_0^T \epsilon(t)^r dt\,,$$

where, once again, we have used a dominated convergence argument based on the monotonicity of κ_J. The conclusion follows from Proposition 2.2.4-(b). □

2.4 Numerical Examples

In this section we consider a selection of positive distributions of the jumps J and we illustrate how such a choice impacts the associated realized variance smile $I(K)$ for a fixed maturity T. The numerical examples we provide are based on the OU subclass (2.23) with $v_0 = 0$, as this specification, in contrast to the full SVJ-v model, allows for both an upward sloping and a downward sloping behavior of the

left wing. For the unit-time jump distribution J_1, we consider the Gamma, the Inverse Gamma, and the Generalized Inverse Gaussian laws and we refer to the corresponding model specifications as the OU-Γ, OU-IΓ and OU-GIG models.

Recall that a Gamma distribution $\Gamma(\alpha, \beta)$ has density function f_Γ and Laplace transform $\mathscr{L}_\Gamma$ given by

$$f_\Gamma(x) = \frac{\beta^\alpha}{\Gamma(\alpha)} x^{\alpha-1} e^{-\beta x}\,,\ x \geq 0$$

$$\mathscr{L}_\Gamma(u) = \left(1 + \frac{u}{\beta}\right)^{-\alpha}\,,\ u \geq -\beta.$$

Since $0 \in \mathring{\mathscr{D}}_J$, Proposition 2.3.1–(b) predicts that in the OU-Γ model, the smile $I(K)$ is downward sloping to zero as $K \to \infty$. Also, we see that $\mathscr{L}_\Gamma$ is a regularly varying function of index $-\alpha$ at infinity. By Proposition 2.3.3–(a) we can conclude that $I(K) \to \infty$ as $K \to 0$, in accordance to the asymptotic equivalence (2.15) with index $q_V = \alpha T$.

In the OU-IΓ specification, we choose J_1 distributed according to an Inverse Gamma law I$\Gamma(\nu, \mu)$. The density function $f_{I\Gamma}$ and Laplace transform $\mathscr{L}_{I\Gamma}$ are given by

$$f_{I\Gamma}(x) = \frac{\mu^\nu}{\Gamma(\nu)} x^{-\nu-1} e^{-\mu/x}\,,\ x \geq 0$$

$$\mathscr{L}_{I\Gamma}(u) = \frac{2(\mu u)^{\nu/2}}{\Gamma(\nu)} K_\nu(\sqrt{4\mu u})\,,\ \ u \geq 0$$

where K_ν is the modified Bessel function of the second kind. Since $f_{I\Gamma} \in R_{-\nu-1}$, we see from (2.10) that the corresponding survival function $\overline{F}_{I\Gamma} \in R_{-\nu}$. Hence, Proposition 2.3.1–(a) shows that for large strikes, the volatility curve $I(K)$ implied by the OU-IΓ model follows the asymptotic equivalence (2.4) with $p_V = \nu - 1$. For the small strikes behavior, we can use the fact that for large arguments $K_\nu(z) \sim \sqrt{\frac{\pi}{2z}} e^{-z}$ (see Abramowitz and Stegun [4] p. 378), and show that $\lim_{u\to\infty} \frac{\log \mathscr{L}_{I\Gamma}(u)}{u^{1/2}} = -\sqrt{4\mu} < 0$. Therefore, Proposition 2.3.3–(b), combined with de Bruijn's Tauberian Theorem (2.19), implies that $I(K) \to 0$ as $K \to 0$.

Finally, we consider the OU-GIG specification, where the law of J_1 is given by a Generalized Inverse Gaussian distribution GIG(p, a, b) with density and Laplace transform given by

$$f_{GIG}(x) = \frac{(b/a)^p}{2K_p(ab)} x^{\lambda-1} e^{-\frac{1}{2}\left(a^2 x^{-1} + b^2 x\right)}\,,\ x \geq 0$$

$$\mathscr{L}_{GIG}(u) = \left(\frac{b^2}{b^2+2u}\right)^{p/2} \frac{K_p(\sqrt{a^2(b^2+2u)})}{K_p(ab)}\,, \quad u \geq -b^2/2.$$

As above, K_p denotes the modified Bessel function of the second kind and it is immediate to see that $\lim_{u\to\infty} \frac{\log \mathscr{L}_{GIG}(u)}{u^{\frac{1}{2}}} < 0$. Also, $0 \in \mathring{\mathscr{D}}_{GIG}$, and in virtue of Proposition 2.3.1–(b) and Proposition 2.3.3–(b) we can conclude that $I(K) \to 0$ both at small and at large strikes.

In all the model specifications introduced above, the realized variance call price $C(K)$ and the associated implied volatility $I(K)$ can be computed by means of Fourier transform methods. In fact, Carr et al. [34] show that the Laplace transform $\mathscr{L}_C$ of the call price $C(K)$ can be expressed as

$$\mathscr{L}_C(u) = \int_0^\infty e^{-uK} C(K) dK = \frac{\mathscr{L}_V(u) - 1}{u^2} + \frac{\mathbb{E}[V_T]}{u}\,. \tag{2.37}$$

Applying a Laplace inversion algorithm to (2.37) allows us to obtain prices of options on realized variance for a sequence of variance strikes. Figure 2.1 plots implied volatilities against variance strikes for the three selected models. We consider a maturity of 3 months and we set the parameters of the different jump distributions so that the mean and the variance are the same across the alternative specifications. In particular, we take $\alpha = 18$ and $\beta = 22.8$ in the Gamma case, $\nu = 20$ and $\mu = 15$ for the Inverse-Gamma and $p = -0.5$, $a = 3.7697$ and $b = 4.7749$ for the GIG distribution. The value of λ is the same in all cases and it is equal to 8. The plots confirm that in the OU-Γ case, the implied volatility of variance smile is downward-sloping, clearly at odds with the upward-sloping smile observed in variance markets. In contrast, the OU-IΓ model implies an upward-sloping smile and finally, in the OU-GIG specification, we observe a frown.

To further support these observations, we investigate the sensitivity of the implied volatility of variance with respect to the parameters of the jump distribution in Figures 2.2-2.4. To disclose the ceteris paribus effects on the implied volatility, we change one parameter while keeping any remaining parameters fixed. For each parameter set, we plot the implied volatility curve against variance strikes. For the selected jump distributions, we make the common observation that while altering the parameters of the distribution changes the levels of implied volatility and the wideness of the smile in variance strikes, the shapes of the implied volatility curves persist across different parameter values.

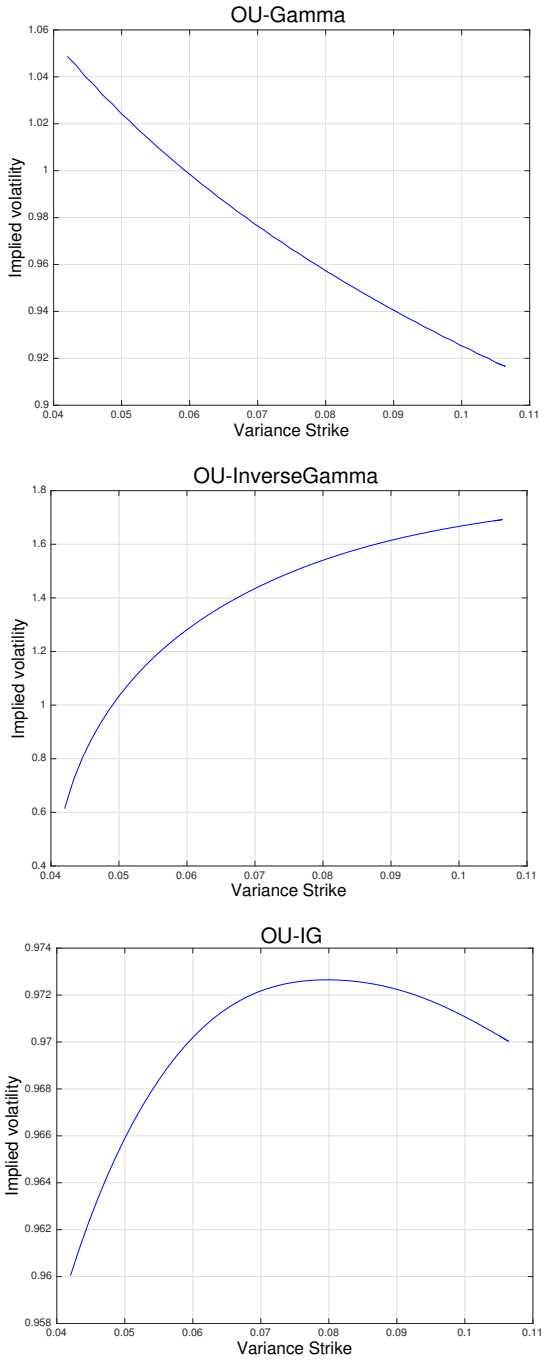

Figure 2.1: *Implied volatilities of variance for the OU-Gamma with parameters* $\alpha = 18$, $\beta = 22.8$ *(top), OU-InverseGamma with* $\nu = 20$, $\mu = 15$ *(middle), and OU-IG with* $a = 3.7697$, $b = 4.7749$ *(bottom). In all cases we take* $\lambda = 8$, *and* $v_0 = 0$ *and we obtain the parameters of the different jump specifications by matching the mean and the variance.*

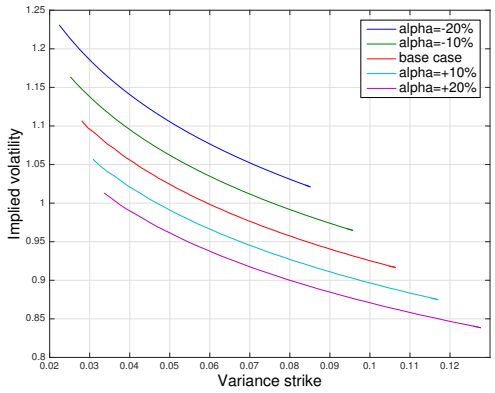

(a) Changes in α

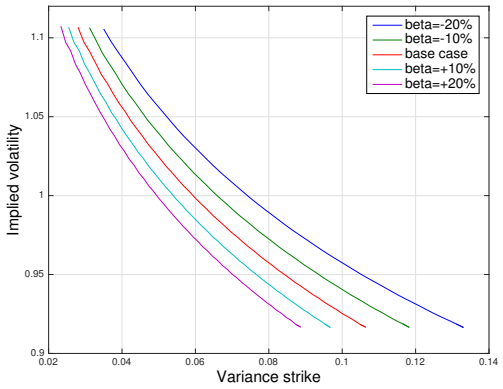

(b) Changes in β

Figure 2.2: *OU-Gamma parameter sensitivities. Base case parameters:* $\alpha = 18$, $\beta = 22.8$, $\lambda = 8$, *and* $v_0 = 0$.

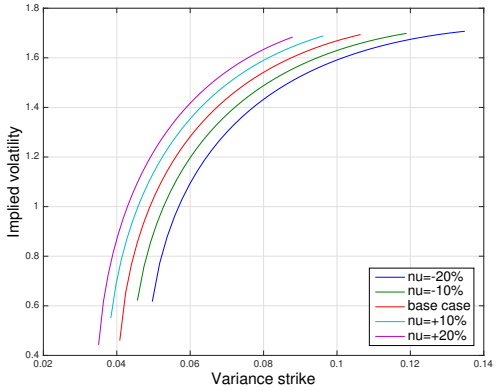

(a) Changes in ν

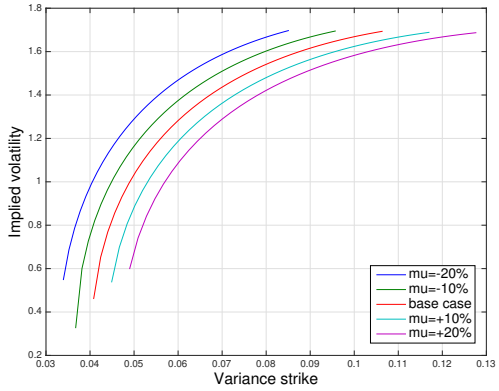

(b) Changes in μ

Figure 2.3: *OU-Inverse Gamma parameter sensitivities. Base case parameters:* $\nu = 20$, $\mu = 15$, $\lambda = 8$, *and* $v_0 = 0$.

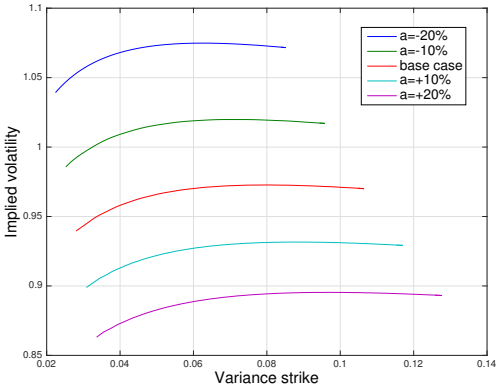

(a) Changes in a

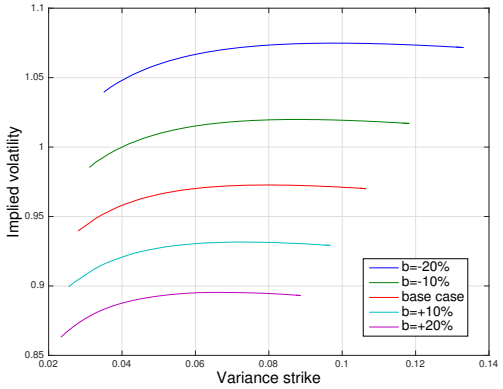

(b) Changes in b

Figure 2.4: *OU-IG parameter sensitivities. Base case parameters:* $a = 3.7697$, $b = 4.7749$, $\lambda = 12$, *and* $v_0 = 0$.

2.5 VIX options

Since 2006 options have traded on CBOE's VIX index and constitute today a relatively liquid market of variance derivatives. The VIX index tracks the price of a portfolio of options on the S&P 500 index (SPX index). As shown by Carr and Wu [38], VIX squared approximates the conditional risk-neutral expectation of the realized variance of SPX over the next 30 calendar days. As such, it can be interpreted as the fair swap rate of a variance swap - an OTC contract in which one exchanges payments of realized variance against receiving a fixed variance swap rate.

It is immediate to show that under the general SVJ-v dynamics (2.21), the VIX squared – the price of future realized variance – is simply given by an affine transformation of the instantaneous variance

$$\mathrm{VIX}_T^2 = \mathbb{E}_T\left[\tfrac{1}{\tau}\int_T^{T+\tau} v_t dt\right] = a v_T + b \tag{2.38}$$

where

$$\begin{aligned} a &= \tfrac{1}{\lambda\tau}(1-e^{-\lambda\tau}), \\ b &= (\tfrac{\mathbb{E}[J_1]}{\lambda}+\theta)(1-a) \end{aligned} \tag{2.39}$$

and $\tau = 30/365$.

Extending the previous analysis of realized variance options, we now examine the impact of the jump-distribution J on the price of VIX options, that is options with payoff

$$(F_{VIX}(T,T)-K)_+$$

where $F_{VIX}(t,T) = \mathbb{E}_t[VIX_T]$ indicates the VIX future price at time t. Using the notation of Section 2.2 and the fact that $F_{VIX}(T,T) = VIX_T$ we are interested in the asymptotic behavior of the volatility curve implied by options with

$$H_T = \mathrm{VIX}_T = \sqrt{a v_T + b}.$$

We see from (2.39) that in the SVJ-v framework the VIX_T is bounded away from zero by the quantity b, for any parameter choice and any maturity T. Thus, we only consider the volatility curve at large strikes $K \to \infty$, as $I(K)$ is not defined for $K \to 0$.

Also, recall that the Laplace transform of the instantaneous variance $\mathscr{L}_v(u,T) = \mathbb{E}[e^{-uv_T}]$ is given by

$$\mathscr{L}_v(u,T) = \exp\left(\alpha(u,T) + v_0\beta(u,T) + \delta(u,T)\right) , \tag{2.40}$$

where the functions α, β and δ satisfy the ODEs

$$\frac{\partial}{\partial t}\alpha = \theta\lambda\beta \tag{2.41}$$

$$\frac{\partial}{\partial t}\beta = -\lambda\beta + \frac{1}{2}\sigma^2\beta^2 , \tag{2.42}$$

$$\frac{\partial}{\partial t}\delta = \kappa_J(-\beta) , \tag{2.43}$$

with initial conditions $\alpha(u,0) = \delta(u,0) = 0$ and $\beta(u,0) = -u$. Similar to the realized variance case, a detailed analysis of the ODEs (2.41)–(2.43) reveals the close connection between the tail of the jump distribution J_1 and the tail of the instantaneous variance v_T. The main results are reported in Lemma 2 below, while the derivations are omitted, as they follow closely the proof of Lemma 1.

Lemma 2. *In the SVJ-v model* (2.21) *the following holds:*

(i) If $p \geq 0$, then $\mathbb{E}[J_1^p] < \infty$ if and only if $\mathbb{E}[v_T^p] < \infty$.

(ii) If $\overline{F}_J \in R_{-\rho}$ with $\rho > 0$ non integer, then $\overline{F}_v \in R_{-\rho}$. In the OU subclass (2.23)*, the statement holds for arbitrary $\rho > 0$.*

We see immediately that in order to price VIX options in the SVJ-v model, we need to assume that $\mathbb{E}\left[J_1^{1/2}\right] < \infty$. Furthermore, the large strikes Lee's formula (2.3) holds with index

$$p_{\text{VIX}} = \sup\left\{p : \mathbb{E}[J_1^{\frac{p+1}{2}}] < \infty\right\} .$$

The analogous of Proposition 2.3.1 for VIX smiles at large strikes reads as follows.

Proposition 2.5.1. *In the SVJ-v model* (2.21) *the following holds:*

(a) Suppose that $\overline{F}_J \in R_{-\rho}$ with $\rho > 1/2$ non integer. Then the large strikes asymptotic equivalence (2.4) *holds with $p_{VIX} = 2\rho - 1$. In the OU subclass* (2.23)*, the statement holds for arbitrary $\rho > 1/2$.*

(b) Suppose that $\overline{F}_J$ is exponentially dominated. Then $p_{VIX} = \infty$ and $I(K) \to 0$ as $K \to \infty$.

Proof. From (2.38), we see that

$$\overline{F}_{VIX}(x) = \overline{F}_v\left(\frac{x^2 - b}{a}\right).$$

Elementary properties of regularly varying functions show that if $\overline{F}_v \in R_{-\rho}$ then $\overline{F}_{VIX} \in R_{-2\rho}$. Therefore part (a) follows immediately from Lemma 2 and Proposition 2.2.2, (a). As for part (b), inspection of (2.41)–(2.43) shows that $\overline{F}_J$ is exponentially dominated if and only if $\overline{F}_v$ is exponentially dominated, which in turns implies that $\overline{F}_{VIX}$ is exponentially dominated. The conclusion follows from Proposition 2.2.2, (b). □

We conclude this section by providing some numerical examples illustrating the behavior of VIX smiles implied by different jump distributions. We consider the full SVJ-v specification obtained by augmenting the Heston model with compound Poisson jumps, i.e.

$$J_t = \sum_{i=1}^{N(t)} Z_i, \quad Z_i \sim i.i.d.\ Z\,, \tag{2.44}$$

where $N(t)$ is a Poisson process with intensity ℓ while Z denotes the positive jump-size distribution. As mentioned in the introduction, this variance process equipped with exponentially distributed jumps has been used, e.g. by Sepp [101], and Lian and Zhu [90], in the attempt to capture the observed upward-sloping skew of VIX options. Here, besides this specification and the purely diffusive Heston model, we also consider the case of inverse gamma jumps $Z \sim \text{I}\Gamma(\nu, \mu)$. Figure 2.5 plots the implied volatilities against strikes in the three different cases. We consider 3-months options and we use Heston parameters from Bakshi et al. [11] $v_0 = 0.0348$, $\lambda = 1.15$, $\theta = 0.0348$, $\sigma = 0.39$, obtained by calibration to out-of-the-money options on the $S\&P500$ index. One observes that, when using parameters fitted to equity option quotes, the VIX implied volatility skew is downward-sloping. Next, we augment the Heston model with exponential jump sizes $Z \sim \Gamma(1, \beta)$ with mean $1/\beta = 0.3429$. The intensity is set to $\ell = 1.5$. Once again, we obtain a downward-sloping skew.

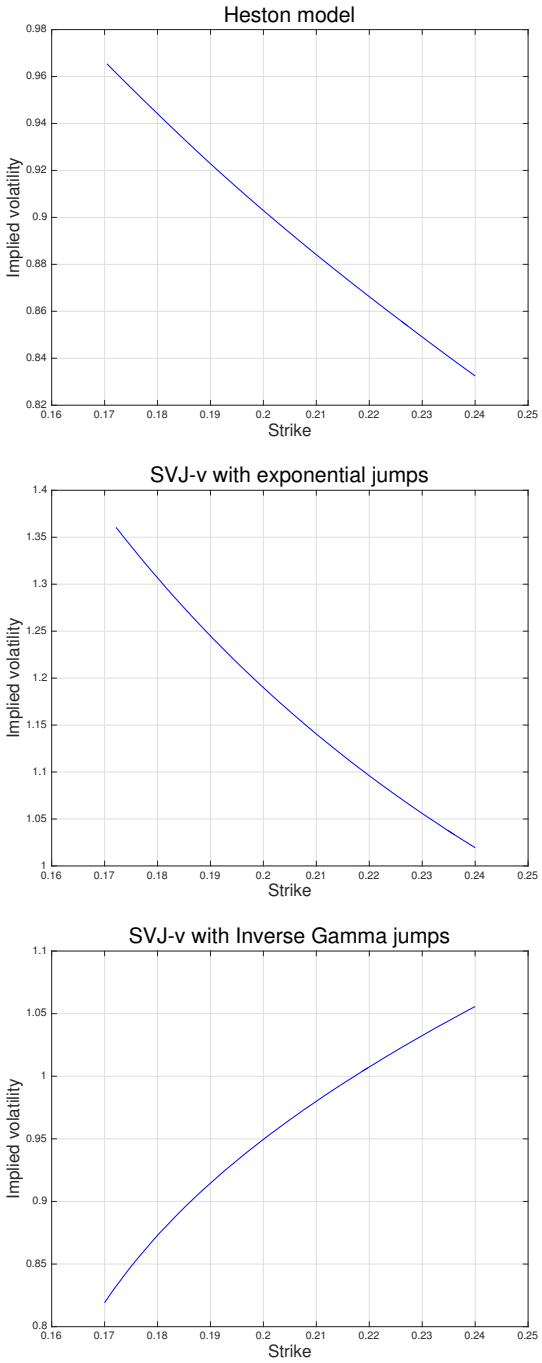

Figure 2.5: *Implied volatilities of VIX options for: the Heston model with* $v_0 = 0.0348$, $\lambda = 1.15$, $\theta = 0.0348$, $\sigma = 0.39$ *(top), the SVJ-v model with exponential jumps with* $\ell = 1.5$ *and* $1/\beta = 0.3429$ *(middle) and the SVJ-v model with Inverse Gamma jumps with* $\ell = 1.5$, $\nu = 4.5$ *and* $\mu = 1.2$ *(bottom). The jump-parameters are chosen so that* $\mathbb{E}[Z]$ *is the same in both jump specifications.*

However, if we maintain the same diffusive component, the same intensity level ℓ, but we substitute the jump size with an Inverse Gamma law $Z \sim \text{I}\Gamma(\nu, \mu)$, we observe a dramatic change in the shape of the VIX implied volatility. Specifically, this leads to an upward-sloping skew as shown in Figure 2.5. The Inverse Gamma jump parameters are $\nu = 4.5$ and $\mu = 1.2$ and they have been obtained so that the first moment of Z is the same as in the exponential case.

2.6 Conclusions

We have considered options on realized variance and VIX options in the SVJ-v model, a tractable affine stochastic volatility model that generalizes the Heston [77] model by augmenting it with jumps in the instantaneous variance. The model allowed us to isolate the unique impact of the jump distribution and we have shown that this has a profound effect on the characteristics and shape of the implied volatility of variance smile. We provided sufficient conditions for the asymptotic behavior of the implied volatility of variance for small and large strikes. In particular, we showed that by selecting alternative jump distributions, one obtains fundamentally different shapes of the implied volatility smile. Some distributions of jumps predict implied volatilities of variance that are clearly at odds with the upward-sloping volatility skew observed in variance markets.

2.7 Appendix

Proof of Lemma 1 part (i) We start by recalling a few basic facts relating the (possibly infinite) moments $\mathbb{E}[H^p]$, $p > 0$ of a non negative random variable H to its Laplace transform $\mathscr{L}_H$. Fix $p > 0$, $n \in \mathbb{Z}^+$ and r so that $n = p + r$ with $0 < r < 1$. Then the moments can be expressed as follows

$$\mathbb{E}[H^n] = (-1)^n \mathscr{L}_H^{(n)}(0+) \tag{2.45}$$

and

$$\mathbb{E}[H^p] = \frac{(-1)^n}{\Gamma(r)} \int_0^\infty u^{r-1} \mathscr{L}_H^{(n)}(u) du \,,$$

where we have employed the usual notation $f^{(n)}(u) = \frac{d^n}{du^n} f$. In particular, it holds that

$$\mathbb{E}[H^p] < \infty \iff (-1)^n \int_0^{u_0} u^{r-1} \mathscr{L}_H^{(n)}(u) du < +\infty \tag{2.46}$$

for an arbitrary $u_0 > 0$. Finally, recall that the n-derivative $\mathscr{L}_H^{(n)}$ can be expressed in terms of Bell's polynomials $B_{n,k}(x_1, x_2, \dots, x_{n-k+1})$ as follows

$$\mathscr{L}_H^{(n)} = \mathscr{L}_H \cdot \sum_{k=1}^{n} B_{n,k}\left(\kappa_H^{(1)}, \kappa_H^{(2)}, \dots, \kappa_H^{(n-k+1)}\right), \tag{2.47}$$

where $\kappa_H(u) = \log \mathscr{L}_H(u)$, and

$$B_{n,k}(x_1, x_2, \dots) = \sum_{\substack{j_1+j_2+\cdots=k \\ j_1+2j_2+\cdots=n}} \frac{n!}{j_1! j_2! \cdots} \left(\frac{x_1}{1!}\right)^{j_1} \left(\frac{x_2}{2!}\right)^{j_2} \cdots . \tag{2.48}$$

Notice that, $B_{n,1}(x_1, x_2, \dots) = x_n$ and $B_{n,n}(x_1, x_2, \dots) = x_1^n$, and if $(-1)^n \kappa_H^{(n)} \geq 0$ for any $n \geq 1$, then also

$$(-1)^n B_{n,k}\left(\kappa_H^{(1)}, \kappa_H^{(2)} \dots\right) \geq 0, \qquad \text{for all } 1 \leq k \leq n. \tag{2.49}$$

Consider now the unit time law J_1 of the jump process. Differentiating expression (2.22) we obtain

$$(-1)^n \kappa_J^{(n)}(u) = \int_0^\infty x^n e^{-ux} \nu_J(dx),$$

for any $n \geq 1$. So, from (2.45), (2.47), (2.49) it follows that

$$\mathbb{E}[J_1^n] < \infty \iff \int_0^\infty x^n \nu_J(dx) < \infty \tag{2.50}$$

and, for a non integer $p > 0$,

$$\begin{aligned} \mathbb{E}[J_1^p] < \infty &\iff (-1)^n \int_0^{u_0} u^{r-1} \kappa_J^{(n)}(u) du < \infty, \\ &\iff \int_0^\infty x^{n-r} \gamma(x u_0; r) \nu_J(dx) < \infty, \end{aligned} \tag{2.51}$$

for a $u_0 > 0$, where $\gamma(x; r)$ denotes the incomplete Gamma function $\gamma(x; r) = \int_0^x q^{r-1} e^{-q} dq$. We now apply similar arguments to moments of the integrated variance V_T. First differentiate expressions (2.24) and (2.25)–(2.27) to obtain that

$$\kappa_V^{(n)}(u, T) = \alpha^{(n)}(u, T) + v_0 \beta^{(n)}(u, T) + \delta^{(n)}(u, T), \qquad q > 0, \tag{2.52}$$

where $\beta^{(1)}, \beta^{(2)} \dots$ solve the ODEs

$$\frac{\partial}{\partial t}\beta^{(1)} = -\lambda\beta^{(1)} + \sigma^2\beta\beta^{(1)} - \frac{1}{T}\,, \tag{2.53}$$

$$\frac{\partial}{\partial t}\beta^{(n)} = -\lambda\beta^{(n)} + \frac{1}{2}\sigma^2\sum_{i=0}^{n}\binom{n}{i}\beta^{(i)}\beta^{(n-i)} \qquad n \geq 2\,, \tag{2.54}$$

with initial condition $\beta^{(1)}(u,0) = \beta^{(2)}(u,0) = \cdots = 0$, while $\alpha^{(n)}, \delta^{(n)}$ solve

$$\frac{\partial}{\partial t}\alpha^{(n)} = \theta\lambda\beta^{(n)} \tag{2.55}$$

$$\frac{\partial}{\partial t}\delta^{(n)} = \frac{\partial^n}{\partial u^n}\left(\kappa_J(-\beta)\right)\,, \tag{2.56}$$

with $\alpha^{(n)}(u,0) = \delta^{(n)}(u,0) = 0$ for all $n \geq 1$. Since $\beta \leq 0$, from (2.53)–(2.54) it follows that $(-1)^n\beta^{(n)} \geq 0$ and $(-1)^n\alpha^{(n)} \geq 0$ for any $n \geq 1$. As for $\delta^{(n)}$, set

$$L(u,t,x) = e^{\beta(u,t)x}$$

and integrate (2.56) to obtain

$$\begin{aligned}\delta^{(n)}(u,T) &= \int_0^T\int_0^\infty L^{(n)}(u,t,x)\nu_J(dx)dt \\ &= \sum_{k=1}^{n}\int_0^T\int_0^\infty x^k L(u,t,x)B_{n,k}\left(\beta^{(1)}(u,t)\,,\beta^{(2)}(u,t)\dots\right)\nu_J(dx)dt\,,\end{aligned} \tag{2.57}$$

where, similar to (2.47), we have expressed the n-derivative $L^{(n)}$ in terms of Bell's polynomials. Since $(-1)^n\beta^{(n)} \geq 0$ for all $k \geq 1$, observation (2.49) implies that $(-1)^nL^{(n)}$, $(-1)^n\delta^{(n)}$, and $(-1)^n\kappa_V^{(n)}$ are all non negative functions. In view of (2.45), (2.47), we obtain that

$$\mathbb{E}\big[V_T^n\big] < \infty \iff (-1)^n\kappa_V^{(n)}(0+,T) < \infty \iff (-1)^n\delta^{(n)}(0+,T) < \infty\,,$$

where the last equivalence follows from observing, e.g., from (2.28)–(2.29), that both $\alpha(u,T)$ and $\beta(u,T)$ are finite and infinitely differentiable in an open neighborhood of $u = 0$. Expression (2.57) shows that

$$(-1)^n\delta^{(n)}(0+,T) = \sum_{k=1}^{n}\int_0^\infty x^k\nu_J(dx)\cdot\int_0^T(-1)^nB_{n,k}\left(\beta^{(1)}(0,t)\,,\beta^{(2)}(0,t)\dots\right)dt,$$

and we see that for the case of n integer, statement (i) follows from (2.50).

Consider now $\mathbb{E}\big[V_T^p\big]$ for non-integer p. Based on similar arguments as above, the equivalence (2.46) shows that

$$\begin{aligned}\mathbb{E}\big[V_T^p\big] < \infty \iff (-1)^n \int_0^{u_0} u^{r-1} \kappa_V^{(n)}(u,T) du < \infty \\ \iff (-1)^n \int_0^{u_0} u^{r-1} \delta^{(n)}(u,T) du < \infty \,. \end{aligned} \tag{2.58}$$

Next, a simple inspection of the ODEs (2.26), (2.53), and (2.54) shows that for all $(u,t) \in \mathbb{R}_+^2$, the functions $\beta, \beta^{(1)}, \dots, \beta^{(n)}$ satisfy the following bounds

$$-u\,\epsilon(t) \leq \qquad \beta(u,t) \qquad \leq -u\left(1 - \frac{\sigma^2}{2\lambda^2 T} u\right) \epsilon(t)\,, \tag{2.59}$$

$$\left(1 - \frac{\sigma^2}{\lambda^2 T} u\right) \epsilon(t) \leq \quad (-1)\beta^{(1)}(u,t) \quad \leq \epsilon(t)\,, \tag{2.60}$$

$$0 \leq \quad (-1)^n \beta^{(n)}(u,t) \quad \leq b\,, \qquad \text{for all } n \geq 1\,, \tag{2.61}$$

where $\epsilon(t)$ is the function given in (2.32), and $b > 0$ is a large enough constant. In particular, the upper bounds in (2.61) imply that we can find a $\tilde{b} > 0$ large enough such that

$$(-1)^n B_{n,k}\left(\beta^{(1)}(u,t)\,, \beta^{(2)}(u,t)\,, \dots\right) \leq \tilde{b}\,, \qquad \forall (u,t) \in \mathbb{R}_+^2\,,$$

for all $1 \leq k \leq n$. Furthermore, choosing $u_0 < \frac{2\lambda^2 T}{\sigma^2}$ and setting $b_0 = u_0 \frac{\epsilon(T)}{T}$, from (2.59) it follows that

$$\beta(u,t) \leq -u b_0 t \qquad \forall (u,t) \in [0,u_0] \times [0,T]\,.$$

Substituting this estimates in (2.57) we obtain that

$$\begin{aligned}(-1)^n \int_0^{u_0} u^{r-1} \delta^{(n)}(u,T) du &\leq \tilde{b} \sum_{k=1}^n \int_0^\infty \int_0^T \int_0^{u_0} x^k u^{r-1} e^{-x b_0 t u} \, du \; dt \; \nu_J(dx) \\ &= \frac{\tilde{b}}{b_0^r} \sum_{k=1}^n \int_0^\infty \int_0^T \int_0^{x b_0 t u_0} x^{k-r} t^{-r} \zeta^{r-1} e^{-\zeta} d\zeta \, dt \, \nu_J(dx) \\ &\leq \frac{\tilde{b}}{b_0^r} \sum_{k=1}^n \left(\int_0^T t^{-r} dt\right) \int_0^\infty x^{k-r} \int_0^{x b_0 T u_0} \zeta^{r-1} e^{-\zeta} d\zeta \, \nu_J(dx) \\ &= \frac{\tilde{b} T^{1-r}}{(1-r) b_0^r} \sum_{k=1}^n \int_0^\infty x^{k-r} \gamma(x b_0 T u_0; r) \, \nu_J(dx)\,, \end{aligned}$$

and in view of (2.51), (2.58) we can conclude that $\mathbb{E}[J_1^p] < \infty$ implies $\mathbb{E}\big[V_T^p\big] < \infty$. For the converse implication, notice that (2.59) implies

$$\beta(u,t) \geq -\frac{u}{\lambda T} \qquad \forall (u,t) \in \mathbb{R}_+^2\,,$$

choose $u_0 < \frac{\lambda^2 T}{\sigma^2}$ and set $a_0 = u_0 \frac{\epsilon(T)}{T}$, so (2.60) implies

$$(-1)\beta^{(1)}(u,t) \geq a_0 t \qquad \forall (u,t) \in [0,u_0] \times [0,T]\,.$$

Substituting these estimate in (2.57) we obtain

$$\begin{aligned}(-1)^n \int_0^{u_0} u^{r-1}\delta^{(n)}(u,T)du &\geq a_0^n \int_0^\infty \int_0^T \int_0^{u_0} x^n t^n u^{r-1} e^{-xu/\lambda T}\, du\; dt\; \nu_J(dx) \\ &= \frac{a_0^n}{\lambda^r}\frac{T^{n+1-r}}{n+1}\int_0^\infty \int_0^{xu_0/T\lambda} x^{n-r}\zeta^{r-1}e^{-\zeta} d\zeta\, \nu_J(dx) \\ &= \frac{a_0^n}{\lambda^r}\frac{T^{n+1-r}}{n+1}\int_0^\infty x^{n-r}\gamma(xu_0/T\lambda; r)\, \nu_J(dx)\,,\end{aligned}$$

and from (2.51)–(2.58) we see that $\mathbb{E}\big[V_T^p\big] < \infty$ implies $\mathbb{E}[J_1^p] < \infty$, which concludes the proof of part (i).

Proof of Lemma 1 part (ii) We start by proving the statement for the OU subclass (2.23). First, recall that for a positive and infinitely divisible distribution H with Lévy measure ν_H it holds that

$$\overline{F}_H(x) \in R_{-\rho} \quad \text{if and only if} \quad \nu_H(x,\infty) \in R_{-\rho} \tag{2.62}$$

and in this case $\overline{F}_H(x) \sim \nu_H(x,\infty)$. See, e.g., Remark 25.14 in Sato [99]. Next, from (2.33) we see that

$$\begin{aligned}\kappa_V(u,T) &= -u\epsilon(T)v_0 + \int_0^T \int_0^\infty \big(e^{-u\epsilon(t)x} - 1\big)\, \nu_J(dx)\, dt \\ &= -u\epsilon(T)v_0 + \int_0^\infty \big(e^{-ux} - 1\big)\, \nu_V(dx)\,,\end{aligned}$$

where ν_V is the measure defined by

$$\nu_V(x,\infty) = \int_0^T \nu_J(x/\epsilon(t),\infty)dt\,, \qquad \text{for } x > 0\,. \tag{2.63}$$

Thus, the distribution of V_T is infinitely divisible with Lévy measure ν_V. In view of (2.62), we proceed to show that $\nu_J(x,\infty) \in R_{-\rho}$ implies $\nu_V(x,\infty) \in R_{-\rho}$. In (2.63), use (2.2) and apply the change of variable $z := x/\epsilon(t)$ in (2.63), to show that for $\xi > 0$, $\nu_V(\xi x,\infty)$ takes the form

$$\nu_V(\xi x,\infty) = \xi^{-\rho} x T \int_{x/\epsilon(T)}^{\infty} \ell(\xi z) \frac{z^{-\rho-1}}{z - \lambda T x} dz.$$

Since $\ell(\xi z)/\ell(z) \to 1$ as $z \to \infty$, for a given $\varepsilon > 0$ we can find z_* such that

$$(1-\varepsilon)\frac{z^{-\rho-1}}{z-\lambda T x}\ell(z) \;\le\; \frac{z^{-\rho-1}}{z-\lambda T x}\ell(\xi z) \;\le\; (1+\varepsilon)\frac{z^{-\rho-1}}{z-\lambda T x}\ell(z)$$

holds for all $z \ge x/\epsilon(T) \ge z_*$. So, integrating the chain of inequalities above, we see that

$$(1-\varepsilon)\xi^{-\rho}\nu_V(x,\infty) \;\le\; \nu_V(\xi x,\infty) \;\le\; (1+\varepsilon)\xi^{-\rho-1}\nu_V(x,\infty)$$

for any $x \ge x_* = z_*\epsilon(T)$, and we can conclude that $\nu_V(\xi x,\infty)/\nu_V(x,\infty) \to \xi^{-\rho}$ as $x \to \infty$.

Consider now the full SVJ-v specification (2.21) and assume $\overline{F}_J \in R_{-\rho}$ for a non integer $\rho > 0$. In view of the Tauberian equivalence (2.12), we aim to show that

$$\frac{\mathscr{L}_V^{(n)}(\xi u, T)}{\mathscr{L}_V^{(n)}(u, T)} \to \xi^{-r} \quad \text{as} \quad u \to 0\,, \tag{2.64}$$

for all $\xi > 0$, where $n \in \mathbb{Z}_+$, $0 < r < 1$ and $n = \rho + r$. Notice that (2.9) implies that $\int_0^\infty x^k \nu_J(dx) < \infty$ for $k = 1, \ldots, n-1$. Thus, using (2.47) and expressions (2.52), (2.57), we can represent $(-1)^n \mathscr{L}_V^{(n)}$ as follows

$$(-1)^n \mathscr{L}_V^{(n)}(u,T) = \mathscr{L}_V(u,T)\,\mathscr{G}_V(u,T) + \ell_V(u,T) \tag{2.65}$$

where

$$\mathscr{G}_V(u,T) = \int_0^T \int_0^\infty x^n \left(-\beta^{(1)}(u,t)\right)^n e^{x\beta(u,t)} \nu_J(dx)dt\,, \tag{2.66}$$

while ℓ_V is such that $\ell_V(0+,T) < \infty$. Therefore, (2.64) is equivalent to

$$\frac{\mathscr{G}_V(\xi u, T)}{\mathscr{G}_V(u, T)} \to \xi^{-r} \quad \text{as} \quad u \to 0\,. \tag{2.67}$$

To show the above, fix $\xi > 0$, consider an arbitrary $0 < \varepsilon < 1$, and choose $u_\varepsilon < \min(1, \xi^{-1}) \frac{\sigma^2}{\lambda^2 T} \varepsilon$. Then (2.59), (2.60) imply that, for all $u \le u_\varepsilon$, the following holds

$$\begin{aligned}(1-\varepsilon)\,\mathscr{G}_{\mathrm{OU}}(u,T) \;&\le\; \mathscr{G}_V(u,T) \;\le\; \mathscr{G}_{\mathrm{OU}}\left(u(1-\varepsilon),T\right)\\ (1-\varepsilon)\,\mathscr{G}_{\mathrm{OU}}(\xi u,T) \;&\le\; \mathscr{G}_V(\xi u,T) \;\le\; \mathscr{G}_{\mathrm{OU}}\left(\xi u(1-\varepsilon),T\right)\end{aligned}$$

where

$$\mathscr{G}_{\mathrm{OU}}(u,T) = \int_0^T \int_0^\infty x^n \epsilon(t)^n e^{-u\epsilon(t)x} \nu_J(dx)dt\,.$$

Notice that $\mathscr{G}_{\mathrm{OU}}$ corresponds to $\mathscr{G}_V$ defined in (2.65)–(2.66) when V_T is specified in the OU model. Therefore, $\mathscr{G}_{\mathrm{OU}}$ satisfies (2.67) for any $\xi > 0$, implying that

$$(1-\varepsilon)\,\xi^{-r} \le \lim_{u\to 0} \frac{\mathscr{G}_V(\xi u,T)}{\mathscr{G}_V(u,T)} \le \frac{1}{(1-\varepsilon)^{r+1}}\,\xi^{-r}\,.$$

Since ε is arbitrary, we see that $\mathscr{G}_V$ satisfies (2.67), which concludes the proof of part (ii).

Chapter 3

Pricing Realized Variance Options using Laplace transforms: a comparison of inversion methods

Pricing Realized Variance Options using Laplace transforms: a comparison of inversion methods

Camilla Pisani
Dept. of Economics and Business Economics, Aarhus University

Abstract

We provide a description of different algorithms for the inversion of Laplace transforms and we analyze how they perform when applied to the computation of prices of realized variance options. The model we consider is a generalization of the Heston model where the dynamics of the instantaneous variance are augmented with cPp jumps, the jump size follows an Inverse Gamma law. Under this framework, an explicit expression of the Laplace transform of the realized variance is available and therefore Laplace inversion techniques can be easily applied.

However, we show that when using a formulation of the Laplace transform which leads to discontinuities, wrong option prices may be obtained. Hence, attention must be paid before applying this pricing technique.

3.1 Introduction

Numerical inversion of Laplace transforms (see Bellman and Roth [16] for an overview of Laplace transforms and their properties) appears in various fields other than finance such as e.g., probability, physics, queueing theory and control engineering. Due to numerical errors stemming in part from discontinuities in the Laplace function or its derivatives, the numerical computation of the inverse of a Laplace transform is not an easy task. This problem, described by Kendall [83] as

the *"Laplace curtain obscuring the understanding of system behaviour"*, has been addressed by several authors, among others Epstein and Schotland [54] and Davis and Martin [48].

The purpose of this paper is to provide a review of some Laplace inversion algorithms and show numerical issues that might appear when these algorithms are used for pricing of call options on the realized variance of an asset.

Realized variance options and in general, volatility derivatives such as VIX options have recently gained great popularity. It is therefore important to find efficient methods for their pricing. Classical Monte Carlo methods appear to be quite easy to implement and reliable enough, as shown by the fact that they are currently spread among researchers and practitioners. However, they can be quite time consuming. This is why we need to look for alternative pricing methods. The starting point of our analysis will be the formula recently proposed in Carr et al. [34], expressing the Laplace transform of a call function on the realized variance V_T in terms of the Laplace transform of the realized variance itself:

$$\mathscr{L}_C(u) = \int_0^\infty e^{-uK} C(K) dK = \frac{\mathscr{L}_V(u) - 1}{u^2} + \frac{V_0}{u}\,. \tag{3.1}$$

As a consequence of the equation above, if an explicit expression of $\mathscr{L}_V$ exists, call prices can be found by applying some inversion algorithm to $\mathscr{L}_C$. However, when computing option prices by means of equation (3.1) several numerical issues may appear.

In this paper, we focus on a generalization of the Heston model where the dynamics of the instantaneous variance are augmented with compound Poisson jumps. In particular, we consider jump sizes following an Inverse Gamma density as this has proved to be capable of reproducing the upward sloping volatility skew of realized variance and VIX options (see Chapter 2). In this framework, we test the performance of some of the most popular algorithms available in the literature, comparing the results with those obtained through Monte Carlo simulations. As we shall see under the considered model, the realized variance is the same as the integrated variance. This implies a further error component in Monte Carlo simulations, due to the approximation of an integral as a finite sum. However, pricing through Monte Carlo simulations is not as sensitive to the lack of smoothness of the integrand as the inversion algorithms. Therefore, it can be assumed to be a good comparison method. A similar analysis in the context of Asian options pric-

ing can be found in Fu et al. [59] and Craddock et al. [44], and indeed options on the integrated variance of an asset can be considered continuous arithmetic Asian options on the instantaneous variance.

Finally, we mention the use of the Laplace transform and its inversion in pricing of other financial derivatives such as double barrier options, as in Geman and Yor [65], Pelsser [97] and Labart and Lelong [85], interest rate derivatives as in Leblanc and Scaillet [88] and credit risk as in Di Graziano and Rogers [49].

The rest of the paper is organized as follows: Section 3.2 gives an overview of the inversion algorithms we will test, namely the Bromwich-trapezoidal rule, Weeks' algorithm and Iseger's algorithm. Section 3.3 describes the framework we work on and in particular the model we consider, i.e., the SVJ-v model with Inverse Gamma jumps in the instantaneous variance. Section 3.4 provides numerical illustrations. Section 3.5 points to a possible extension of the model considered. Finally, Section 3.6 concludes.

3.2 A survey of inversion methods

In this section, we recapitulate some algorithms for the inversion of Laplace transforms that we will later apply to the specific case of pricing of call options on the realized variance V_T. They are all based on some expansion of f in terms of orthogonal functions with coefficients that are written in terms of the Laplace transform of f. The algorithms we consider are: the Bromwich-trapezoidal rule, Weeks' algorithm and Iseger's algorithm. These allow to show some of the numerical issues that might appear when applying Laplace inversion techniques in option pricing.

Other methods include the Gaver-Stehfest algorithm, [64] and [103], which is based on combinations of Gaver functionals and the method in Talbot [105], which is based on a contour deformation technique. For a comprehensive overview of Laplace inversion methods we refer to Cohen [41] and finally to Chapter 7 in Fusai and Roncoroni [60] where applications to option pricing are also shown.

Notation

- R^+ indicates the non-negative real line
- Given $f \in R^+$ we denote $L^p[0,\infty) = \left\{ f \text{ s.t.} \int_0^\infty |f(x)|^p dx < \infty \right\}$

– Given $f \in R^+$ we denote its Laplace transform by $\mathscr{L}_f = \int_0^\infty e^{-st} f(t)dt$

– $i = \sqrt{-1}$ denotes the imaginary unit

The Bromwich integral

The first method we describe is based on an application of the trapezoidal rule to the Bromwich inversion integral, a formula expressing a positive real valued function f as an integral involving its Laplace transform. This leads to an approximation of f as a trigonometric sum. A main reference for a full description of this algorithm is Abate et al. [3] where applications in the field of queuing theory are provided. The obtained algorithm can be considered a variant of the Fourier-series method (we refer again to Abate et al. [3] for an overview on the topic).

Theorem 3.2.1 (The Bromwich inversion integral)**.** *Let f be a real function on R^+, with Laplace transform $\mathscr{L}_f$ and b any real number to the right of all singularities of $\mathscr{L}_f$. For any $t > 0$ the three following equivalent formulae hold:*

$$f(t) = \frac{1}{2\pi i} \int_{b-i\infty}^{b+i\infty} e^{st} \mathscr{L}_f(s)ds \tag{3.2}$$

$$f(t) = \frac{2e^{bt}}{\pi} \int_0^\infty Real(\mathscr{L}_f(b+is))cos(st)ds \tag{3.3}$$

$$f(t) = \frac{-2e^{bt}}{\pi} \int_0^\infty Im(\mathscr{L}_f(b+is))sen(st)ds \tag{3.4}$$

where the integrals are intended to be zero for $t < 0$.

Proof. Equation (3.2) is a classical formula for the inversion of Laplace transforms, see e.g., Doetsch [50] for details. Formulae (3.3) and (3.4) can be easily recovered by the elementary equality $e^{ist} = cos(st) + isen(st)$ (see Abate et al. [3] for details). □

The problem of computing the inverse of $\mathscr{L}_f$ is therefore reduced to the computation of an integral. Different approaches can be carried out using various numerical integration techniques (see e.g., Smyth [102] for a survey on the topic). In what follows we will focus on equation (3.3) which, together with equation (3.4), involve integration with respect to real numbers, and not complex numbers as equation (3.2). A possible approach in order to approximate the integral above

consists in the use of the trapezoidal rule leading to the formula below which we denominate the *Bromwich-trapezoidal rule*

$$f(t) \sim \tilde{f}(t) = \frac{he^{bt}}{\pi}\mathscr{L}_f(b) + \frac{2he^{bt}}{\pi}\sum_{n=1}^{\infty} Real(\mathscr{L}_f(b+inh))cos(nht), \;\; t>0 \quad (3.5)$$

where h is a chosen step size. An analogous formula in terms of $sen(u)$ rather than $cos(u)$ can be easily derived.

When applying the approximation in equation (3.5), three main sources of error arise: a discretization error, a truncation error, and finally a roundoff error. The first error is due to the application of the trapezoidal rule, or in other words, to the approximation of the integral in equation (3.3) with a sum. It can be shown however that if $|f(x)| \leq C$ for all $x > t + 2\pi/h$ then

$$|f(t) - \tilde{f}(t)| \leq \frac{Ce^{-2\pi b/h}}{1 - e^{-2\pi b/h}}. \quad (3.6)$$

In our case, $f = C(K)$ is bounded by a constant if V_T has finite first moment. As a consequence, we can control the discretization error by increasing b/h.

Once we have control of the discretization error, we need to compute the final summation in equation (3.5). Hence, we need to approximate the infinite series with a finite sum (leading to truncation errors), and compute the single terms. When performing the last task, roundoff errors appear due to the computation of elementary functions such as addition and multiplication.

In order to bound these last two sources of errors and therefore improve the final convergence of the approximation, different acceleration procedures can be applied. Abate et al. [2] suggest the Euler acceleration technique according to which $f(t)$ is approximated as

$$f(t) \sim \tilde{f}^e_{m,n}(t) = \sum_{k=0}^{m} \binom{m}{k} 2^{-m} s_{n+k}(t) \quad (3.7)$$

where

$$s_n(t) = \sum_{k=0}^{n} (-1)^k \frac{e^{A/2L}}{2Lt} b_k(t) \tag{3.8}$$

$$b_0(t) = \mathscr{L}_f(A/2Lt) + 2\sum_{j=1}^{l} Real[\mathscr{L}_f(A/2Lt + ij\pi/Lt)e^{ij\pi/L}] \tag{3.9}$$

$$b_k(t) = 2\sum_{j=1}^{l} Real[\mathscr{L}_f(A/2Lt + ij\pi/Lt + ik\pi/t)e^{ij\pi/L}],\ k \geq 1 \tag{3.10}$$

This is obtained by letting $h = \pi/Lt$ and $b = A/2Lt$ be a function of t rather than a constant, and by taking the average of $s_n, s_{n+1}, \ldots, s_{n+m}$, weighted by a binomial probability distribution with parameters m and $p = 1/2$.

The main advantage of the Euler acceleration technique is that a smaller number of terms in the summation is required with respect to the case without acceleration. The parameters A, L, m, n play a fundamental role in the outcome of the approximation. In particular, A allows control of the discretization error, and equation (3.6) can be reformulated as

$$|f(t) - \tilde{f}^e_{m,n}(t)| \leq \frac{Ce^{-A}}{1 - e^{-A}}. \tag{3.11}$$

Finally, when applying the algorithm in practice, a good test for the convergence is to compute $\tilde{f}^e_{m,n}(t)$ for two different couples (A, L). In case the values obtained are not close enough to each other, an increment of n is advised. Also, an increment of L can help control roundoff errors. We refer to Abate et al. [2] for a comprehensive discussion about computational errors when applying equation (3.5).

Weeks' algorithm

A different approach involving an expansion as a Laguerre-series can be found in Abate et al. [1]. It is based on the property of the Laguerre functions to be an orthonormal basis for the space $L_2[0, \infty)$.

Theorem 3.2.2 (Laguerre-series representation)**.** *Let f be a real function on R^+, with Laplace transform $\mathscr{L}_f$ and assume $f \in L^2[0, \infty)$. Then*

$$f(t) = \sum_{n=1}^{\infty} q_n l_n(t), \quad t \geq 0 \tag{3.12}$$

where $l_n(t)$ are the Laguerre functions

$$l_n(t) = e^{-t/2} Lag_n(t) \tag{3.13}$$

associated to the Laguerre polynomials

$$Lag_n(t) = \sum_{k=0}^{n} \binom{n}{k} \frac{(-t)^k}{k!} \tag{3.14}$$

and $q_n = \int_0^\infty f(t) l_n(t) dt$ are the Laguerre coefficients which can be computed from the Laguerre generating function given below

$$Q(z) = \sum_{n=1}^{\infty} q_n z^n = (1-z)^{-1} \mathscr{L}_f \left(\frac{1+z}{2(1-z)} \right). \tag{3.15}$$

The idea of inverting Laplace transforms through Laguerre series representations first appeared in Tricomi [106] (see also Gabutti and Lepora [61] and Widder [108]). However, complete algorithms for its implementation were developed later on in Weeks [107] and the procedure is nowadays known as "Week's algorithm".

Before proceeding, we recall that the Laguerre functions in (3.13) can be computed by recursion as follows:

$$\begin{aligned}
l_0(t) &= e^{-t/2}, \\
l_1(t) &= (1-t)e^{-t/2}, \\
l_n(t) &= \left(\frac{2n-1-t}{n} \right) l_{n-1}(t) - \left(\frac{n-1}{n} \right) l_{n-2}(t).
\end{aligned}$$

Two issues appear when using the algorithm above: the computation of the coefficients q_n from $\mathscr{L}_f$ and the truncation of the summation in equation (3.15). The first problem is solved in Abate et al. [1] through a computation formula based on the modification of the Lattice-Poisson algorithm in Choudhury et al. [40]:

$$q_n \sim \tilde{q}_n = \frac{1}{2\ell n r^n} \sum_{j=0}^{\ell-1} \sum_{k=-n}^{n-1} (-1)^j exp(-\pi i k/\ell) Q(r e^{\pi i (j+\ell k)/n\ell}) \tag{3.16}$$

where $0 < r < 1$ is the radius of a circle about the origin on which $Q(z)$ is analytic. Boundedness of the coefficients q_n grants boundedness of the error $e_a = \tilde{q}_n - q_n$, also

called aliasing error, which corresponds to the discretization error when applying formula (3.5). It can be proved that if $|q_{n+2jln}/q_n| \leq C$ then

$$|e_a/q_n| \leq Cr^{2\ell n}/(1-r^{2\ell n}) \approx Cr^{2\ell n}.$$

The number r^{2l} can therefore be chosen in order to control the error e_a. Usually $\ell = 1$ and $r = (0.1)^{4/n}$ are sufficient for a good approximation. However, different values of ℓ can be used as an accuracy test.

Regarding the second issue, which already appeared under the name of truncation error when using (3.5), this is related to the rate of convergence to zero of the coefficients q_n. This in turn depends on the behaviour of the Laplace transform at infinity and on the smoothness of the function f and its derivatives. In order to overcome numerical issues due to lack of smoothness, a scaling technique can be applied. This consists in considering the function $f_{\xi,\phi} = e^{-\xi t} f(t/\phi)$, applying the algorithm to $f_{\xi,\phi}$ and then recovering the original function f from the equality $f(t) = e^{\xi\phi t} f_{\xi,\phi}(bt)$. This is possible by observing that the Laguerre generating function of the scaled function is

$$Q_{f_{\xi,\phi}}(z) = \sum_{n=1}^{\infty} q_n^{\xi,\phi} z^n = \phi(1-z)^{-1} \mathscr{L}_f \left(\frac{\phi(1+z)}{2(1-z)} + \phi\xi \right). \tag{3.17}$$

The presence of the parameter ξ allows elimination of singularities in zero, whereas ϕ can potentially help with singularities at infinity. Both parameters can also work as accuracy check by applying the algorithm for different couples (ϕ, ξ) and comparing the results obtained.

Finally, additional roundoff errors can occur when computing the coefficients q_n through equation (3.16). Different techniques can be applied in order to overcome this problem, depending on the rate of convergence of q_n to zero (see Abate et al. [2] for further details).

Remark 3.2.3 (A conclusive remark on the applicability of the Laguerre expansion to $C(K)$)**.** *By standard calculations*

$$\int_0^{\infty} C(K)^2 dK \leq \frac{\mathbb{E}[V_T^3]}{3}$$

from which it is evident that if $\mathbb{E}[V_T^3] < +\infty$ *then* $C(K) \in L_2[0, \infty)$*, and it is therefore possible to apply the Laguerre-series expansion. On the other hand, also in*

the case when $C(K)$ is not initially integrable, it is usually possible to pre-multiply it by a damping factor ξ^*, in a similar way as the scaling technique above, and apply the Laguerre representation to the corresponding integrable function $C^*(K) = e^{-\xi^* t}C(K)$ whose Laplace transform is given by $\mathscr{L}^*(s) = \mathscr{L}(s + \xi^*)$.

Remark 3.2.4. *Giunta et al. [66] find the optimal value for ϕ in terms of the singularities of the Laplace transform $\mathscr{L}$. However, when numerically implementing the algorithm further discontinuities may appear, as it will be shown in the numerical illustrations that follow.*

Iseger's algorithm

In this subsection we present the algorithm in Iseger [79] which is based on the Poisson summation formula and an application of the Gaussian quadrature rule. This algorithm was recently applied in the case of pricing of realized variance options by Drimus [51]. We finally refer to Iseger [80] where a generalization of the algorithm working for functions defined on the entire real line is proposed.

Theorem 3.2.5 (The Poisson summation formula)**.** *Let f be a real function on R^+, with Laplace transform $\mathscr{L}_f$, $f \in L_1[0,\infty)$, and f of bounded variation. Then for any $t > 0$ and for any $v \in [0,1)$, it holds:*

$$\sum_{k=-\infty}^{\infty} \mathscr{L}_f(a + 2\pi i(k+v)) = \sum_{k=0}^{\infty} e^{-ak} e^{-i2\pi kv} f(k) \tag{3.18}$$

where $a \in R$ is called damping factor.

Proof. This is a classical result of Fourier analysis, see e.g., Stein and Weiss [104]. □

The idea behind the algorithm is to re-write the left hand side of equation (3.18) as an inner product and then approximate it with a Gaussian quadrature rule. Further manipulations lead to the following algorithm:

given n, M_2, a and M, with M power of 2 define

$$\hat{f}_{jk} = Re\left[\mathscr{L}_f\left(\frac{a + i\lambda_j + \frac{2i\pi k}{M_2}}{\Delta}\right)\right],\ k = 0, 1, \ldots, M_2,\ j = 1, 2, \ldots, n/2 \tag{3.19}$$

and subsequently

$$\hat{f}_0 = \frac{1}{\Delta}\sum_{j=1}^{n/2}\beta_j(\hat{f}_{j0} + \hat{f}_{jM_2})$$

$$\hat{f}_k = \frac{2}{\Delta}\sum_{j=1}^{n/2}\beta_j\hat{f}_{jk}$$

with coefficients as in Appendix A in Iseger [79]. Then for $l = 0, 1, \ldots, M-1$, an approximation of f is given by

$$f(l\Delta) \sim \tilde{f}_a(l) = \frac{e^{al}}{M_2}\sum_{k=0}^{M_2-1}\hat{f}_k cos\left(\frac{2\pi lk}{M_2}\right). \tag{3.20}$$

The algorithm therefore allows the evaluation of the function f on a regular grid of points $0, \Delta, \ldots (M-1)\Delta$, or in other words, it allows us to evaluate the call function $C(K)$ on a regular grid of strikes. Regarding the parameters that appear in the algorithm, Iseger [79] suggests the choice $n = 16$, $M_2 = 8M$, $a = 44/M_2$, whereas M depends upon the number of points we want to evaluate the function on. Finally, the parameter M_2 can be used in order to find an equilibrium between running time and accuracy of the algorithm. In particular, decreasing M_2 accelerates the algorithm but at the same time reduces the precision of the results.

Remark 3.2.6 (A conclusive remark on the applicability of the Poisson summation formula and consequently of Iseger's algorithm)**.** *$C(K)$, being a monotone (decreasing) function, is of bounded variation. Moreover by standard calculations*

$$\int_0^\infty |C(K)|dK \leq \frac{\mathbb{E}[V_T^2]}{2}$$

from which it is evident that if $\mathbb{E}[V_T^2] < +\infty$ then $C(K) \in L_1[0, \infty)$.

3.3 A test model

We consider the SVJ-v model where the square root dynamics of the Heston [77] model are augmented with jumps in the instantaneous variance. Specifically, we consider as jumps compound Poisson processes where the jump size follows an Inverse Gamma law. Inverse Gamma densities have been proved to be able to

reproduce the upward-sloping volatility skew exhibited by volatility derivatives (see Chapter 2). The assumption of no jumps in the log asset price is made in order to simplify computations, since under these hypotheses the realized variance of the asset reduces to its integrated variance. The considered model will allow us to show some of the issues that arise when performing inversion of the Laplace transform in equation (3.1). For completeness we mention the case with jumps both in the log-price and in the instantaneous variance in Section 3.5.

Without loss of generality, we assume zero interest rates and dividend yields. We consider a filtered probability space $(\Omega, \mathbb{F}, \{\mathbb{F}\}_{t\geq 0}, \mathbb{Q})$ where $\{\mathbb{F}\}_{t\geq 0}$ is a filtration the price process S_t is adapted to and $\mathbb{Q}$ is a pricing measure. We assume that the risk-neutral dynamics of the log-price $X_t = \log(S_t)$ and its instantaneous variance v_t are given by

$$\begin{aligned} dX_t &= -\tfrac{1}{2}v_t dt + \sqrt{v_t} dW_t \\ dv_t &= \lambda(\theta - v_t)dt + \sigma\sqrt{v_t} dB_t + dJ_t \end{aligned} \tag{3.21}$$

where the processes W and B are standard Brownian motions with correlation parameter ρ, λ, θ and σ are non-negative constants, and J_v is a compound Poisson process

$$J_v = \sum_{i=1}^{N(t)} Z_i, \quad Z_i \sim i.i.d.\ Z \tag{3.22}$$

with $N(t)$ Poisson process with intensity l. The jump size Z follows an Inverse Gamma law $I\Gamma(\nu, \mu)$ with density

$$f_{I\Gamma}(x) = \frac{\mu^\nu}{\Gamma(\nu)} x^{-\nu-1} e^{-\mu/x} \mathbf{1}_{x\geq 0}$$

and Laplace transform

$$\mathscr{L}_Z(u) = \frac{2(\mu u)^{\nu/2}}{\Gamma(\nu)} K_\nu(\sqrt{4\mu u})$$

where K_ν is the modified Bessel function of the second kind.

We will focus on options on the realized variance of X_t. Given a time interval $[0, T]$ and a grid $0 = t_0 < t_1 < \cdots < t_N = T$ on it, we define *realized variance* over $[0, T]$

$$RV_N = \sum_{n=1}^{N} (X_{t_n} - X_{t_{n-1}})^2.$$

RV_N can therefore be considered a measure of the variation in the price realized over the time interval $[0, T]$. The realized variance is often approximated by the quadratic variation $[X]_T$ of the log-price

$$[X]_T = \lim_{\Pi \to 0} \sum_{n=1}^{N} (X_{t_n} - X_{t_{n-1}})^2.$$

This is justified by the fact that the realized variance converges to $[X]_T$ as the mesh-size of the time-grid, $\Pi = \sup_{n=1,\ldots,N}(t_n - t_{n-1})$, goes to zero. This is proved to work quite well in practice when considering daily data (see e.g., Broadie and Jain [31]). We will adopt this assumption and indicate with the term of realized variance its continuous-time limit given by the quadratic variation. Under the dynamics in (3.21), the (annualized) realized variance reduces to the (annualized) integrated variance

$$V_T = \frac{1}{T} \int_0^T v_t dt, \tag{3.23}$$

which is more tractable from a mathematical point of view. We refer to Sepp [100] for a description of realized variance options under the Heston model with jumps. We also suggest Carr and Lee [37], Drimus [51], [52], Fatone et al. [57] and Kallsen [82] as further references on this topic.

An explicit expression of the Laplace transform of V_T under the dynamics in (3.21) is available. Indeed, denote by $\mathscr{L}_Z(u) = \mathbb{E}[e^{-uZ}]$ the Laplace transform of the jump size Z and by

$$\kappa_J(u) = \log \mathbb{E}[e^{-uJ_1}] = l(\mathscr{L}_Z(u) - 1) \tag{3.24}$$

the cumulant exponent of the jump process J. The Laplace transform of V_T is then given by

$$\mathscr{L}_{V_T}(u) = \mathbb{E}[e^{-uV_T}] = e^{\alpha_1(u,T) + \beta_1(u,T)\, v_0}, u \geq 0 \tag{3.25}$$

with functions $\alpha_1(u, t)$ and $\beta_1(u, t)$ as below

$$\begin{aligned} \beta_1(u,t) &= \tfrac{1-e^{-\gamma(u)t}}{c_1(u)+d_1(u)e^{-\gamma(u)t}} \\ \alpha_1(u,t) &= -\tfrac{2\lambda\theta}{\sigma^2} \log \tfrac{c_1(u)+d_1(u)e^{-\gamma(u)t}}{c_1(u)+d_1(u)} + \tfrac{\lambda\theta t}{c_1(u)} + \int_0^t \kappa_J(-\beta_1(u,s))ds \end{aligned}$$

and $c_1(u) = \frac{\lambda+\gamma(u)}{-2u/T}$, $d_1(u) = \frac{\lambda-\gamma(u)}{2u/T}$ and $\gamma(u) = \sqrt{\lambda^2 + 2\sigma^2 u/T}$ (see Duffie et al. [53] for details). We can therefore apply equation (3.1) and recover call prices by inversion algorithms.

3.4 Numerical experiments

The aim of this section is to test how the different algorithms presented in Section 3.2 perform when applied to pricing of call options on the realized variance.

Although equation (3.1) does not seem to involve any complex number, all the previous algorithms for inverting Laplace transforms do fall in the set of complex numbers. This is because we actually need to invert equation (3.1) in order to recover the function $C(K)$. Going into the complex number set can cause discontinuities leading to wrong option prices, in a similar way as already pointed out in Albrecher et al. [6] and Lord and Kahl [92]. However, their analysis is mainly restricted to the Heston model with applications to pricing of equity options, whereas here we consider a case with jumps in the instantaneous variance, with focus on realized variance options. Specifically, we consider jump sizes following an Inverse Gamma density which leads to further discontinuities because of the presence, in the corresponding Laplace transform, of Bessel functions combined with the square root.

We compare the results from the different inversion algorithms with those obtained from Monte Carlo simulations. Prices under the risk-neutral probability measure $\mathbb{Q}$ can be computed through the usual formula

$$C(K) = \mathbb{E}[(V_T - K)_+] \sim \frac{1}{Q}\sum_{q=1}^{Q}(V_T^q - K)_+ \tag{3.26}$$

where $\{V_T^q\}_{q=1,\dots Q}$ are Q different simulations of V_T (usually $Q = 10^5$ or 10^6 is enough to obtain good approximations). In order to simulate V_T, we first need to simulate a path of v_T and then approximate the integral in equation (3.23) with a finite sum. A path of the instantaneous variance v_t can be obtained for example by applying the Euler discretization scheme modified with the Full Truncation method (see Lord et al. [93]):

$$v_{t+1} = v_t + \lambda(\theta - (v_t)_+)\Delta t + \sigma\sqrt{(v_t)_+}\sqrt{\Delta t}W_t + \sum_{n=1}^{N_{t_{n+1}}} z_n \tag{3.27}$$

where x_+ denotes the positive part of x, W_t is a standard normal random variable, N_t is a Poisson process with intensity $l\Delta t$, and $z_n \sim \text{I}\Gamma(\nu, \mu)$.

We refer to Glasserman [67] for a complete review on Monte Carlo methods and to Platen and Bruti-Liberati [98] for an overview of different methods for simulation of processes with jumps.

Before testing the different inversion procedures, we show how different formulations of the Laplace transform in (3.25) may lead to different results of the Laplace transform in (3.1) and therefore to different option prices.

Two formulations of the Laplace transform

The Laplace transform of the realized variance under the model in equation (3.21) can be rewritten as

$$\mathscr{L}_V(u) = \mathbb{E}[e^{-uV_T}] = e^{\alpha_2(u,T)+\beta_2(u,T)\,v_0}\,, u \geq 0 \tag{3.28}$$

with functions $\alpha_2(u,t)$ and $\beta_2(u,t)$ as below

$$\begin{aligned}
\beta_2(u,t) &= \tfrac{1-e^{\gamma(u)t}}{c_2(u)+d_2(u)e^{\gamma(u)t}} \\
\alpha_2(u,t) &= -\tfrac{2\lambda\theta}{\sigma^2}\log\tfrac{c_2(u)+d_2(u)e^{\gamma(u)t}}{c_2(u)+d_2(u)} + \tfrac{\lambda\theta T}{c_2(u)} + \int_0^t \kappa_J(-\beta_2(u,s))ds
\end{aligned}$$

and $c_2(u) = \frac{\lambda-\gamma(u)}{-2u/T}$, $d_2(u) = \frac{\lambda+\gamma(u)}{2u/T}$ and $\gamma(u) = \sqrt{\lambda^2 + 2\sigma^2 u/T}$. In the following, we will refer to equation (3.25) and equation (3.28) as Formulation 1 and Formulation 2, respectively.

Inspired by Albrecher et al. [6] and Lord and Kahl [92], we perform some numerical studies showing how the two formulations may lead to completely different option prices, especially when considering long maturities.

Figure 3.1 (left) shows the case corresponding to prices with maturity of 1 year and parameters $v_0 = 0.0348$, $\lambda = 1.15$, $\theta = 0.0218$, $\sigma = 0.3788$, $\nu = 4.8$, $\mu = 0.02$, $l = 1.5$. Prices are computed through the Bromwich-trapezoidal approximation in (3.5) with $b = 0.1$, $h = 0.01$ and the two different formulations. The difference between the two formulations becomes even bigger when considering maturities longer than 1 year. The reason for this difference is that, for maturities large enough, Formulation 2 leads to discontinuities in the Laplace transform of the realized variance and therefore in the corresponding Laplace transform of the call function, which is the one to be inverted. This is evident from Figure 3.2 where we plot real and imaginary part of $\mathscr{L}_C$ computed in $b+inh$ with $b = 0.1$, $h = 0.01$ and n ranging from 62000 to 64000. Note that those values enter in the approximation

(3.5). Observe also that, in this example, the two obtained price curves look both reasonable and the presence of discontinuities is not so evident from Figure 3.1 (left), without looking at Figure 3.2.

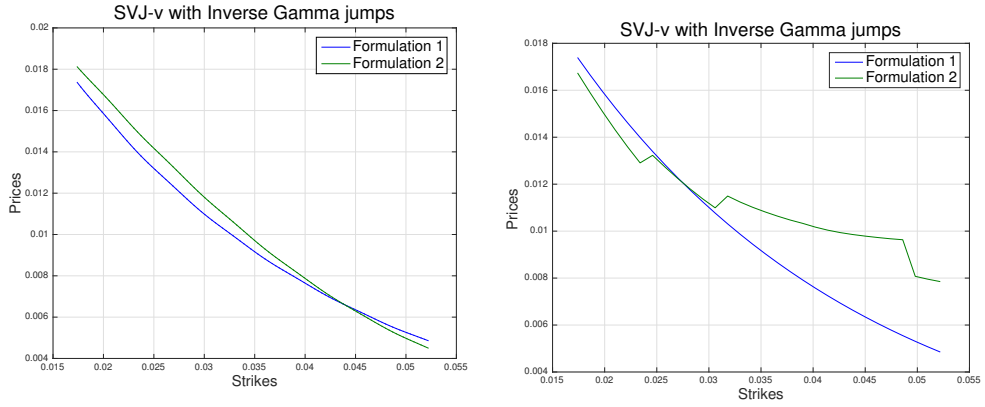

Figure 3.1: *Prices of call options on V_T in the SVJ-v model with Inverse Gamma jumps, $T = 1$ year, $v_0 = 0.0348$, $\lambda = 1.15$, $\theta = 0.0218$, $\sigma = 0.3788$, $\nu = 4.8$, $\mu = 0.02$, $l = 1.5$. Prices are computed using the two formulations and applying the Bromwich-trapezoidal rule with $b = 0.1$, $h = 0.01$ (left) and making use of the Euler acceleration technique with $A = 29$, $L = 4$, $m = 11$, $n = 40$ (right).*

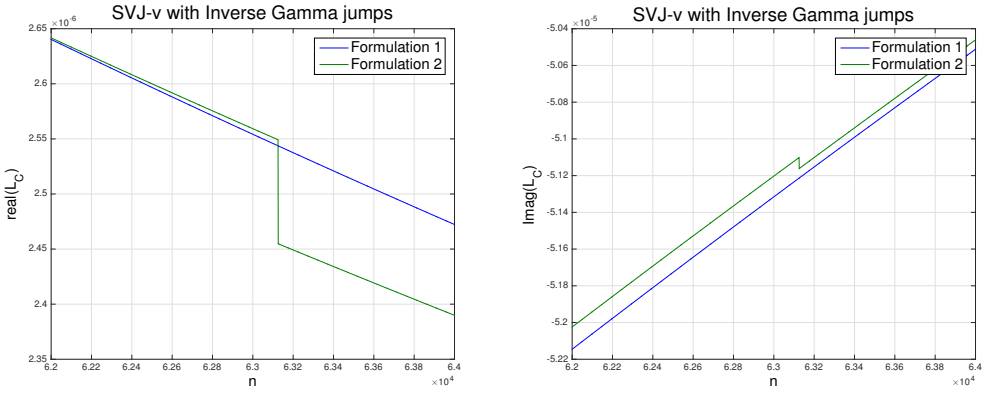

Figure 3.2: *Real and imaginary part of $\mathscr{L}_C(u)$ in the SVJ-v model with Inverse Gamma jumps, $T = 1$ year, $v_0 = 0.0348$, $\lambda = 1.15$, $\theta = 0.0218$, $\sigma = 0.3788$, $\nu = 4.8$, $\mu = 0.02$ and $l = 1.5$ computed using the two formulations. The Laplace transform is evaluated in $b + inh$ with $b = 0.1$, $h = 0.01$.*

Subsequently, we test the performance of the Euler summation formula applied

to the Bromwich-trapezoidal rule, when using Formulation 2. We assume the same model-parameters as above, a maturity of 1 year and parameters in the algorithm $A = 29$, $L = 4$, $m = 11$, $n = 40$. These lead to discontinuities as shown in Figure 3.1 (right). Changing the parameters A and L or increasing n and m the results do not improve much. Also, the default parameters of the algorithm $A = 19$, $L = 1$, $m = 11$, $n = 38$ lead to negative prices in correspondence to a few strikes

Next, we test the sensitivity of Weeks' algorithm to discontinuities in the Laplace transform. In this case, prices computed with the two different formulations lead to analogous results. Figure 3.3 (left) shows the case corresponding to model-parameters as above and a maturity of 1 year. Weeks' algorithm is implemented with $N = 10^3$ and $\ell = 1$.

On the other hand, the use of Iseger's algorithm together with Formulation 2 leads to numerical instabilities. This is shown in Figure 3.3 (right) which represents the analogous of Figure 3.3 (left). Iseger's algorithm is implemented with $n = 16$.

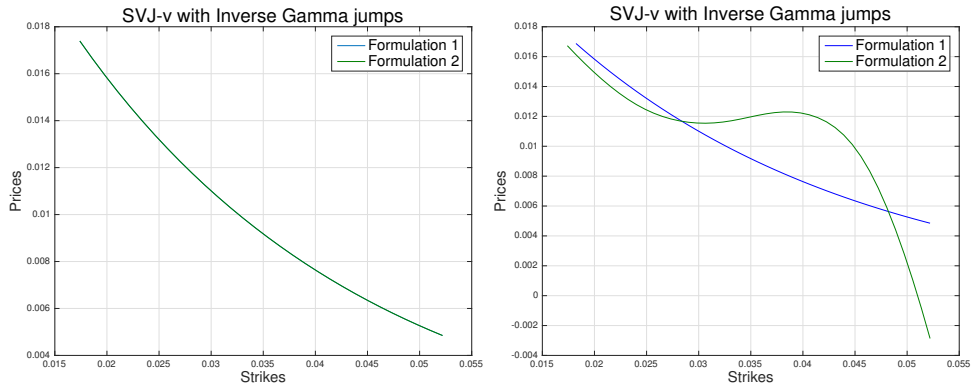

Figure 3.3: *Prices of call options on V_T in the SVJ-v model with Inverse Gamma jumps, $T = 1$ year, $v_0 = 0.0348$, $\lambda = 1.15$, $\theta = 0.0218$, $\sigma = 0.3788$, $\nu = 4.8$, $\mu = 0.02$, $l = 1.5$. Prices are computed using the two formulations and applying Weeks' algorithm with $N = 10^3$ and $\ell = 1$ (left) and Iseger's algorithm with $n = 16$(right).*

In the following numerical experiments, we will test the performance of the different algorithms when using Formulation 1 which, we do believe, avoids discontinuities and therefore performs better than Formulation 2.

Finally, we remark that the implied volatility is quite sensitive to differences in option prices, and therefore errors are amplified when looking at implied volatilities

rather than prices.

Numerical tests on the Bromwich-trapezoidal rule

We start from an application of formula (3.5) showing how the specific choice of the parameters h and b in the algorithm may have a considerable impact on the corresponding results. We consider parameters $v_0 = 0.0348$, $\lambda = 1.15$, $\theta = 0.0218$, $\sigma = 0.3788$, $\nu = 4.8$, $\mu = 0.02$, $l = 1.5$ and a maturity of 3 months. First, we fix the value $b = 0.1$ and perform the algorithm for different values of h. Then, we fix $h = 0.01$ and perform for different values of b. In all cases, we truncate the infinite sum at the 10^5th term. In the first case, we observe sensitivity with respect to h, see e.g., Figure 3.4 (left). On the contrary, in the second case, represented in Figure 3.4 (right), the approximation reveals to be independent on the value of b.

We observe that the performance of the approximation also depends on the specific parameters we choose for the model. For example, modifying the parameters to $v_0 = 0.0653$, $\lambda = 3.8$, $\theta = 0.0918$, $\sigma = 0.9271$ and keeping the same jumps-parameters and maturity as above, we obtain Figure 3.5 where sensitivity to h is less evident than in Figure 3.4.

Here we focussed on options with a maturity of 3 months. Implementing the algorithm with the same parameters and different maturities, we obtained analogous results.

Finally, numerical tests on the Euler summation formula, which corresponds to parameters $h = \pi/LK$, $b = A/2LK$, dependent on the specific strike, provide good results, as shown in Figure 3.6. The algorithm works well also for different maturities.

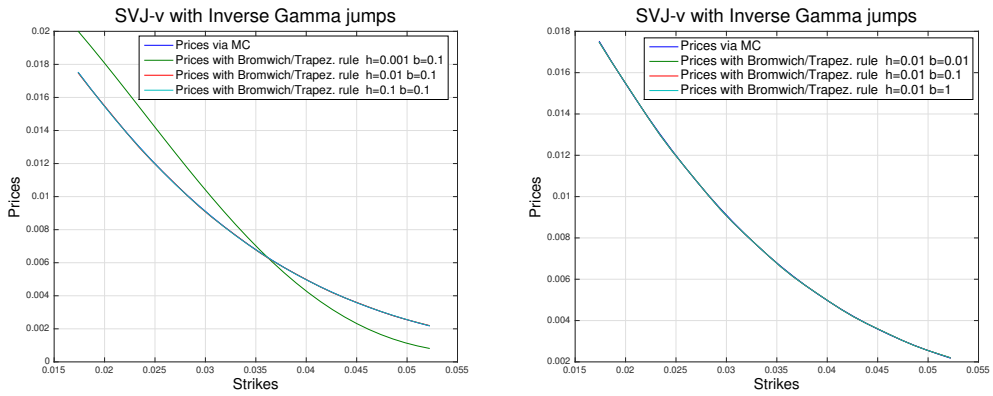

Figure 3.4: *Prices of call options on V_T in the SVJ-v model with Inverse Gamma jumps with $v_0 = 0.0348$, $\lambda = 1.15$, $\theta = 0.0218$, $\sigma = 0.3788$, $\nu = 4.8$, $\mu = 0.02$, $l = 1.5$, $T = 3$ months, computed using Monte Carlo simulation and the Bromwich-Trapezoidal rule. Sensitivity with respect to h (left) and to b (right) are analyzed. In all the cases the truncation is made at $N = 10^5$. For the case on the left, red, light blue and dark blue lines coincide.*

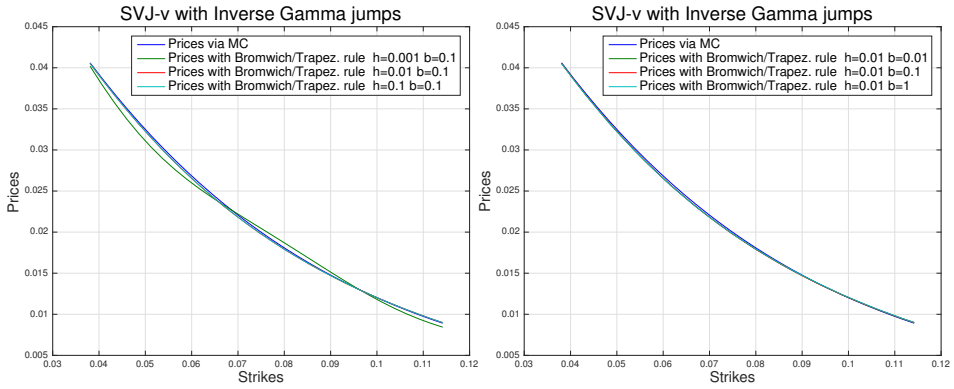

Figure 3.5: *Prices of call options on V_T in the SVJ-v model with Inverse Gamma jumps with $v_0 = 0.0653$, $\lambda = 3.8$, $\theta = 0.0918$, $\sigma = 0.9271$, $\nu = 4.8$, $\mu = 0.02$, $l = 1.5$, $T = 3$ months, computed using Monte Carlo simulation and the Bromwich-Trapezoidal rule. Sensitivity with respect to h (left) and to b (right) are analyzed. In all the cases the truncation is made at $N = 10^5$. For the case on the left, red, light blue and dark blue lines coincide.*

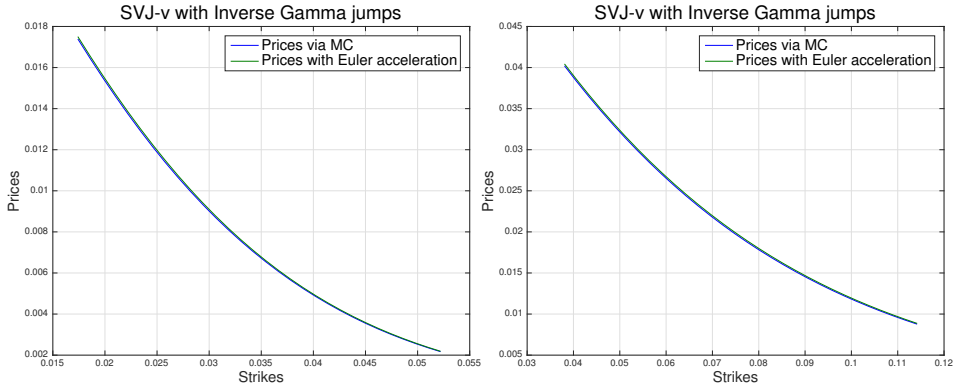

Figure 3.6: *Prices of call options on V_T in the SVJ-v model with Inverse Gamma jumps with $v_0 = 0.0348$, $\lambda = 1.15$, $\theta = 0.0218$, $\sigma = 0.3788$ (left), and $v_0 = 0.0653$, $\lambda = 3.8$, $\theta = 0.0918$, $\sigma = 0.9271$ (right). In both cases $\nu = 4.8$, $\mu = 0.02$, $l = 1.5$ and the maturity is 3 months. Prices are computed using Monte Carlo simulation and the Bromwich-Trapezoidal rule with Euler acceleration technique, with $A = 19$, $L = 1$, $m = 11$, $n = 38$.*

Numerical tests on Weeks' algorithm

We now perform numerical tests on Weeks' algorithm. We use the same model parameters as before and we compare the results obtained with prices computed via Monte Carlo simulations.

We start by using the default parameters in Weeks' [107], namely $\ell = 1$, $r = (0.1)^{4/n}$ and $N = 100$, N number of terms in the summation 3.12. In this case prices computed by inversion of the Laplace transform differ considerably from prices computed through Monte Carlo simulations. However, when increasing N to 10^3 good results are obtained, as shown in Figure 3.7.

For maturities of 6 months or 1 year good results are still produced, whereas when reducing the maturity to below 3 months, numerical issues arise.

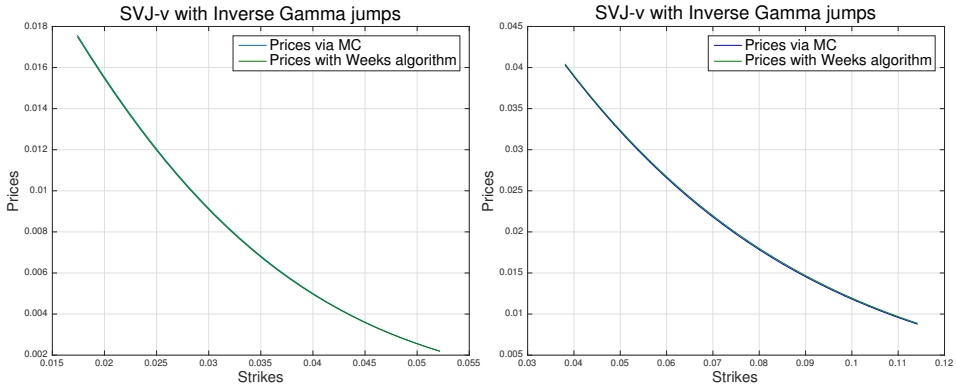

Figure 3.7: *Prices of call options on V_T in the SVJ-v model with Inverse Gamma jumps, $v_0 = 0.0348$, $\lambda = 1.15$, $\theta = 0.0218$, $\sigma = 0.3788$ (left) and $v_0 = 0.0653$, $\lambda = 3.8$, $\theta = 0.0918$, $\sigma = 0.9271$(right). The jump-parameters are $\nu = 4.8$, $\mu = 0.02$, $l = 1.5$ and the maturity is 3 months. Prices are computed using Monte Carlo simulation and Weeks' algorithm. In both cases $\ell = 1$, $r = 0.1^{4/n}$ and the truncation is made at $N = 10^3$.*

Numerical tests on Iseger's algorithm

Finally, we test the inversion procedure in Iseger [79]. The numerical experiments performed confirm the accuracy of the algorithm, as shown in Figure 3.8 corresponding to $n = 16$ and $M = 2^6$, for a maturity of 3 months. Good results are also obtained for different maturities, including those less than 3 months in which case Weeks' algorithm works poorly.

However, keep in mind that Iseger's algorithm is extremely sensitive to discontinuities in $\mathscr{L}_V(u)$ and therefore attention must be paid to the used expression of the Laplace transform.

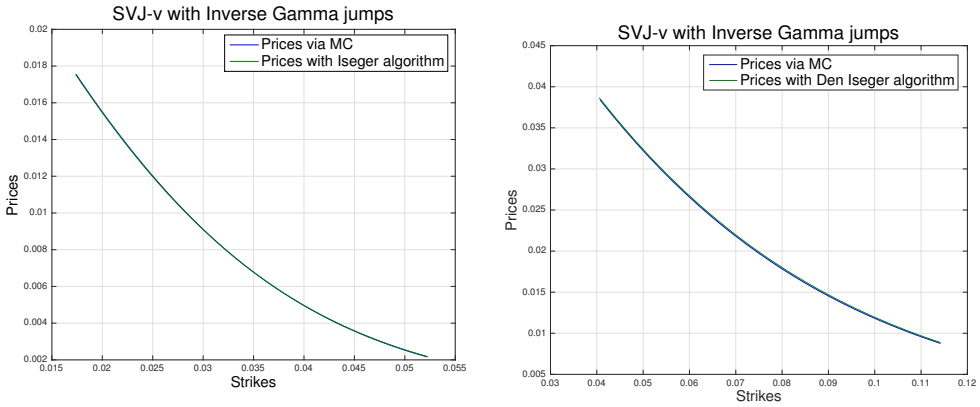

Figure 3.8: *Prices of call options on V_T in the SVJ-v model with Inverse Gamma jumps, $v_0 = 0.0348$, $\lambda = 1.15$, $\theta = 0.0218$, $\sigma = 0.3788$ (left) and $v_0 = 0.0653$, $\lambda = 3.8$, $\theta = 0.0918$, $\sigma = 0.9271$ (right). In both cases $\nu = 4.8$, $\mu = 0.02$, $l = 1.5$ and the maturity is 3 months. Prices are computed using Monte Carlo simulation and Iseger's algorithm.*

Control Variates

Numerical performances of the previous algorithms may possibly be enhanced by a careful application of a control variate. This technique was introduced in Andersen and Andreasen [9] who apply Fourier transform methods for pricing of equity options. Later, it was extended in the context of realized variance options by Drimus [51]. The main idea behind it is the use of a distribution for the realized variance, for which call option-prices are available in closed-form. Denoting by $\mathscr{L}_{\hat{V}}(u)$ and $\mathscr{L}_{\hat{C}}(u)$ the Laplace transform of the realized variance and of the call funtion under the control variate distribution, the idea is to compute the Laplace transform

$$\mathscr{L}_{C-\hat{C}}(u) = \mathscr{L}_C(u) - \mathscr{L}_{\hat{C}}(u) = \frac{\mathscr{L}_V(u) - \mathscr{L}_{\hat{V}}(u)}{u^2},$$

invert it, thus obtaining $C - \hat{C}$, and finally recovering C by adding $\hat{C}$ which is known in closed-form.

For example, when using a Gamma Control Variate with density

$$f_\Gamma(x) = \frac{\hat{\beta}^\alpha}{\Gamma(\hat{\alpha})} x^{\hat{\alpha}-1} e^{-\hat{\beta}x} \mathbf{1}_{x\geq 0},$$

the corresponding price of a call option on the realized variance is

$$\hat{C}(K) = \frac{\hat{\alpha}}{\hat{\beta}}(1 - F(K; \hat{\alpha} + 1, \hat{\beta})) - K(1 - F(K; \hat{\alpha}, \hat{\beta}))$$

with F cumulative distribution function of a Gamma distribution $\Gamma(\hat{\alpha}, \hat{\beta})$. This is the Control Variate used e.g., in Drimus [51] in order to compute prices under the Heston model and the 3/2 model.

The parameters of the Gamma distribution are chosen in order to match its mean with $C(0)$ and its second moment with that of a log-normal distribution of the form

$$C(0)e^{\hat{\sigma}\sqrt{T}N(0,1) - \frac{\hat{\sigma}^2 T}{2}},$$

thus obtaining

$$\hat{\alpha} = \frac{\mathbb{E}[V_T]}{\hat{\beta}}$$
$$\hat{\beta} = \frac{1}{\mathbb{E}[V_T](e^{\hat{\sigma}^2 T} - 1)}.$$

As a first experiment, we also apply this distribution as control variate when using the Bromwich-trapezoidal rule and Iseger's algorithm. We compare the performances of the technique when using the two different formulations of the Laplace transform. The numerical experiments performed show that when using Formulation 2, which leads to discontinuities, a Gamma control variate technique does not improve the results. This is shown for example in Figure 3.9 and Figure 3.11, corresponding to parameters $v_0 = 0.0348$, $\lambda = 1.15$, $\theta = 0.0218$, $\sigma = 0.3788$, $\nu = 4.8$, $\mu = 0.02$, $l = 1.5$ and a maturity of 1 year. On the left, prices with the 2 different formulations are presented. On the right, real part of the Laplace transform $\mathscr{L}_{C-\hat{C}}(u)$ to be inverted is shown. The case in the Figure corresponds to $\hat{\sigma} = 1$. Different values of $\hat{\sigma}$ lead to analogous results.

Afterwards, we perform the same experiment using an Inverse Gamma Control variate, which is more in line with the distribution of the jumps. Given an Inverse Gamma distribution, with density

$$f_{I\Gamma}(x) = \frac{\hat{\mu}^{\hat{\nu}}}{\Gamma(\hat{\nu})} x^{-\hat{\nu}-1} e^{-\hat{\mu}/x} \mathbf{1}_{x \geq 0},$$

the corresponding price of a call option on the realized variance is

$$\hat{C}(K) = \frac{\hat{\mu}}{\hat{\nu} - 1} F(1/K; \hat{\nu} - 1, \hat{\mu}) - KF(1/K; \hat{\nu}, \hat{\mu}).$$

The parameters can be chosen by matching the first two moments in an analogous way as before

$$\hat{\nu} = \frac{1}{e^{\hat{\sigma}^2 T} - 1} + 2$$
$$\hat{\mu} = \mathbb{E}[V_T](\hat{\nu} - 1).$$

The numerical results are analogous to those obtained in the previous case and are shown in Figure 3.10 and Figure 3.12, corresponding to the case $\hat{\sigma} = 1$.

Remark 3.4.1. *The control variates applied above help eliminate discontinuities in zero, see Drimus [51]. However, further discontinuities might be introduced when implementing the codes in Matlab, e.g., when evaluating logarithms or Bessel functions in the complex domain. This is a possible explanation of why in the numerical experiments above the control variate performs poorly. Observe also that when applying Inverse Gamma control variates, additional discontinuities could be created by the presence of an additional Bessel function in the Laplace transform of the Inverse Gamma control variate.*

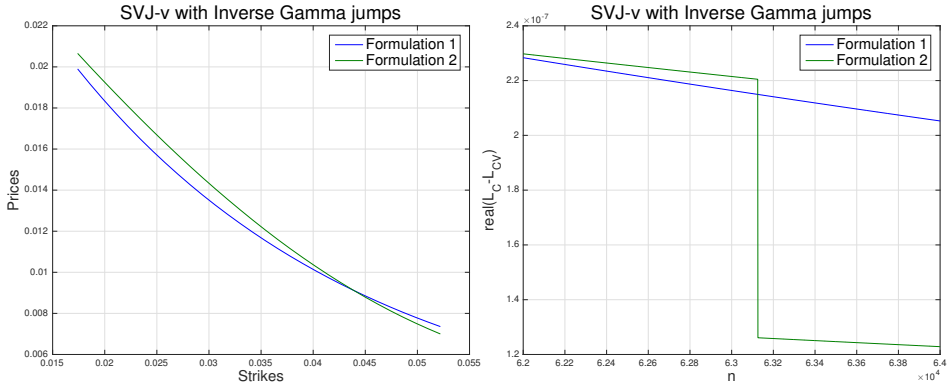

Figure 3.9: *On the left, prices of call options on V_T in the SVJ-v model with Inverse Gamma jumps, $T = 1$ year, $v_0 = 0.0348$, $\lambda = 1.15$, $\theta = 0.0218$, $\sigma = 0.3788$, $\nu = 4.8$, $\mu = 0.02$, $l = 1.5$. Prices are computed using the two formulations, applying the Bromwich-trapezoidal rule with $b = 0.1$, $h = 0.01$ and making use of a Gamma control variate. On the right, real part of $\mathscr{L}_{C-\hat{C}}(u)$ evaluated in $b + inh$ with $b = 0.1$, $h = 0.01$.*

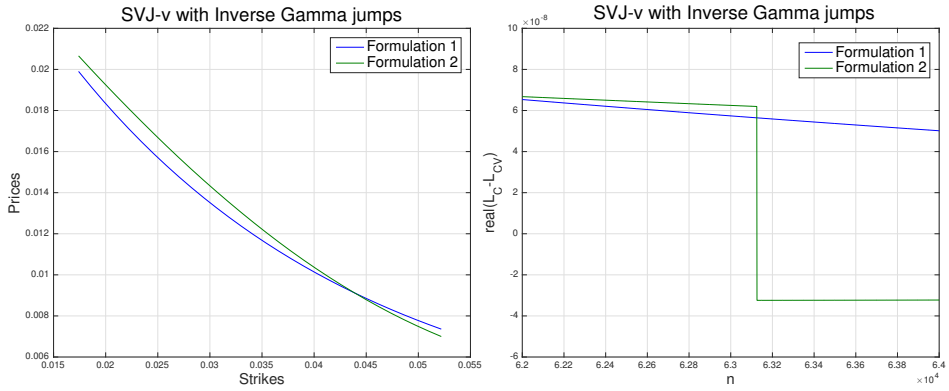

Figure 3.10: *On the left, prices of call options on V_T in the SVJ-v model with Inverse Gamma jumps, $T = 1$ year, $v_0 = 0.0348$, $\lambda = 1.15$, $\theta = 0.0218$, $\sigma = 0.3788$, $\nu = 4.8$, $\mu = 0.02$, $l = 1.5$. Prices are computed using the two formulations, applying the Bromwich-trapezoidal rule with $b = 0.1$, $h = 0.01$ and making use of an Inverse Gamma control variate. On the right, real part of $\mathscr{L}_{C-\hat{C}}(u)$ evaluated in $b + inh$ with $b = 0.1$, $h = 0.01$.*

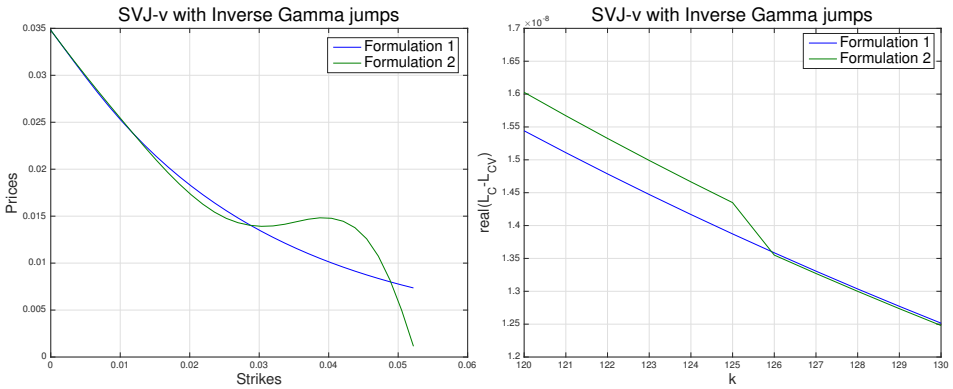

Figure 3.11: *On the left, prices of call options on V_T in the SVJ-v model with Inverse Gamma jumps, $T = 1$ year, $v_0 = 0.0348$, $\lambda = 1.15$, $\theta = 0.0218$, $\sigma = 0.3788$, $\nu = 4.8$, $\mu = 0.02$, $l = 1.5$. Prices are computed using the two formulations, applying Iseger's algorithm with $n = 16$, and making use of a Gamma control variate. On the right, real part of $\mathscr{L}_{C-\hat{C}}(u)$ evaluated in $\frac{a+i\lambda_j+2i\pi k/M_2}{\Delta}$, $M_2 = 256$, $a = 0.1719$, $j = 1$.*

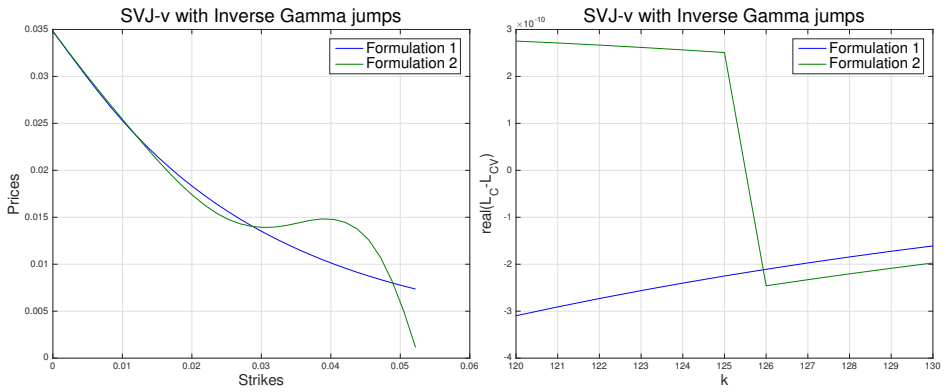

Figure 3.12: *On the left, prices of call options on V_T in the SVJ-v model with Inverse Gamma jumps, $T = 1$ year, $v_0 = 0.0348$, $\lambda = 1.15$, $\theta = 0.0218$, $\sigma = 0.3788$, $\nu = 4.8$, $\mu = 0.02$, $l = 1.5$. Prices are computed using the two formulations, applying Iseger's algorithm with $n = 16$, and making use of an Inverse Gamma control variate. On the right, real part of $\mathscr{L}_{C-\hat{C}}(u)$ evaluated in $\frac{a+i\lambda_j+2i\pi k/M_2}{\Delta}$, $M_2 = 256$, $a = 0.1719$, $j = 1$.*

3.5 Adding jumps in the asset price dynamics

In this section we introduce an extension of the model in (3.21) where we add jumps to the asset price dynamics. This allows for a better fit of the short term implied volatility from equity options. The joint dynamics of the log-price and the instantaneous variance under this model are given by

$$\begin{aligned} dX_t &= (-\gamma m_J - \tfrac{1}{2}v_t)dt + \sqrt{v_t}dW_t + dJ_t^S \\ dv_t &= \lambda(\theta - v_t)dt + \sigma\sqrt{v_t}dB_t + dJ_t^V \end{aligned} \tag{3.29}$$

where

$$\begin{aligned} J_S &= \textstyle\sum_{i=1}^{N(t)} Z_i^S, \quad Z_i^S \sim i.i.d.\ Z^S \\ J_V &= \textstyle\sum_{i=1}^{N(t)} Z_i^V, \quad Z_i^V \sim i.i.d.\ Z^V \end{aligned}$$

with $N(t)$ Poisson process with intensity l. We keep all the hypotheses made when introducing the model in (3.21), including the Inverse Gamma as distribution of the jump size Z^V, whereas Z^S follows a normal distribution $\mathscr{N}(m, v^2)$ with density

$$f_{\mathscr{N}}(x) = \frac{1}{\sqrt{2\pi v^2}} e^{-\frac{(x-m)^2}{v^2}}.$$

Finally,

$$m_J = e^{m+\frac{1}{2}v^2} - 1$$

is the compensator. Note that the same Poisson process is considered for jumps in the log-price and jumps in the instantaneous variance, meaning that they occur simultaneously. This is in line with the existing literature (Sepp [100], Eraker [55]). The model in (3.29) can be considered an alternative to the model in Sepp [100], the only difference being an Inverse Gamma distribution for J_V rather than an exponential distribution. As in Sepp [100], we do not assume any correlation between the volatility and the asset return jumps, as opposed to Duffie et al. [53]. Under the dynamics in (3.29) the realized variance presents a further component due to jumps in X_t

$$V_T = \frac{1}{T}\left(\int_0^T v_t dt + \sum_{i=1}^{N(T)} (Z_i^S)^2\right) \tag{3.30}$$

(see e.g., Sepp [100]). Nonetheless, an explicit expression for the Laplace transform of V_T is available in this case as well, and it is given by

$$\mathscr{L}_V(u) = \mathbb{E}[e^{-uV_T}] = e^{\alpha_1(u,T)+\beta_1(u,T)\,v_0+\delta(u,T)}\,, u \geq 0 \tag{3.31}$$

with functions $\alpha_1(u,t)$ and $\beta_1(u,t)$ as below

$$\begin{aligned}
\beta_1(u,t) &= \tfrac{1-e^{-\gamma(u)t}}{c_1(u)+d_1(u)e^{-\gamma(u)t}} \\
\alpha_1(u,t) &= -\tfrac{2\lambda\theta}{\sigma^2}\log\tfrac{c_1(u)+d_1(u)e^{-\gamma(u)t}}{c_1(u)+d_1(u)} + \tfrac{\lambda\theta t}{c_1(u)} + \int_0^t \kappa_J(-\beta_1(u,s))ds \\
\delta(u,t) &= lt\left[\tfrac{e^{-\frac{um^2}{T+2v^2u}}}{\sqrt{2v^2u/T+1}} - 1\right]
\end{aligned}$$

with k_J as in equation (3.24) and $c_1(u) = \frac{\lambda+\gamma(u)}{-2u/T}$, $d_1(u) = \frac{\lambda-\gamma(u)}{2u/T}$ and $\gamma(u) = \sqrt{\lambda^2 + 2\sigma^2 u/T}$. Again, we can substitute α_1, β_1 with α_2, β_2 in (3.28) thus obtaining an alternative expression of the Laplace transform, which however may lead to discontinuities, especially for long maturities. This is shown for example in Figure 3.13 corresponding to prices with maturity of 1 year and parameters $v_0 = 0.0317$, $\lambda = 3.2501$, $\theta = 0.0179$, $\sigma = 0.2897$, $\nu = 3.8$, $\mu = 0.1728$, $m = -0.1$, $v = 0.1$, $l = 1.0727$. These are obtained from the parameters in Sepp [100], by fixing $\nu = 3.8$, computing μ by matching the first moment with that of the exponential distribution in [100] and keeping all the other parameters unchanged.

The analysis of the previous chapters can be easily extended to this case, where further discontinuities potentially arise due to the square root in the Laplace transform of the asset-jumps.

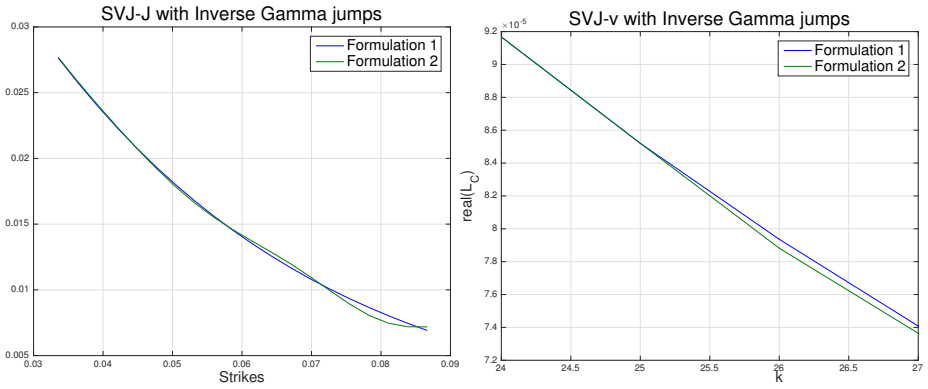

Figure 3.13: *On the left, prices of call options on V_T in the SVJ-J model with Inverse Gamma jumps, $T = 1$ year, $v_0 = 0.0317$, $\lambda = 3.2501$, $\theta = 0.0179$, $\sigma = 0.2897$, $\nu = 3.8$, $\mu = 0.1728$, $m = -0.1$, $v = 0.1$, $l = 1.0727$. Prices are computed using the two formulations, applying Iseger's algorithm with $n = 16$, and making use of a Gamma control variate. On the right, real part of $\mathscr{L}_{C-\hat{C}}(u)$ evaluated in $\frac{a+i\lambda_j+2i\pi k/M_2}{\Delta}$, $M_2 = 256$, $a = 0.1719$, $j = 1$.*

Table 3.1: *Summary of our numerical experiments*

Bromwich-trapezoidal rule	Weeks' algorithm	Iseger's algorithm
Sensitivity to discontinuities		Sensitivity to discontinuities
Sensitivity to h		
	Issues for $T < 3M$	

Table 3.2: *Parameters providing good results in our experiments with Formulation 1*

Brom-trap. rule with Euler	Weeks' algorithm	Iseger's algorithm
$A = 19$	$r = (0.1)^{4/n}$ or $r = (0.1)^{6/n}$	$n = 16$
$L = 1$	$\ell = 1$	$M = 32$
$m = 11$	$N = 10^3$	
$n = 38$		

3.6 Conclusions

We provided a description of some algorithms for the inversion of Laplace transforms and we investigated their performance in the context of pricing of realized variance call-options, showing numerical issues that may appear when using these methods. The algorithms investigated are the Bromwhich-trapezoidal rule [2], Weeks' algorithm [107] and Iseger's algorithm [79], whereas the model considered is a generalization of the Heston stochastic volatility model including jumps in the instantaneous variance dynamics.

First of all, we showed that (theoretically) equivalent expressions of the Laplace transform of the realized variance may lead to different option prices. This is due to the fact that depending on the particular expression we use, discontinuities may appear because of the presence of the complex logarithm, and in the case with Inverse Gamma jumps, because of complex square roots as argument of Bessel functions. The numerical experiments performed showed that both the Bromwich-trapezoidal rule and Iseger's algorithm are really sensitive to different formulations of the Laplace transform of the realized variance. On the other hand, Weeks' algorithm seems to overcome discontinuities.

Afterwards, we analyzed the performance of the different algorithms when using a formulation of the Laplace transform which seems not to lead to discontinuities. In the case of the Bromwich-trapezoidal rule we observed some sensitivity to the parameter h in the algorithm, whereas for Weeks' algorithm numerical issues appear for short maturities. Finally, Iseger's algorithm performs well. The results of our numerical investigations are summarized in Table 3.1.

Lastly, we showed that a control variate technique which might potentially help overcoming discontinuities of the Laplace transform, does not work in our case. Indeed, this technique helps eliminating discontinuities of the call-price Laplace transform in zero, but do not eliminate discontinuities in the Laplace transform of the realized variance.

In the paper we focussed on the case where jumps are allowed in the instantaneous variance only. Similar numerical issues also appear when jumps are included both in the dynamics of the log-price and of the instantaneous variance.

In conclusion, before applying a Laplace transform method, it is fundamental to verify whether there are discontinuities in the Laplace transform, check the

accuracy of the algorithm and compare with prices obtained by other methods, such as Monte Carlo simulations. In fact, an inaccurate use of inversion methods might lead to wrong option prices. On the other hand, by properly choosing an inversion algorithm and optimizing it (e.g., choosing opportune parameters, introducing some damping factor in order to eliminate discontinuities), it is possible to obtain efficient and reliable methods for the inversion of Laplace transforms. Having reliable inversion algorithms is important not only for pricing but also for risk management purposes. Indeed, as observed e.g., in Drimus [51], realized variance options can naturally be hedged by variance swaps (see also Carr and Lee [36]). The corresponding deltas can be easily computed by inversion methods, as long as the Laplace transform of the call price can be differentiated in closed form. This is the case for the model considered in this paper.

It is left for future work to investigate, from a theoretical point of view, the stability of the different expressions of the Laplace transform of the realized variance. This could be done in a similar fashion as in Albrecher et al. [6], who investigate stability of the characteristic function of the log-asset price in the Heston model. Our guess is that a similar lenghtly calculation could be readapted to the case of realized variance options in the Heston model, whereas the same proof in the case of jumps, might potentially be too difficult or not applicable. Finally, it could also be interesting to check whether possible discontinuities can be avoided using a rotation-count algorithm, as that one in Kahl and Jäckel [81], of which a deep analysis can be found in Lord and Kahl [91].

Chapter 4

The Multivariate Mixture Dynamics Model: Shifted dynamics and correlation skew

The Multivariate Mixture Dynamics Model: Shifted dynamics and correlation skew

Damiano Brigo
Dept. of Mathematics, Imperial College, London

Camilla Pisani
Dept. of Economics and Business Economics, Aarhus University

Francesco Rapisarda [1]
Bloomberg

Abstract

The Multi Variate Mixture Dynamics Model is a tractable, dynamical, arbitrage-free multivariate model characterized by transparency in the dependence structure, since closed form formulae for terminal correlations, average correlations and copula functions are available. It also allows for complete decorrelation between assets and instantaneous variances. Each single asset is modelled according to a lognormal mixture dynamics model and this univariate version is widely used in the industry due to its flexibility and accuracy. The same property holds for the multivariate process of all assets whose density is a mixture of multivariate basic densities. This allows for consistency of single asset and index/portfolio smile.

In this paper, we generalize the MVMD model by introducing shifted dynamics and we propose a definition of implied correlation in this model. We investigate whether the model is able to consistently reproduce the implied volatility of FX cross rates once the single components are calibrated to

[1]This paper solely reflects the author's personal opinion and does not represent the opinions of the author's employers, present and past, in any way.

univariate shifted lognormal mixture dynamics models. We compare the performance of the shifted MVMD model in terms of implied correlation with those of the shifted Simply Correlated Mixture Dynamics model where the dynamics of the single assets are naively connected by introducing correlation among their Brownian motions. Finally, we introduce a model with uncertain volatilities and correlation. The Markovian projection of this model is a generalization of the shifted MVMD model.

4.1 Introduction to the Multivariate Mixture Dynamics

The Multi Variate Mixture Dynamics model (MVMD) introduced by Brigo, Mercurio and Rapisarda [28] and recently described in a deeper way in Brigo, Rapisarda and Sridi [29] is a tractable dynamical arbitrage-free model defined as the multidimensional version of the lognormal mixture dynamics model (LMD) in [24] and [25] (see also [27]). The single-asset LMD model is a no-arbitrage model widely used among practitioners because of its practical advantages in calibration and pricing (analytical formulae for European options, explicit expression for the local volatility) and of its flexibility and accuracy. In fact, a variant of this model is presently used in the calibration of implied volatility surfaces for single stocks and equity indices in the Bloomberg terminal [23], and in the subsequent pricing of European, American and path-dependent options on single assets and baskets of assets. The main advantage of the MVMD over other multidimensional models, such as e.g., the Wishart model ([46] and [69]) is in its tractability and flexibility which allows the MVMD to calibrate index volatility smiles consistently with the univariate assets smiles. In addition, a full description of its dependence structure (terminal correlations, average correlations, copula functions) is available.

The MVMD model also enjoys some interesting properties of Markovian projection. First of all, the model can be seen as a Markovian projection of a model with uncertain volatilities denominated MUVM model. As a consequence, European option prices under the MVMD model can more easily be computed under the MUVM model instead. However, the MVMD model remains superior in terms of smoothness and dynamics. Secondly, the Geometric average basket under the

MVMD model can be projected into a univariate lognormal mixture dynamics model. Consequently, European option prices on the basket can be easily computed through the Black and Scholes formula.

Finally, under the MVMD model, the terminal correlation between assets and squared volatilities is zero. This mitigates the common drawback of local volatility models of having perfect instantaneous correlation between assets and squared volatilities.

In this paper we generalize the MVMD model, including shifts to the dynamics of the single assets, and we study the correlation skew under this framework.

Before going into details, we recapitulate the definition of the MVMD model (in the non-shifted case), starting with the univariate LMD model and then generalizing to the multidimensional case.

The volatility smile mixture dynamics model for single assets

Given a maturity $T > 0$, we denote by $P(0,T)$ the price at time 0 of the zero-coupon bond maturing at T, and by $(\Omega, \mathscr{F}, \mathbb{P})$ a probability space with a filtration $(\mathscr{F}_t)_{t\in[0,T]}$ which is $\mathbb{P}$-complete and satisfying to the usual conditions. We assume the existence of a measure $\mathbb{Q}$ equivalent to $\mathbb{P}$, called the risk–neutral or pricing measure, ensuring arbitrage freedom in the classical setup, for example, of Harrison, Kreps and Pliska [75, 76]. In this framework we consider N purely *instrumental* diffusion processes $Y^i(t)$ with dynamics

$$dY^i(t) = \mu Y^i(t)dt + v^i(t, Y^i(t))Y^i(t)dW(t) \tag{4.1}$$

and a deterministic initial value $Y^i(0)$, marginal densities p_t^i and diffusion coefficient v_i. We define S_t as the solution of

$$dS(t) = \mu S(t)dt + s(t, S(t))S(t)dW(t) \tag{4.2}$$

where s is a local volatility function, namely a deterministic function of t and S only, and it is computed so that the marginal density p_t of $S(t)$ is a linear convex combination of the densities p_t^i [24, 25, 26]:

$$p_t = \sum_i \lambda^i p_t^i \text{ with } \lambda^i \geq 0, \forall i \text{ and } \sum_i \lambda^i = 1. \tag{4.3}$$

In what follows we restrict ourselves to the case

$$\begin{cases} Y^i(0) & = S(0), \\ v_i(t,x) & = \sigma^i(t), \\ V^i(t) & = \sqrt{\int_0^t \sigma^i(s)^2 ds} \\ p_t^i(x) & = \frac{1}{\sqrt{2\pi}xV^i(t)} \exp\left[-\frac{1}{2V_i^2(t)}\left(\ln\left(\frac{x}{S(0)}\right) - \mu t + \frac{1}{2}V^i(t)^2\right)^2\right] = \ell_t^i(x) \end{cases} \tag{4.4}$$

with σ^i deterministic. The parameter μ is completely specified by $\mathbb{Q}$. If the asset is a stock paying a continuous dividend yield q and r is the time T constant risk-free rate, then $\mu = r - q$. If the asset is an exchange rate and r_d and r_f are the (deterministic) domestic and foreign rates at time T, respectively, then $\mu = r_d - r_f$. If the asset is a forward price, then $\mu = 0$.

Brigo and Mercurio [25] proved that defining

$$s(t,x) = \left(\frac{\sum_{k=1}^N \lambda^k \sigma^k(t)^2 \ell_t^k(x)}{\sum_{k=1}^N \lambda^k \ell_t^k(x)}\right)^{1/2} \tag{4.5}$$

and assuming a few additional nonstringent assumptions on the σ_i, the corresponding dynamics for S_t admits a unique strong solution.

Theorem 4.1.1. ***Existence and uniqueness of solutions for the LMD model****. Assume that all the real functions $\sigma^i(t)$, defined on the real numbers $t \geq 0$, are once continuously differentiable and bounded from above and below by two positive real constants. Assume also that in a small initial time interval $t \in [0, \epsilon]$, $\epsilon > 0$, the functions $\sigma^i(t)$ have an identical constant value σ_0. Then the Lognormal Mixture Dynamics model (LMD) defined by*

$$dS_t = \mu S_t dt + s(t, S_t) S_t dW_t, \quad S_0, \quad s(t,x) = \left(\frac{\sum_{k=1}^N \lambda^k \sigma^k(t)^2 \ell_t^k(x)}{\sum_{k=1}^N \lambda^k \ell_t^k(x)}\right)^{1/2}, \tag{4.6}$$

admits a unique strong solution and the forward Kolmogorov equation (Fokker Planck equation) for its density admits a unique solution satisfying (4.3)*, which is a mixture of lognormal densities.*

An important consequence of the above construction is that European option prices on S can be written as linear combinations of Black-Scholes prices with weights λ_i. The same combination holds for the Greeks at time 0.

Combining mixture dynamics on several assets: SCMD

Consider now, n different asset prices $S_1 \dots S_n$ each calibrated to an LMD model as in equation (4.6), and denote by λ_i^k, σ_i^k the parameters relative to the k-th instrumental process of the asset i. There are two possible ways in order to combine the dynamics of the single assets into a multivariate model. The first more immediate way consists in introducing a non-zero quadratic covariation between the Brownian motions driving the LMD models of equation (4.6) for $S_1 \dots S_n$ leading to the so-called SCMD model.

Definition 4.1.2. ***The SCMD Model.*** *We define the Simply Correlated Multivariate Mixture Dynamics (SCMD) model for $\underline{S} = [S_1, \dots, S_n]$ as a vector of univariate LMD models, each satisfying Theorem 4.1.1 with diffusion coefficients $s_1, \dots, s_n$ given by equation* (4.6) *and densities $\ell_1, \dots, \ell_n$ applied to each asset, and connected simply through quadratic covariation ρ_{ij} between the Brownian motions driving assets i and j. This is equivalent to the following n-dimensional diffusion process where we keep the Ws independent and where we embed the Brownian covariation into the diffusion matrix $\bar{C}$, whose i-th row we denote by $\bar{C}_i$:*

$$d\underline{S}(t) = diag(\underline{\mu})\underline{S}(t)dt + diag(\underline{S}(t))\bar{C}(t, \underline{S}(t))d\underline{W}(t), \quad \bar{a}_{i,j}(t, \underline{S}) := \bar{C}_i \bar{C}_j^T \tag{4.7}$$

$$\bar{a}_{i,j}(t, \underline{S}) = s_i(t, S_i)s_j(t, S_j)\rho_{ij} = \begin{pmatrix} \frac{\sum_{k=1}^N \lambda_i^k \sigma_i^k(t)^2 \ell_{i,t}^k(S_i)}{\sum_{k=1}^N \lambda_i^k \ell_{i,t}^k(S_i)} & \frac{\sum_{k=1}^N \lambda_j^k \sigma_j^k(t)^2 \ell_{j,t}^k(S_j)}{\sum_{k=1}^N \lambda_j^k \ell_{j,t}^k(S_j)} \end{pmatrix}^{1/2} \rho_{ij} \tag{4.8}$$

where T represents the transposition operator.

Assumption. We assume $\rho = (\rho_{ij})_{i,j}$ to be positive definite.

It is evident from the previous construction that the SCMD is consistent with both the dynamics of the single assets S_i and the instantaneous correlation matrix ρ. Moreover, we can easily simulate a path of S by exogenously computing ρ for example from historical data, assuming it constant over time and applying a naive Euler scheme. However, an explicit expression for the density of $\underline{S} = [S_1, \dots, S_n]$ under the SCMD dynamics is not available. As a consequence, if we aim at computing prices of options whose payoff depends on the value at time T only we still need to simulate entire paths of $\underline{S}$ over the interval $[0, T]$, which can be quite time consuming.

Lifting the mixture dynamics to asset vectors: MVMD

A different approach, still consistent with the single assets' dynamics, lies in merging the dynamics of the single assets in such a way that the mixture property is lifted to the multivariate density and the corresponding model gains some further tractability property with respect to the SCMD model. This can be achieved by mixing the densities of the instrumental processes of each individual asset in all possible ways and by imposing the correlation structure ρ at the level of the single instrumental processes, rather than of the assets as we did for the SCMD model. This has important consequences for the actual structure of the correlation, see [28]. Below we summarize the construction leading to the MVMD model, while referring to Brigo et al. [29] for further details.

Assume we have calibrated an LMD model for each $S_i(t)$. If $p_{S_i(t)}$ is the density of S_i, we write

$$p_{S_i(t)}(x) = \sum_{k=1}^{N_i} \lambda_i^k \ell_{i,t}^k(x), \text{ with } \lambda_i^k \geq 0, \forall k \text{ and } \sum_k \lambda_i^k = 1 \tag{4.9}$$

where $(\ell_{i,t}^k)_k$ are the densities of $(Y_i^k)_k$, instrumental processes for S_i evolving lognormally according to the stochastic differential equation:

$$dY_i^k(t) = \mu_i Y_i^k(t)dt + \sigma_i^k(t)Y_i^k(t)dZ_i(t), \quad d\langle Z_i, Z_j\rangle_t = \rho_{ij}dt, \quad Y_i^k(0) = S_i(0). \tag{4.10}$$

For notational simplicity we assume the number of base densities N_i to be the same, N, for all assets. The exogenous correlation structure ρ_{ij} is given by the symmetric, positive–definite matrix ρ.

Denote by $\underline{S}(t) = [S_1(t), \cdots, S_n(t)]^T$ the vector of asset prices with

$$d\underline{S}(t) = diag(\underline{\mu})\underline{S}(t)dt + diag(\underline{S}(t))C(t, \underline{S}(t))d\underline{W}(t). \tag{4.11}$$

As we did for the one dimensional case, we look for a matrix C such that

$$p_{\underline{S}(t)}(\underline{x}) = \sum_{k_1,k_2,\cdots k_n=1}^{N} \lambda_1^{k_1} \cdots \lambda_n^{k_n} \ell_{1,\ldots,n;t}^{k_1,\ldots,k_n}(\underline{x}), \qquad \ell_{1,\ldots,n;t}^{k_1,\ldots,k_n}(\underline{x}) := p_{\left[Y_1^{k_1}(t),\ldots,Y_n^{k_n}(t)\right]^T}(\underline{x}), \tag{4.12}$$

or more explicitly

$$\ell_{1,\ldots,n;t}^{k_1,\ldots,k_n}(\underline{x}) = \frac{1}{(2\pi)^{\frac{n}{2}}\sqrt{\det \Xi^{(k_1\cdots k_n)}(t)}\Pi_{i=1}^n x_i} \qquad \exp\left[-\frac{\tilde{x}^{(k_1\cdots k_n)T}\Xi^{(k_1\cdots k_n)}(t)^{-1}\tilde{x}^{(k_1\cdots k_n)}}{2}\right]$$

where $\Xi^{(k_1\cdots k_n)}(t)$ is the integrated covariance matrix whose (i,j) element is

$$\Xi_{ij}^{(k_1\cdots k_n)}(t) = \int_0^t \sigma_i^{k_i}(s)\sigma_j^{k_j}(s)\rho_{ij}ds \tag{4.13}$$

and

$$\tilde{x}_i^{(k_1\cdots k_n)} = \ln x_i - \ln x_i(0) - \mu_i t + \int_0^t \frac{\sigma_i^{k_i^2}(s)}{2}ds. \tag{4.14}$$

Computations show that if a solution exists, it must satisfy the definition below.

Definition 4.1.3. ***The MVMD Model.*** *The (lognormal) Multi Variate Mixture Dynamics (MVMD) model is given by*

$$\begin{aligned} d\underline{S}(t) &= diag(\underline{\mu})\ \underline{S}(t)\ dt + diag(\underline{S}(t))\ C(t,\underline{S}(t))B\ d\underline{W}(t), \qquad (4.15)\\ C_i(t,\underline{x}) &:= \frac{\sum_{k_1,\ldots,k_n=1}^N \lambda_1^{k_1}\ldots\lambda_n^{k_n}\ \sigma_i^{k_i}(t)\ \ell_{1,\ldots,n;t}^{k_1,\ldots,k_n}(\underline{x})}{\sum_{k_1,\ldots,k_n=1}^N \lambda_1^{k_1}\ldots\lambda_n^{k_n}\ \ell_{1,\ldots,n;t}^{k_1,\ldots,k_n}(\underline{x})}, \end{aligned}$$

$\ell_{1,\ldots,n;t}^{k_1,\ldots,k_n}(\underline{x}) := p_{\left[Y_1^{k_1}(t),\ldots,Y_n^{k_n}(t)\right]^T}(\underline{x})$ *and defining* B *such that* $\rho = BB^T$, $a = CB(CB)^T$,

$$a_{i,j}(t,\underline{x}) = \frac{\sum_{k_1,\ldots,k_n=1}^N \lambda_1^{k_1}\ldots\lambda_n^{k_n}\ V^{k_1,\ldots,k_n}(t)\ \ell_{1,\ldots,n;t}^{k_1,\ldots,k_n}(\underline{x})}{\sum_{k_1,\ldots,k_n=1}^N \lambda_1^{k_1}\ldots\lambda_n^{k_n}\ \ell_{1,\ldots,n;t}^{k_1,\ldots,k_n}(\underline{x})} \tag{4.16}$$

where

$$V^{k_1,\ldots,k_n}(t) = \left[\sigma_i^{k_i}(t)\ \rho_{i,j}\ \sigma_j^{k_j}(t)\right]_{i,j=1,\ldots,n}. \tag{4.17}$$

From the previous definitions it is evident that the dynamics of the single assets S_i in the SCMD model are Markovian. On the other hand, in the MVMD model, while the dynamics of the whole vector S is Markovian, those of the single assets are not. This leads to more realistic dynamics.

Under mild assumptions, the existence and uniqueness of a solution can be proved through the following Theorem.

Theorem 4.1.4. *Assume that the volatilities* $\sigma_i^{k_i}(t)$ *for all* i *are once continuously differentiable, uniformly bounded from below and above by two positive real numbers* $\tilde{\sigma}$ *and* $\hat{\sigma}$*, respectively, and that they take a common constant value* σ_0 *for* $t \in [0,\epsilon]$

for a small positive real number ϵ, namely

$$\tilde{\sigma} = \inf_{t\geq 0}\left(\min_{i=1\cdots n, k_i=1,\cdots N} (\sigma_i^{k_i}(t))\right),$$
$$\hat{\sigma} = \sup_{t\geq 0}\left(\max_{i=1\cdots n, k_i=1\cdots N} (\sigma_i^{k_i}(t))\right),$$
$$\sigma_i^{k_i}(t) = \sigma_0 > 0 \quad \textit{for all} \quad t \in [0,\epsilon].$$

Also assume the matrix ρ to be positive definite. Then the MVMD n-dimensional stochastic differential equation (4.15) admits a unique strong solution. The diffusion matrix $a(t,\underline{x})$ in (4.16) is positive definite for all t and x.

4.2 Introducing a shift in MVMD

When modelling a one dimensional asset price through an LMD model, implied volatilities with minimum exactly at a strike equal to the forward asset price are the only possible outcome. In order to gain greater flexibility and therefore move the smile minimum point from the ATM forward, we can shift the overall density by a deterministic function of time, carefully chosen in order to preserve risk–neutrality and therefore guarantee no–arbitrage. This is the so–called *shifted lognormal mixture dynamics model* [26]. Under this model the new asset price process S is defined as

$$S_t = \beta e^{\mu t} + X_t \tag{4.18}$$

with β real constant and X_t satisfying (4.6). Under the assumption $K - \beta e^{\mu T} > 0$, the price at time 0 of a European call option with strike K and maturity T can be written as

$$P(0,T)\mathbb{E}^T\{(S_T - K)^+\} = P(0,T)\mathbb{E}^T\{(X_T - [K - \beta e^{\mu T}])^+\} \tag{4.19}$$

and thus, as a combination of Black and Scholes prices with strike $K - \beta e^{\mu T}$. The model therefore preserves the same level of tractability as in the non-shifted case with the advantage of gaining more flexibility.

Once each asset is calibrated to a shifted LMD model, we have two possibilities for reconstructing the dynamics of the multidimensional process. The first possibility is to reconnect the single assets by introducing a non-zero quadratic covariation

between the Brownian motions (as we did for the SCMD model), leading to what we call the *shifted SCMD model*. The second possibility going on the same lines as the approach leading to the MVMD model, lies in applying the same shift $\beta_i e^{\mu_i t}$ to each instrumental process Y_i^k of each asset X_i

$$S_i^k(t) = Y_i^k(t) + \beta_i e^{\mu_i t}$$

where Y_i^k satisfies the dynamics in (4.10) (this is equivalent to applying the shift $\beta_i e^{\mu_i t}$ directly to the i-th asset) and then mix the corresponding densities $p_{S_i^k(t)}(x)$ in all possible ways. Computations similar to those for the non-shifted case show that if a solution exists, it must satisfy the definition below (details on the computations are shown in the Appendix).

Definition 4.2.1. ***The Shifted MVMD Model.*** *The shifted Multi Variate Mixture Dynamics model is given by*

$$\begin{aligned} d\underline{S}(t) &= diag(\underline{\mu})\underline{S}(t)dt + diag(\underline{S}(t))\widetilde{C}(t,\underline{S}(t))Bd\underline{W}(t), \qquad (4.20)\\ \widetilde{C}_i(t,\underline{x}) &:= \frac{\sum_{k_1,\ldots,k_n=1}^N \lambda_1^{k_1}\ldots\lambda_n^{k_n}\ \sigma_i^{k_i}(t)(x_i-\beta_i e^{\mu_i t})\ \tilde{\ell}_{1,\ldots,n;t}^{k_1,\ldots,k_n}(\underline{x})}{x_i\sum_{k_1,\ldots,k_n=1}^N \lambda_1^{k_1}\ldots\lambda_n^{k_n}\ \tilde{\ell}_{1,\ldots,n;t}^{k_1,\ldots,k_n}(\underline{x})}, \end{aligned}$$

$$\tilde{\ell}_{1,\ldots n;t}^{k_1,\ldots,k_n}(\underline{x}) = p_{[S_1^{k_1}(t),\ldots,S_n^{k_n}(t)]^T}(\underline{x}) = \ell_{1,\ldots,n;t}^{k_1,\ldots,k_n}(\underline{x}-\underline{\beta}e^{\underline{\mu}t}) \qquad (4.21)$$

and defining B such that $\rho = BB^T$, $\tilde{a} = \widetilde{C}B(\widetilde{C}B)^T$,

$$\tilde{a}_{ij}(t,\underline{x}) = \frac{\sum_{k_1,k_2,\ldots k_n=1}^N \lambda_1^{k_1}\cdots\lambda_n^{k_n}\ V^{k_1,\ldots,k_n}(t)(x_i-\beta_i e^{\mu_i t})(x_j-\beta_j e^{\mu_j t})\tilde{\ell}_{1,\ldots n;t}^{k_1,\ldots,k_n}(\underline{x})}{x_i x_j\sum_{k_1,k_2,\ldots k_n=1}^N \lambda_1^{k_1}\cdots\lambda_n^{k_n}\tilde{\ell}_{1,\ldots n;t}^{k_1,\ldots,k_n}(\underline{x})} \qquad (4.22)$$

with $V^{k_1,\ldots,k_n}$ as in (4.17).

We now have all the instruments to introduce the correlation skew and study its behaviour under shifted SCMD and shifted MVMD dynamics.

4.3 The correlation skew

The aim of this section is to introduce a definition of *correlation skew* and to study its behaviour under shifted MVMD dynamics in comparison with the correlation

skew under shifted SCMD dynamics. It is observed in practice under normal market conditions that assets are relatively weakly correlated with each other. However, during periods of market stress stronger correlations are observed. This fact suggests that a single correlation parameter for all options quoted on a basket of assets, or an index, say, may not be sufficient to reproduce all option prices on the basket/index for a given expiry. In fact, this is what is observed empirically when inferring a multidimensional dynamics from a set of single–asset dynamics. Among others, this has been shown in Bakshi et al. [12] for options on the S&P 100 index and in Langnau [87] for options on the Euro Stoxx 50 index and on the DAX index.

When computing the implied volatility, European call prices (or equivalently put prices) are considered and the reference model is the benchmark Black & Scholes [22] model. It seems then natural to consider as a multidimensional benchmark a model where the single assets follow geometric Brownian motions and constant correlation among the single Brownian shocks is introduced. However, when moving from the one-dimensional to the multidimensional framework, a bigger variety of possible option instruments for comparing prices under the reference model and the model under analysis appears, the particular choice depending on the specific product we are interested in. Austing [10] recently provided a discussion of some of the most popular multi-assets products. He suggested the use of composite options as benchmark on which defining the implied correlation. In this paper we adopt a different approach based on the comparison with options on $S_1(t)$, $S_2(t)$ with payoff

$$(S_1(T)S_2(T) - K)^+ . \tag{4.23}$$

Assume that the pair (S_1, S_2) follows a bi-dimensional Black and Scholes model, in other words S_1 and S_2 follow two geometric Brownian motions with correlation ρ and consider the payoff in equation (4.23). Given the Black and Scholes implied volatilities for S_1 and S_2, the value ρ_{impl} such that prices under the bi-dimensional Black and Scholes model are the same as market prices

$$\text{MKT\_Prices}(S_1(0), S_2(0), K, T) = \text{BS\_Prices}(S_1(0), S_2(0), K, T, \rho_{impl}(K, T))$$

is called *implied correlation*. If we try to match option prices for a given maturity T and two different strikes K_1, K_2, we will observe two different values of the

implied correlation. This is contrary to the hypothesis of constant correlation in the bi-dimensional Black and Scholes model.

The curve $K \to \rho_{impl}(K,T)$ is called correlation skew. Thus, the correlation skew can be considered as a descriptive tool/metric similar to the volatility smile in the one-dimensional case, with the difference that it primarily describes implied dependence instead of volatility.

Explaining the skew in MVMD with the single parameter ρ via MUVM

The aim of this section is to introduce a definition of implied correlation under shifted MVMD dynamics, when using options with payoff as in equation (4.23). This leads to a straightforward application in the foreign exchange market within the study of triangular relationships. Imagine, for example, that S_1 and S_2 represent the exchange rates USD/EUR and EUR/JPY, respectively. The cross asset $S_3 = S_1 S_2$ then represents the USD/JPY exchange rate, and the corresponding payoff in equation (4.23) is the payoff of a call option on the USD/JPY FX rate. In the following, we will investigate whether the shifted MVMD model is able to consistently reproduce the implied volatility of S_3, once the single components S_1, S_2 are calibrated to univariate shifted LMD models. Consistency properties of this kind are important, for example, in order to reconstruct the time series of less liquid cross currency pairs from more liquid ones.

Before proceeding we make a remark on the interpretation of ρ. Keeping in mind the definition of instantaneous local correlation in a bivariate diffusion model

$$\rho_L(t) := \frac{d\langle S_1, S_2\rangle_t}{\sqrt{d\langle S_1, S_1\rangle_t \; d\langle S_2, S_2\rangle_t}}$$

and making use of Schwartz's inequality, we obtain that the absolute value of the local correlation under the shifted MVMD model is smaller than the value under the shifted SCMD model. The result is contained in the Proposition below.

Proposition 4.3.1 (Local correlation in the shifted MVMD and shifted SCMD)**.** *The instantaneous local correlation under the shifted SCMD model is ρ, whereas*

for the shifted MVMD model we have

$$\rho_L(t) = \frac{\rho \sum_{k,k'=1}^{N} {\lambda_1}^k {\lambda_2}^{k'} \sigma_1^{(k)} \sigma_2^{(k')} \tilde{\ell}_t^{(kk')}(x_1, x_2)}{\sqrt{\left(\sum_{k,k'=1}^{N} {\lambda_1}^k {\lambda_2}^{k'} \sigma_1^{(k)2} \tilde{\ell}_t^{(kk')}(x_1, x_2)\right)\left(\sum_{k,k'=1}^{N} {\lambda_1}^k {\lambda_2}^{k'} \sigma_2^{(k')2} \tilde{\ell}_t^{(kk')}(x_1, x_2)\right)}},$$

$|\rho_L(t)| \leq |\rho|$

where $\tilde{\ell}_t^{(kk')}(x_1, x_2)$ *is defined as in equation (4.21).*

We see that ρ enters the formula for the instantaneous local correlation ρ_L in the MVMD model, even though the latter is more complex than the constant value ρ. Our aim is to find a value of ρ which matches the prices of options with payoff as in equation (4.23) under shifted MVMD dynamics with market prices.

In order to do that we will make use of a model with uncertain parameters of which the shifted MVMD is a Markovian projection. Indeed, as shown in Brigo et al. [29], the MVMD model as in Definition 4.1.3 (without shift) is a Markovian projection of the model

$$d\xi_i(t) = \mu_i \ \xi_i(t)dt + \sigma_i^{I_i}(t) \ \xi_i(t)dZ_i(t), \quad i = 1, ..., n. \tag{4.24}$$

Each Z_i is a standard one dimensional Brownian motion with $d\langle Z_i, Z_j\rangle_t = \rho_{i,j}dt$, μ_i are constants, $\sigma^I := [\sigma_1^{I_1}, \ldots, \sigma_n^{I_n}]^T$ is a random vector independent of Z and representing uncertain volatilities with $I_1, \ldots, I_n$ being mutually independent. More specifically, each $\sigma_i^{I_i}$ takes values in a set of N deterministic functions σ_i^k with probability λ_i^k. Thus, for all times in $(\varepsilon, +\infty)$ with small ε we have

$$(t \longmapsto \sigma_i^{I_i}(t)) = \begin{cases} (t \longmapsto \sigma_i^1(t)) & \text{with } \mathbb{Q} \text{ probability } \lambda_i^1 \\ (t \longmapsto \sigma_i^2(t)) & \text{with } \mathbb{Q} \text{ probability } \lambda_i^2 \\ \vdots & \\ (t \longmapsto \sigma_i^N(t)) & \text{with } \mathbb{Q} \text{ probability } \lambda_i^N \end{cases}$$

Now, if we add a shift to each component as follows

$$\tilde{\xi}_i(t) = \xi_i(t) + \beta_i e^{\mu_i t}, \tag{4.25}$$

we obtain a model having the shifted MVMD model (4.20)-(4.22) as a Markovian projection. This can easily be shown by Gyöngy's lemma [74].

Theorem 4.3.2. *The shifted MVMD model is a Markovian projection of the shifted MUVM model.*

Proof. A straightforward application of Ito's lemma shows that $\tilde{\xi}(t)$ satisfies the system of SDEs

$$d\underline{\tilde{\xi}}(t) = diag(\underline{\mu})\ \underline{\tilde{\xi}}(t)\ dt + diag(\underline{\tilde{\xi}}(t) - \underline{\alpha}(t))\ A^I(t)\ d\underline{W}(t) \tag{4.26}$$

where $diag(\underline{\alpha}(t))$ is a deterministic matrix whose i-th diagonal element is the shift $\beta_i e^{\mu_i t}$ and $A^I(t)$ is the Cholesky decomposition of the covariance matrix $\Sigma^I_{i,j}(t) := \sigma_i^{I_i}(t)\sigma_j^{I_j}(t)\ \rho_{ij}$.

Define $\tilde{v}(t, \underline{\xi}(t)) = diag(\underline{\tilde{\xi}}(t) - \underline{\alpha}(t))A^I(t)$. In order to show that the MVMD model is a Markovian projection of the MUVM model, we need to show that

$$\mathbb{E}[\tilde{v}\tilde{v}^T|\underline{\tilde{\xi}}(t) = \underline{\tilde{x}}] = \tilde{\sigma}\ \tilde{\sigma}^T(t, \underline{x}) \tag{4.27}$$

where $\tilde{\sigma}(t, \underline{x}) = diag(\underline{x})\widetilde{C}(t, \underline{x})B$ and $\widetilde{C}$ is defined as in (4.20).

Observing that

$$\mathbb{E}[\tilde{v}\tilde{v}^T|\underline{\xi}(t) \in d\underline{x}] = \frac{\mathbb{E}[diag(\underline{\tilde{\xi}}(t) - \underline{\alpha}(t))\ \Sigma\ diag(\underline{\tilde{\xi}}(t) - \underline{\alpha}(t))\ 1_{\{\underline{\tilde{\xi}}(t) \in d\underline{x}\}}]}{\mathbb{E}[1_{\{\underline{\tilde{\xi}}(t) \in d\underline{x}\}}]} =$$

$$\frac{diag(\underline{x} - \underline{\alpha}(t)) \sum_{k_1,\ldots,k_n=1}^N \lambda_1^{k_1} \ldots \lambda_n^{k_n}\ V^{k_1,\ldots,k_n}(t) \tilde{\ell}^{k_1,\ldots,k_n}_{1,\ldots,n;t}(\underline{x})\ diag(\underline{x} - \underline{\alpha}(t))\ d\underline{x}}{\sum_{k_1,\ldots,k_n=1}^N \lambda_1^{k_1} \ldots \lambda_n^{k_n}\ \tilde{\ell}^{k_1,\ldots,k_n}_{1,\ldots,n;t}(\underline{x})\ d\underline{x}}$$

and performing simple matrix manipulations, equation (4.27) is easily obtained. □

Since we will infer the value of ρ from prices of options with payoff as in (4.23), depending on the value of (S_1, S_2) at time T only, we can make computations under the shifted MUVM rather than under the shifted MVMD, as these two models have the same one-dimensional (in time) distributions. Computations under the shifted MUVM model are easier to do (with respect to the shifted MVMD case) since conditioning on $\{I_i = j\}$, ξ_i follows a shifted geometric Brownian motion with volatility σ_i^j.

In particular we will focus on the bidimensional specification in which case the shifted MUVM reduces to

$$\begin{aligned} dS_1(t) &= \mu_1\ S_1(t)dt + \sigma_1^{I_1}(t)\ (S_1(t) - \beta_1 e^{\mu_1 t})dW_1(t) \\ dS_2(t) &= \mu_2\ S_2(t)dt + \sigma_2^{I_2}(t)\ (S_2(t) - \beta_2 e^{\mu_2 t})dW_2(t) \end{aligned} \tag{4.28}$$

where the Brownian motions W_1, W_2 have correlation ρ.

Once we have calibrated S_1 and S_2 independently, each to a univariate shifted LMD model, we notice that the only parameter missing when we compute prices of options having payoff as in (4.23) is ρ.

Definition 4.3.3. *We define the implied correlation parameter in the shifted MVMD model as the value ρ minimizing the squared percentage difference between implied volatilities from options with payoff (4.23) under the shifted MVMD model and market implied volatilities.*

The correlation skew in SCMD via ρ

Now, assume to model the joint dynamics of (S_1, S_2) as a shifted SCMD model instead. In this case

$$\begin{aligned} dS_1(t) &= \mu S_1(t)dt + \nu_1(t, S_1(t) - \beta_1 e^{\mu t})(S_1(t) - \beta_1 e^{\mu t})dW_1(t), \\ dS_2(t) &= \mu S_2(t)dt + \nu_2(t, S_2(t) - \beta_2 e^{\mu t})(S_2(t) - \beta_2 e^{\mu t})dW_2(t) \end{aligned} \tag{4.29}$$

with

$$\begin{aligned} \nu_1(t,x) &= \left(\frac{\sum_{k=1}^N \lambda_1^k \sigma_1^k(t)^2 \ell_t^k(x)}{\sum_{k=1}^N \lambda_1^k \ell_t^k(x)}\right)^{1/2}, \\ \nu_2(t,x) &= \left(\frac{\sum_{k=1}^N \lambda_2^k \sigma_2^k(t)^2 \ell_t^k(x)}{\sum_{k=1}^N \lambda_2^k \ell_t^k(x)}\right)^{1/2} \end{aligned} \tag{4.30}$$

where the Brownian motions W_1, W_2 have correlation ρ. In this case the parameter ρ really represents the true value of the instantaneous local correlation, as opposed to the MVMD case. We still define the *implied correlation* as the value ρ minimizing the squared percentage difference between implied volatilities from options with payoff (4.23) under the shifted SCMD model and market implied volatilities.

Pricing under the shifted MUVM

Now, we consider computing the price of options such as (4.23), namely options on cross FX rates, under the shifted model. In general one has a loss of tractability with respect to the non-shifted case. However, one can still express the price via a semi-analytic formula involving double integration:

$$e^{-rT}\mathbb{E}[(B-K)_+] =$$
$$e^{-rT}\sum_{i,j=1}^{N}\lambda_1^i\lambda_2^j\int_K^\infty dB(B-K)\int_{-\infty}^{\infty}dx_1\frac{n(x_1;0,\Sigma_{1,1}^{i,j})n(D^{i,j}(B,x_1);0,(1-\rho^2)\Sigma_{2,2}^{i,j})}{B-\alpha_2F_1(T)e^{x_1-\Sigma_{1,1}^{i,j}}-\alpha_1\alpha_2} \tag{4.31}$$

where $n(x;m,S)$ is the density function of a one-dimensional Gaussian random variable with mean m and standard deviation S,

$$D^{i,j}(B,x_1) = ln\left(\frac{B}{F_1(t)e^{x_1-\frac{\Sigma_{11}^{i,j}}{2}}+\alpha_1}-\alpha_2\right) - ln(F_2(t)) + \frac{\Sigma_{22}^{i,j}}{2} - \rho x_1\sqrt{\frac{\Sigma_{22}^{i,j}}{\Sigma_{11}^{i,j}}},$$

and $\Sigma_{h,k}^{i,j} = \sigma_h^i\sigma_k^j$ for $h,k=1,2$ and $i,j=1,\dots N$. This follows from the fact that the density of the product

$$B = S_1S_2 = (\xi_1+\beta_1e^{\mu_1T})(\xi_2+\beta_2e^{\mu_2T})$$

can be written as

$$p_{B_T}(B)dB = \mathbb{Q}(B_T\in dB) = \mathbb{E}[1_{\{B_T\in dB\}}] = \sum_{i,j=1}^{N}\lambda_1^i\lambda_2^j\mathbb{E}\left[1_{\{(\xi_1^i+\beta_1e^{\mu_1T})(\xi_2^j+\beta_2e^{\mu_2T})\in dB\}}\right] \tag{4.32}$$

where

$$d\xi_1(t) = \mu_1\ \xi_1(t)dt + \sigma_1^i(t)\ \xi_1(t)dW_1(t)$$
$$d\xi_2(t) = \mu_2\ \xi_2(t)dt + \sigma_2^j(t)\ \xi_2(t)dW_2(t).$$

Now, we focus on a single term in the summation (4.32) and for simplicity we drop the index i, j. Calling $F_1(t)$, $F_2(t)$ the t-forward asset prices and defining $x_i = \ln\frac{\xi_i}{F_i(t)} + \frac{\Sigma_{ii}}{2}$, we can rewrite a single term as

$$\int dx_1dx_2 1_{\{(F_1(t)e^{x_1-\Sigma_{11}/2}+\alpha_1)(F_2(t)e^{x_2-\Sigma_{22}/2}+\alpha_2)\in dB\}}n(\underline{x};0,\Sigma) =$$
$$\left(-\frac{d}{dB}\int_{D_B}dx_1dx_2n(\underline{x};0,\Sigma)\right)dB$$

where $n(\underline{x};0,\Sigma)$ is the density of a bivariate normal distribution with mean equal to zero and covariance matrix Σ defined as

$$\Sigma = \begin{pmatrix}\Sigma_{11} & \rho\sqrt{\Sigma_{11}\Sigma_{22}}\\ \rho\sqrt{\Sigma_{11}\Sigma_{22}} & \Sigma_{22}\end{pmatrix}. \tag{4.33}$$

Observing that $n(\underline{x}; 0, \Sigma) = n(x_1; 0, \Sigma_{11}) n(x_2 - \rho x_1 \sqrt{\Sigma_{22}/\Sigma_{11}}; 0, (1-\rho^2)\Sigma_{22})$, integrating with respect to x_2 and adding up the single terms in (4.32), we obtain

$$p(B_T) = \sum_{i,j=1}^{N} \lambda_1^i \lambda_2^j \int_{-\infty}^{\infty} dx_1 \frac{n(x_1; 0, \Sigma_{1,1}^{i,j}) n(D^{i,j}(B, x_1); 0, (1-\rho^2)\Sigma_{2,2}^{i,j})}{B - \alpha_2 F_1(T) e^{x_1 - \Sigma_{1,1}^{i,j}} - \alpha_1 \alpha_2}$$

from which equation (4.31) is easily derived.

4.4 Comparing correlation skews in the shifted MVMD and SCMD

The aim of this section is to compare the shifted MVMD and the shifted SCMD models in terms of implied correlation, analysing their performance in reproducing triangular relationships.

Numerical case study with cross FX rates

Specifically, we consider the exchanges $S_1 = \text{USD/EUR}$, $S_2 = \text{EUR/JPY}$ under a shifted MUVM model with 2 components

$$S_1(t) = X_1(t) + \beta_1 e^{(r^{€} - r^{\$})t}$$
$$S_2(t) = X_2(t) + \beta_2 e^{(r^{Y} - r^{€})t}$$

with

$$dX_1(t) = (r^{€} - r^{\$}) X_1(t) dt + \sigma_1^{I_1}(t) X_1(t) dW_t^{1,€}$$
$$dX_2(t) = (r^{Y} - r^{€}) X_2(t) dt + \sigma_2^{I_2}(t) X_2(t) dW_t^{2,Y}$$

where $r^{€}$, $r^{\$}$, r^{Y} are the euro, dollar and yen interest rates, respectively, and $\sigma_1^{I_1}(t)$, $\sigma_2^{I_2}(t)$ are as in equation (4.24). $W_t^{1,€}$ and $W_t^{2,Y}$ indicate that we are considering the dynamics of S_1 and of S_2, each under its own domestic measure, that is the euro in the case of S_1 and the yen in the case of S_2.

We calibrate S_1 and S_2 independently, each to its own volatility curve, using 2 components and minimizing the squared percentage difference between model and market implied volatilities. Then, we look at the product $S_1 S_2$, representing the

cross exchange USD/JPY, and we check whether the model is able to reproduce the cross smile consistently with the smiles of the single assets. In particular, we find ρ that minimizes the squared percentage difference between implied volatilities from options on the basket $S_3 = S_1 S_2$ under the shifted MVMD model (the shifted SCMD model) and market implied volatilities. In other words, we look at the implied correlations under the MVMD model and the SCMD model.

When performing calibration on S_3, we express both the dynamics of X_1 and of X_2 under the yen:

$$\begin{aligned} dX_1(t) &= (r^{€} - r^{\$} - \rho\sigma^1(t)\sigma^2(t))X_1(t)dt + \sigma^1(t)X_1(t)dW_t^{1,Y} \\ dX_2(t) &= (r^{Y} - r^{€})X_2(t)dt + \sigma^2(t)X_2(t)dW_t^{2,Y}, \end{aligned}$$

and then we calculate prices of options on

$$S_3(t) = (X_1(t) + \beta_1 e^{(r^{€} - r^{\$})t})(X_2(t) + \beta_2 e^{(r^{Y} - r^{€})t}).$$

All the data for our numerical experiments are downloaded from a Bloomberg terminal. We start by considering data from 19th February 2015. The initial values of S_1, S_2 are $S_1(0) = 0.878$, $S_2(0) = 135.44$. First we calibrate S_1 and S_2 using implied volatilities from options with maturity of 6 months. Denoting

$$\begin{aligned} \eta_1 &= \left(\sqrt{\frac{\int_0^T \sigma_1^1(s)^2 ds}{T}}, \sqrt{\frac{\int_0^T \sigma_1^2(s)^2 ds}{T}} \right) \\ \eta_2 &= \left(\sqrt{\frac{\int_0^T \sigma_2^1(s)^2 ds}{T}}, \sqrt{\frac{\int_0^T \sigma_2^2(s)^2 ds}{T}} \right) \end{aligned}$$

the T-term volatilities of the instrumental processes of S_1 and S_2, respectively,

$$\begin{aligned} \lambda_1 &= (\lambda_1^1, \lambda_1^2), \\ \lambda_2 &= (\lambda_2^1, \lambda_2^2) \end{aligned}$$

the vector of probabilities of each component and β_1, β_2 the shift parameters, we obtain

$$\eta_1 = (0.1952, 0.0709),\ \lambda_1 = (0.1402, 0.8598),\ \beta_1 = 0.00068$$

for the asset S_1 and

$$\eta_2 = (0.1184, 0.0962),\ \lambda_2 = (0.2735, 0.7265),\ \beta_2 = 0.9752$$

for the asset S_2. Then, we perform a calibration on the cross product S_3 =USD/JPY using volatilities from call options with maturity of 6 months, finding the values:

$$\rho_{MVMD}(6M) = -0.6015$$

for the shifted MVMD model and

$$\rho_{SCMD}(6M) = -0.5472$$

for the shifted SCMD model. The higher value (in absolute terms) of the correlation parameter in the shifted MVMD model is due to higher state dependence in the diffusion matrix with respect to the shifted SCMD model. This is partly related to Proposition 4.3.1. In other words, in order to achieve the same local correlation as in the shifted SCMD model, the shifted MVMD model needs a higher absolute value of ρ.

The corresponding prices and implied volatilities are plotted in Figure 4.1 whereas Table 4.1 reports the absolute differences between market and model values corresponding to a few strikes. The reported plot shows that the shifted MVMD model is better at reproducing market prices than the shifted SCMD model. What is very remarkable in this example is that the shifted MVMD fits the whole correlation skew with just one value of ρ.

As a second numerical experiment we repeat the calibration using prices with maturity of 9 months. Specifically, we first calibrate S_1 and S_2 obtaining the values

$$\eta_1 = (0.2236, 0.0761),\ \lambda_1 = (0.0262, 0.9738),\ \beta_1 = 0.0100$$

for the asset S_1 and

$$\eta_2 = (0.1244, 0.0497),\ \lambda_2 = (0.7584, 0.2416),\ \beta_2 = 0.7856$$

for the asset S_2. We observe that the higher volatility now has the highest probability as opposed to the results found for 6 months options. Then, we perform a calibration on the cross product S_3 =USD/JPY using volatilities from call options with maturity of 9 months, finding the values:

$$\rho_{MVMD}(9M) = -0.6199$$

for the shifted MVMD model and

$$\rho_{SCMD}(9M) = -0.5288$$

for the shifted SCMD model. These values are comparable with those found for 6 months options. This shows that the model is quite consistent.

The corresponding prices and implied volatilities are shown in Figure 4.2 whereas Table 4.2 reports some absolute differences between model and market values. Overall, also in this case the shifted MVMD model outperforms the shifted SCMD in terms of ability to reproduce market prices on the cross product.

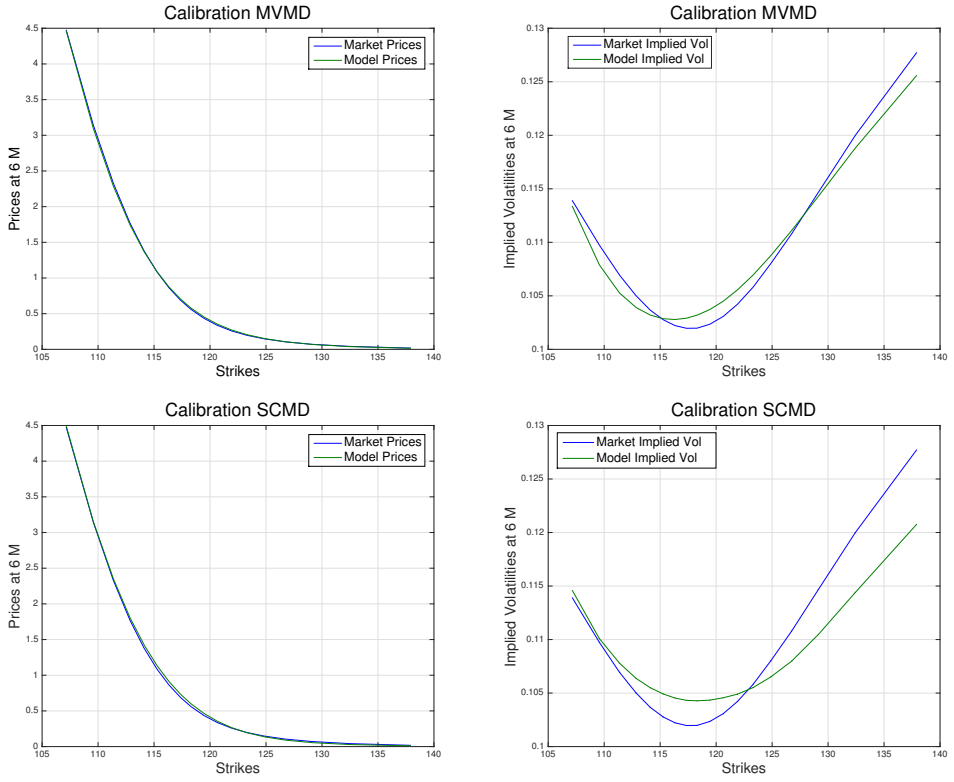

Figure 4.1: *Calibration on* 6 *months options, from 19th February 2015. The implied correlation parameter is* $\rho = -0.6015$ *for the shifted MVMD model (top) and* $\rho = -0.5472$ *for the shifted SCMD model (bottom).*

$T = 6$ Months		
K	Shifted MVMD	Shifted SCMD
107.16	0.0107	0.0188
114.12	0.0095	0.0463
118.3	0.019	0.0394
124.88	0.0045	0.0104
137.9	0.0026	0.0073

$T = 6$ Months		
K	Shifted MVMD	Shifted SCMD
107.16	0.0004	0.0007
114.12	0.0004	0.0018
118.3	0.0011	0.0023
124.88	0.0006	0.0015
137.9	0.0022	0.007

Table 4.1: *Calibration on* 6 *months options, from 19th February 2015. The tables report absolute differences between market and model prices (top) and absolute differences between the corresponding market and model implied volatilities (bottom).*

4.5 Introducing random correlations in the mixture dynamics

A single correlation parameter ρ may not be enough to fit prices on the cross asset. To overcome this, we can allow for random correlations between the single assets in the shifted MUVM model (4.28). Specifically,

$$\begin{aligned} dS_1(t) &= \mu_1 \; S_1(t)dt + \sigma_1^{I_1}(t) \; (S_1(t) - \beta_1 e^{\mu_1 t})dW_1^{I_1}(t) \\ dS_2(t) &= \mu_2 \; S_2(t)dt + \sigma_2^{I_2}(t) \; (S_2(t) - \beta_2 e^{\mu_2 t})dW_2^{I_2}(t) \end{aligned} \tag{4.34}$$

where the Brownian motions $W_1^{I_1}$, $W_2^{I_2}$ now have correlation ρ^{I_1,I_2}. The correlation parameter will therefore assume the value $\rho^{h,k}$ in correspondence with a couple (σ_1^h, σ_2^k) with probability $\lambda_h \lambda_k$.

Theorem 4.5.1. *The shifted MUVM model with an uncertain correlation parameter has, as a Markovian projection, a shifted MVMD model solution of the SDE*

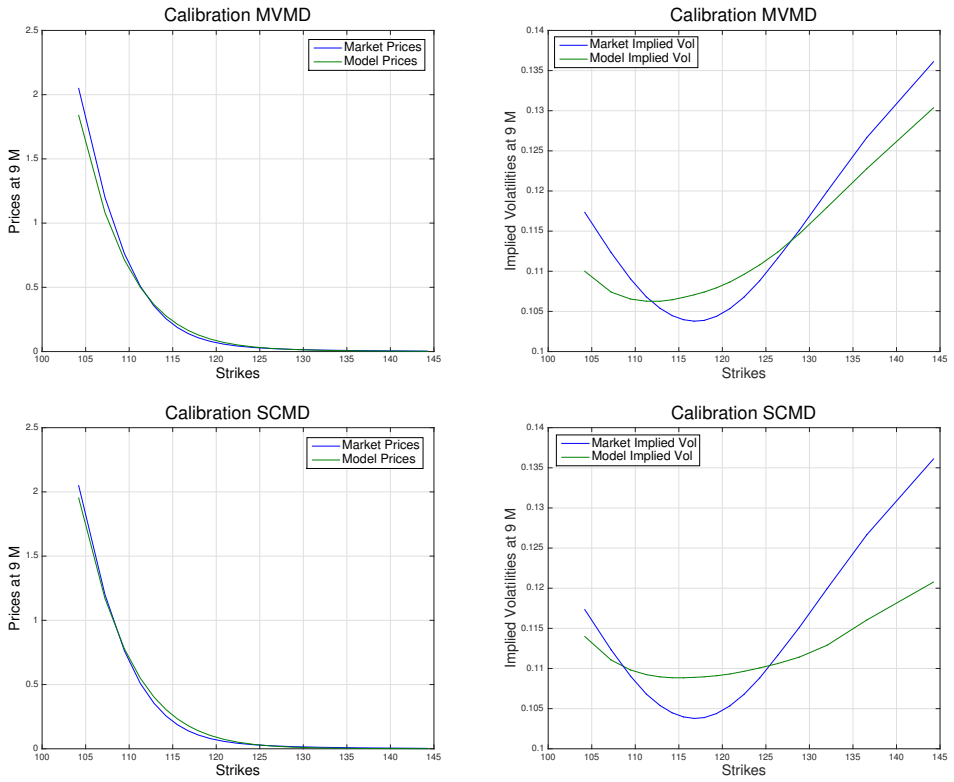

Figure 4.2: *Calibration on* 9 *months options, from 19th February 2015. The implied correlation parameter is* $\rho = -0.6199$ *for the shifted MVMD model (top) and* $\rho = -0.5288$ *for the shifted SCMD model (bottom). The results are comparable with the values obtained using* 6 *months options.*

(4.20) but with equation (4.17) transformed into

$$V^{k_1,\dots,k_n}(t) = \left[\sigma_i^{k_i}(t)\ \rho_{i,j}^{k_i,k_j}\ \sigma_j^{k_j}(t)\right]_{i,j=1,\dots,n}. \tag{4.35}$$

Proof. The Markovian projection property can be easily shown by an application of Gyöngy's lemma, in a similar was as in the proof of Theorem 4.3.2. □

In other words, the correlation between two generic instrumental processes Y_i^k, Y_j^h will depend not only on the assets S_i, S_j, but will correspond to a specific choice of the instrumental processes Y_i^k, Y_j^h themselves.

$T = 9$ Months		
K	Shifted MVMD	Shifted SCMD
104.2	0.2098	0.0961
112.84	0.0116	0.0485
117.91	0.0223	0.0329
122.49	0.0088	0.0089
144.25	0.0013	0.0025

$T = 9$ Months		
K	Shifted MVMD	Shifted SCMD
104.2	0.0073	0.0034
112.84	0.0008	0.0024
117.91	0.0035	0.005
122.49	0.0028	0.0029
144.25	0.005	0.01

Table 4.2: *Calibration on* 9 *months options, from 19th February 2015. The tables report absolute differences between market and model prices (top) and absolute differences between the corresponding market and model implied volatilities (bottom).*

Cross FX rates study for shifted MVMD with random correlations

As a numerical illustration we performed on the shifted MVMD model the same experiment as in Section 4.4. We used 6 months options from 7th September 2015. The initial values of the single FX rates are $S_1(0) = 0.8950$, $S_2(0) = 133.345$. In this case the calibration of the shifted SCMD model is much worse, to the point that there is no value of ρ that can fit any of the prices obtained through this model. On the other hand, in the case of the shifted MVMD model, in particular when introducing random correlations, the fit leads to quite good results. As in the previous cases we independently calibrate S_1=USD/EUR and S_2=EUR/JPY on the corresponding implied volatilities obtaining

$$\eta_1 = (0.1803, 0.0916),\ \lambda_1 = (0.0274, 0.9726),\ \beta_1 = 0.0128$$

$$\eta_2 = (0.1230, 0.0501),\ \lambda_2 = (0.6575, 0.3425),\ \beta_2 = 0.1867$$

and then we look at the cross exchange rate $S_3 = S_1 S_2$=USD/JPY. When performing calibration using a shifted MVMD model with one correlation parameter

only, we obtain

$$\rho = -0.6147,$$

whereas when using random correlations, we have

$$\rho^{1,1} = -0.8717,\ \rho^{1,2} = -0.1762,\ \rho^{2,1} = -0.6591,\ \rho^{2,2} = -0.2269.$$

The corresponding plots are shown in Figure 4.3, in connection with Table 4.3. In this case we also see that using random correlations improves the fit with respect to the case with a single correlation parameter. Moreover, computing the expectation and the standard deviation for the random correlation under the risk-neutral measure $\mathbb{Q}$, we obtain

$$\mathbb{E}^{\mathbb{Q}}(\rho^{i,j}) = -0.5144$$

$$\mathrm{Std}^{\mathbb{Q}}(\rho^{i,j}) = 0.2105$$

satisfying $|\mathbb{E}^{Q}(\rho^{i,j}) - \rho| < \frac{\mathrm{Std}^{Q}(\rho^{i,j})}{2}$. In other words, the absolute difference between the $\mathbb{Q}$-expected random correlation and the deterministic correlation is smaller than half the $\mathbb{Q}$-standard deviation. This means that the random correlation is on average not that far from the deterministic value.

Finally, we repeat the same experiment using options with maturity of 9 months. We find:

$$\eta_1 = (0.2228, 0.0894),\ \lambda_1 = (0.0177, 0.9823),\ \beta_1 = 0.0104$$

$$\eta_2 = (2.0968, 0.1064),\ \lambda_2 = (0.000943, 0.999057),\ \beta_2 = 1.1098.$$

When looking at the cross product S_1S_2=USD/JPY, we obtain

$$\rho = -0.7488$$

in the case of one single correlation parameter, and

$$\rho^{1,1} = -0.8679,\ \rho^{1,2} = -0.2208,\ \rho^{2,1} = -0.8303,\ \rho^{2,2} = -0.3270$$

in the case where random correlations are introduced. Corresponding plots and absolute differences between market and model prices/implied volatilities can be found in Figure 4.4 and Table 4.4, which show that the shifted MVMD model with

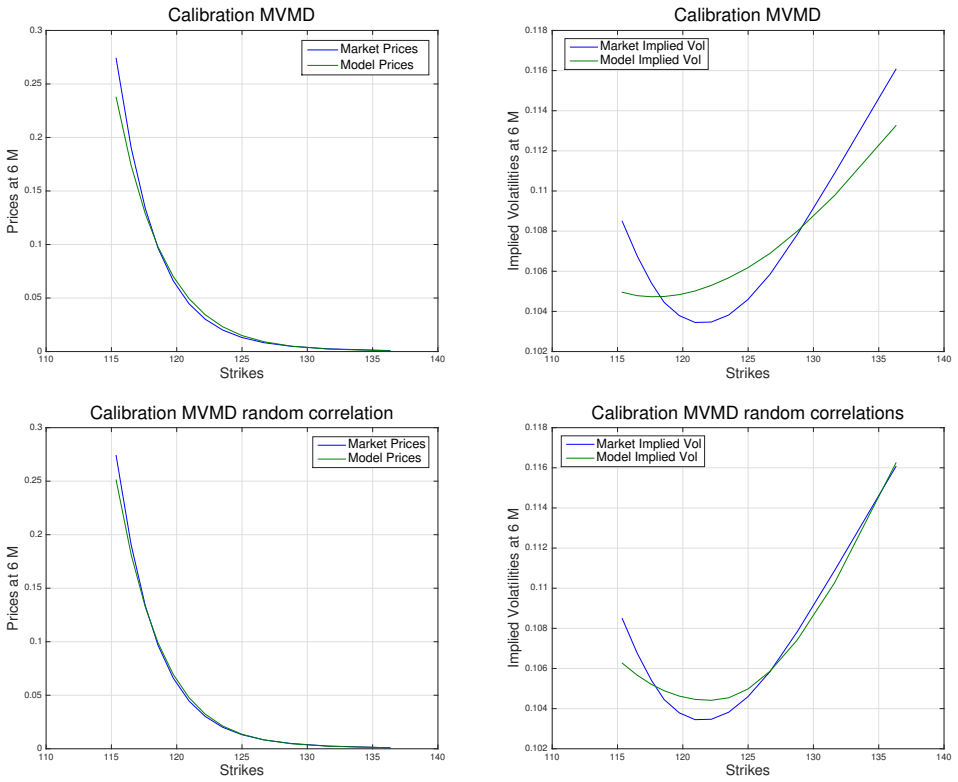

Figure 4.3: *Calibration of the MVMD model on* 6 *months options, from 7th September 2015. The calibration using one single correlation parameter is shown in the top part which corresponds to a fitted value equal to* $\rho = -0.6147$. *The calibration using multiple correlation parameters is shown in the bottom part, which corresponds to* $\rho^{1,1} = -0.8717,\ \rho^{1,2} = -0.1762,\ \rho^{2,1} = -0.6591,\ \rho^{2,2} = -0.2269$.

random correlations outperforms the constant-deterministic correlation model in this case as well.

The values of expected random correlation and standard deviation under the $\mathbb{Q}$ measure are

$$\mathbb{E}^{\mathbb{Q}}(\rho^{i,j}) = -0.5063$$

$$\mathrm{Std}^{\mathbb{Q}}(\rho^{i,j}) = 0.2411.$$

With respect to the case of 6 months options, we observe a movement of the $\mathbb{Q}$-expected random correlation away from the constant correlation. Moreover, if we look at the terminal correlations, that is the correlation between $S_1(T)$ and $S_2(T)$,

$T = 6$ Months		
K	Shifted MVMD	Shifted MVMDRC
115.36	0.0359	0.02228
118.57	0.0016	0.0024
122.18	0.0042	0.0022
126.68	0.0008	$1.18 * 10^{-5}$
136.32	0.0003	$1.94 * 10^{-5}$

$T = 6$ Months		
K	Shifted MVMD	Shifted MVMDRC
115.36	0.0036	0.0022
118.57	0.0002	0.0004
122.18	0.0018	0.0009
126.68	0.0011	$1.159 * 10^{-5}$
136.32	0.0025	0.0002

Table 4.3: *Calibration on* 6 *months options, from 7th September 2015. The tables report absolute differences between market and model prices (top) and absolute differences between the corresponding market and model implied volatilities (bottom).*

for $T = 9$ months, we obtain

$$\hat{\rho}(9M) = -0.6835$$

in case ρ is deterministic and

$$\hat{\rho}_{\text{random}}(9M) = -0.5546$$

in case ρ is random. As a final observation, we remark that in case ρ is constant, an application of Schwartz's inequality shows that the absolute value of the terminal correlation is always smaller than the absolute value of the instantaneous correlation, as verified by the results above. One may wonder whether the same inequality holds in case of random correlations, if we substitute the instantaneous value with the mean of the random correlations. In this case it is not possible to use Schwartz's inequality as we did before and, indeed, the results obtained show that the inequality does not hold, at least not for the example considered above.

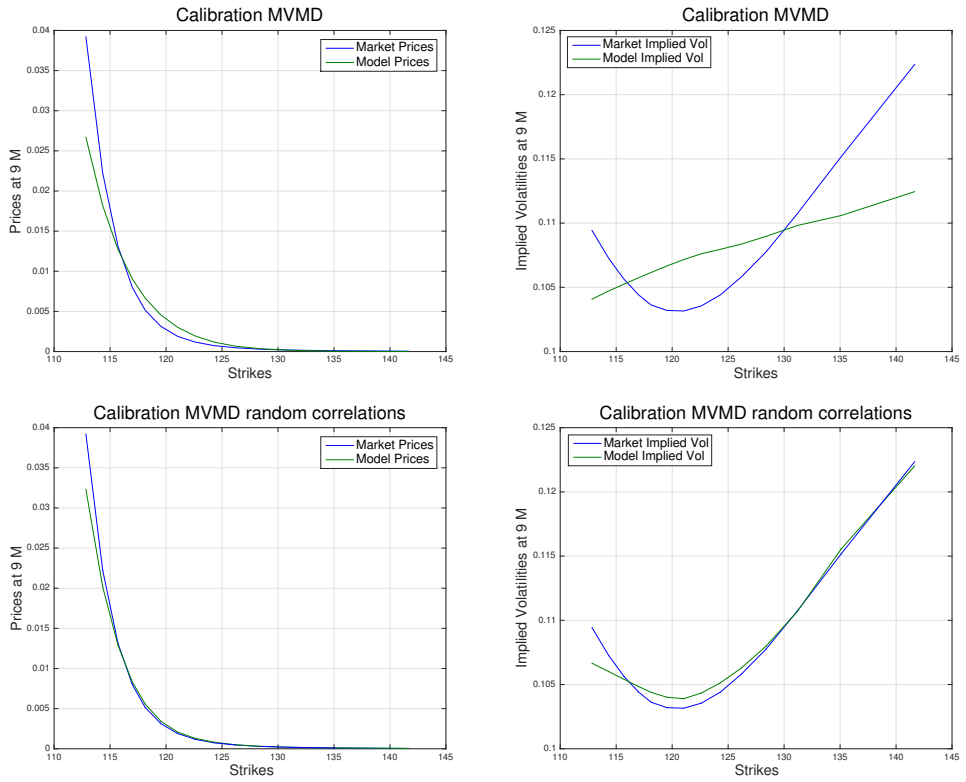

Figure 4.4: *Calibration of the MVMD model on* 9 *months options, from 7th September 2015. The calibration using one single correlation parameter is shown in the top part which corresponds to a fitted value equal to* $\rho = -0.7488$. *The calibration using multiple correlation parameters is shown in the bottom part, which corresponds to* $\rho^{1,1} = -0.8679,\ \rho^{1,2} = -0.2208,\ \rho^{2,1} = -0.8303,\ \rho^{2,2} = -0.3270$.

4.6 Conclusions

We introduced a shifted MVMD model where each single asset follows shifted LMD dynamics which are combined so that the mixture property is lifted to a multivariate level, in the same way as for the non-shifted case [28]. In this framework, we analysed the implied correlation from cross exchange rates and compared the results with those in the shifted SCMD model where the single assets are connected by simply introducing instantaneous correlations among the Brownian motions driving each asset.

Finally, we generalized the MUVM model in [28], having MVMD as a Markovian projection, to a shifted model with random correlation, achieving more flexi-

$T = 9$ Months		
K	Shifted MVMD	Shifted MVMDRC
112.84	0.0125	0.0069
116.99	0.0011	0.0003
121.04	0.0011	0.0002
126.18	0.0002	$3.29 * 10^{-5}$
141.66	$3.46 * 10^{-5}$	$2.2 * 10^{-5}$

$T = 9$ Months		
K	Shifted MVMD	Shifted MVMDRC
112.84	0.0054	0.0028
116.99	0.0013	0.0004
121.04	0.004	0.0007
126.18	0.0026	0.0005
141.66	0.01	0.0003

Table 4.4: *Calibration on* 9 *months options, from 7th September 2015. The tables report absolute differences between market and model prices (top) and absolute differences between the corresponding market and model implied volatilities (bottom).*

bility. This allows one to capture the correlation skew better. Indeed, the numerical experiments which we have conducted show that this model may be able to consistently reproduce triangular relationships among FX cross rates, or in other words to reproduce the implied volatility of a cross exchange rate in a consistent way with the implied volatilities of the single exchange rates.

One possible further use of the models given here is in proxying the smile for illiquid cross FX rates resulting from the product of two liquid FX rates. While one would have to find the relevant correlation parameters, possibly based on historical estimation with some adjustments for risk premia, the models presented here allow us to infer the detailed structure of the cross FX rate smile in an arbitrage free way.

4.7 Appendix

In this Appendix we provide the details leading to definition 4.2.1. We start by applying a shift to each component Y_i^k of each asset as follows

$$S_i^k(t) = Y_i^k(t) + \beta_i e^{\mu_i t}.$$

Keeping in mind that Y_i^k satisfies

$$dY_i^k(t) = \mu_i Y_i^k(t)dt + \sigma_i^k(t)Y_i^k(t)dZ_i(t) \;\; d\langle Z_i, Z_j\rangle = \rho_{ij}dt, \tag{4.36}$$

we obtain, by applying Ito's formula

$$dS_i^k(t) = \mu_i S_i^k(t)dt + \sigma_i^k(t)\left(S_i^k(t) - \beta_i e^{\mu_i t}\right)dZ_i(t). \tag{4.37}$$

The corresponding asset price S_i will therefore be a shifted LMD model with shift equal to $\beta_i e^{\mu_i t}$. In order to find the dynamics of the whole multidimensional process $S(t)$, that is the process corresponding to $S(t)$ after having applied the shift, we look for an SDE of the type

$$d\underline{S}(t) = diag(\underline{\mu})\underline{S}(t)dt + diag(\underline{S}(t))\widetilde{C}(t,\underline{S}(t))Bd\underline{W}(t) \tag{4.38}$$

where $\rho = BB^T$ such that the corresponding density satisfies

$$p_{\underline{S}(t)}(\underline{x}) = \sum_{k_1,k_2,\dots k_n=1}^{N} \lambda_1^{k_1}\cdots\lambda_n^{k_n}\tilde{\ell}^{k_1,\dots,k_n}_{1,\dots n;t}(\underline{x}) \tag{4.39}$$

$$\tilde{\ell}^{k_1,\dots,k_n}_{1,\dots n;t}(\underline{x}) = p_{[S_1^{k_1}(t),\dots,S_n^{k_n}(t)]^T}(\underline{x}). \tag{4.40}$$

In other words, the density $p_{S(t)}$ is obtained by mixing the single densities $p_{S_i^k(t)}(x)$ in all the possible ways.

In order to find the diffusion matrix $\widetilde{C}$, we compute the Fokker-Planck equations for $p_{\underline{S}(t)}$ and $\tilde{\ell}^{k_1,\dots,k_n}_{1,\dots n;t}$. Defining $\tilde{a}(t,\underline{S}(t)) = (\widetilde{C}B)(\widetilde{C}B)^T$ where $\widetilde{C}_i$ denotes the i-th row of $\widetilde{C}$, we obtain

$$\frac{\partial}{\partial t}p_{\underline{S}(t)}(x) = -\sum_{i=1}^{n}\frac{\partial}{\partial x_i}\left[\mu_i x_i p_{\underline{S}(t)}(x)\right] + \frac{1}{2}\sum_{i,j=1}^{n}\frac{\partial^2}{\partial x_i\partial x_j}\left[\tilde{a}_{ij}(t,\underline{x})x_i x_j p_{\underline{S}(t)}(x)\right] \tag{4.41}$$

and

$$\frac{\partial \tilde{\ell}^{k_1,\ldots,k_n}_{1,\ldots n;t}(\underline{x})}{\partial t} = -\sum_{i=1}^{n} \frac{\partial}{\partial x_i}\left(\mu_i^{k_i} x_i \tilde{\ell}^{k_1,\ldots,k_n}_{1,\ldots n;t}(\underline{x})\right) + \frac{1}{2}\sum_{i,j=1}^{n} \frac{\partial^2}{\partial x_i \partial x_j} \sigma_i^{k_i}(t)(x_i - \beta_i e^{\mu_i^{k_i}})\sigma_j^{k_j}(t)(x_j - \beta_j e^{\mu_j^{k_j} t})\rho_{i,j}\tilde{\ell}^{k_1,\ldots,k_n}_{1,\ldots n;t}(\underline{x}).$$

Making use of equation (4.39) and the equation above

$$\begin{aligned}\frac{\partial}{\partial t} p_{\underline{S}(t)}(x) &= \sum_{k_1,k_2,\ldots k_n=1}^{N} \lambda_1^{k_1}\cdots\lambda_n^{k_n} \frac{\partial}{\partial t}\tilde{\ell}^{k_1,\ldots,k_n}_{1,\ldots n;t}(\underline{x}) = \\ &= \sum_{k_1,k_2,\ldots k_n=1}^{N} \lambda_1^{k_1}\cdots\lambda_n^{k_n}\Big[-\sum_{i=1}^{n}\frac{\partial}{\partial x_i}\left(\mu_i x_i \tilde{\ell}^{k_1,\ldots,k_n}_{1,\ldots n;t}(\underline{x})\right) \\ &+ \frac{1}{2}\sum_{i,j=1}^{n}\frac{\partial^2}{\partial x_i\partial x_j}\sigma_i^{k_i}(t)(x_i-\beta_i e^{\mu_i})\sigma_j^{k_j}(t)(x_j-\beta_j e^{\mu_j t})\rho_{i,j}\tilde{\ell}^{k_1,\ldots,k_n}_{1,\ldots n;t}(\underline{x})\Big].\end{aligned}$$

On the other hand, from equation (4.41)

$$\begin{aligned}\frac{\partial}{\partial t} p_{\underline{S}(t)}(x) &= -\sum_{i=1}^{n}\frac{\partial}{\partial x_i}\left[\mu_i x_i\left(\sum_{k_1,k_2,\ldots k_n=1}^{N}\lambda_1^{k_1}\cdots\lambda_n^{k_n}\tilde{\ell}^{k_1,\ldots,k_n}_{1,\ldots n;t}(\underline{x})\right)\right] \\ &+ \frac{1}{2}\sum_{i,j=1}^{n}\frac{\partial^2}{\partial x_i\partial x_j}\left[\tilde{a}_{ij}(t,\underline{x})x_i x_j\left(\sum_{k_1,k_2,\ldots k_n=1}^{N}\lambda_1^{k_1}\cdots\lambda_n^{k_n}\tilde{\ell}^{k_1,\ldots,k_n}_{1,\ldots n;t}(\underline{x})\right)\right].\end{aligned}$$

Finally, comparing the two expressions obtained for $\frac{\partial}{\partial t}p_{\underline{S}(t)}(x)$

$$\begin{aligned}&\frac{1}{2}\sum_{i,j=1}^{n}\frac{\partial^2}{\partial x_i\partial x_j}\sum_{k_1,k_2,\ldots k_n=1}^{N}\lambda_1^{k_1}\cdots\lambda_n^{k_n}\Big[\tilde{a}_{ij}(t,\underline{x})x_i x_j - \\ &\sigma_i^{k_i}(t)(x_i-\beta_i e^{\mu_i})\sigma_j^{k_j}(t)(x_j-\beta_j e^{\mu_j t})\rho_{i,j}\Big]\tilde{\ell}^{k_1,\ldots,k_n}_{1,\ldots n;t}(\underline{x}) = 0\end{aligned}$$

so that

$$a_{ij} = \frac{\sum_{k_1,k_2,\ldots k_n=1}^{N}\lambda_1^{k_1}\cdots\lambda_n^{k_n}\sigma_i^{k_i}(t)(x_i-\beta_i e^{\mu_i})\sigma_j^{k_j}(t)(x_j-\beta_j e^{\mu_j t})\rho_{i,j}\tilde{\ell}^{k_1,\ldots,k_n}_{1,\ldots n;t}(\underline{x})}{x_i x_j\sum_{k_1,k_2,\ldots k_n=1}^{N}\lambda_1^{k_1}\cdots\lambda_n^{k_n}\tilde{\ell}^{k_1,\ldots,k_n}_{1,\ldots n;t}(\underline{x})}.$$

References

[1] J. Abate, G. Choudhury, and W. Whitt. On the Laguerre method for numerically inverting Laplace transforms. *INFORMS Journal on Computing*, 8(4):413–427, 1996.

[2] J. Abate, G. Choudhury, and W. Whitt. *An introduction to numerical transform inversion and its application to probability models.* Computational Probability, W. Grassman (ed.), Kluwer, Boston, 1999.

[3] J. Abate and W. Whitt. The Fourier-series method for inverting transforms of probability distributions. *Queueing Systems*, 10:5–88, 1992.

[4] M. Abramowitz and I. A. Stegun. *Handbook of mathematical functions.* Dover publications, INC. New York, 1987.

[5] A. Ahdida and A. Alfonsi. Exact and high order discretization schemes for Wishart processes and their affine extensions. *Ann. Appl. Probab.*, 23(3):1025–1073, 2013.

[6] H. Albrecher, P. Mayer, W. Schoutens, and J. Tistaert. The little Heston trap, 2007.

[7] C. Alexander and L. Nogueira. Stochastic local volatility. Proceedings of the second IASTED International conference - Financial Engineering and Applications, 2004.

[8] A. Alfonsi. High order discretization schemes for the CIR process: Application to affine term structure and Heston models. *Mathematics of Computations*, 79(269):209–237, 2010.

[9] L. Andersen and J. Andreasen. Volatile volatilities. *RISK*, 15(12):163–168, 2002.

[10] P. Austing. *Smile Pricing Explained*. Palgrave Macmillan, 2014.

[11] G. Bakshi, C. Cao, and Z. Chen. Empirical performance of alternative option pricing models. *The Journal of Finance*, 52(5):2003–2049, 1997.

[12] G. Bakshi, N. Kapadia, and D. Madan. Stock return characteristics, skew laws, and the differential pricing of individual equity options. *Review of Financial Studies*, 16(1):101–143, 2003.

[13] J. Baldeaux and A. Badran. Consistent modeling of VIX and equity derivatives using a 3/2 plus jumps model. *Available on arXiv*, 2012.

[14] O. E. Barndorff-Nielsen and N. Shephard. Non-Gaussian Ornstein–Uhlenbeck-based models and some of their uses in financial economics. *Journal of the Royal Statistical Society*, 63(2):167–241, 2001.

[15] C. Bayer, P. Friz, and J. Gatheral. Pricing under rough volatility. *Quantitative Finance*, November 2015.

[16] R. E. Bellman and R. S. Roth. *The Laplace transform*. Worls Scientific Press, Singapore, 1984.

[17] S. Benaim and P. Friz. Smile asymptotics II: models with known moment generating functions. *Journal of Applied Probability*, 45(1):16–32, 2008.

[18] S. Benaim and P. Friz. Regular variation and smile asymptotics. *Mathematical Finance*, 19(1):1–12, 2009.

[19] L. Bergomi. Smile dynamics II. *Risk*, October:67–73, 2005.

[20] N. H. Bingham, C. M. Goldie, and J. L. Teugels. *Regular variation*. Cambridge University Press, 1987.

[21] T. Björk. *Arbitrage Theory in Continuous Time*. Oxford Finance, 2009.

[22] F. Black and M. Scholes. The pricing of option and corporate liabilities. *Journal of Political Economy*, 1973.

[23] Bloomberg. Local volatility for equity underlyings. retrieved on 9 December 2015 from a Bloomberg terminal, 2012.

[24] D. Brigo and F. Mercurio. A mixed–up smile. *Risk*, 13(9):123–126, 2000.

[25] D. Brigo and F. Mercurio. Displaced and mixture diffusions for analytically-tractable smile models. *Mathematical Finance - Bachelier Congress 2000 , Geman, H., Madan, D.B., Pliska, S.R., Vorst, A.C.F., eds.* Springer Finance*, Springer*, pages 151–174, 2001.

[26] D. Brigo and F. Mercurio. Lognormal–mixture dynamics and calibration to market volatility smiles. *International Journal of Theoretical and Applied Finance*, 5(4):427–446, 2002.

[27] D. Brigo, F. Mercurio, and Sartorelli G. Alternative asset-price dynamics and volatility smile. *Quantitative Finance*, 3(3):173–183, 2003.

[28] D. Brigo, F. Mercurio, and F. Rapisarda. Connecting univariate smiles and basket dynamics: a new multidimensional dynamics for basket options, 2004. Available at http://www.ima.umn.edu/talks/workshops/4-12-16.2004/rapisarda/MultivariateSmile.pdf.

[29] D. Brigo, F. Rapisarda, and A. Sridi. The arbitrage-free multivariate mixture dynamics model: Consistent single-assets and index volatility smiles, 2014. Available on SSRN & arXiv.

[30] M. Broadie, M. Chernov, and M. Johannes. Model specification and risk premia: Evidence from futures options. *Journal of Finance*, 62(3):1453–1490, 2007.

[31] M. Broadie and A. Jain. The effect of jumps and discrete sampling on volatility and variance swaps. *International Journal of Theoretical and Applied Finance*, 11(08):761–797, 2008.

[32] M. F. Bru. Diffusions of perturbed principal component analysis. *Journal of Multivariate Analysis*, 29(1):127–136, 1989.

[33] M.F. Bru. Wishart processes. *Journal of Theoretical Probability*, 4(4):725–751, 1991.

[34] P. Carr, H. Geman, D. B Madan, and M. Yor. Pricing options on realized variance. *Finance and Stochastics*, 9(4):453–475, 2005.

[35] P. Carr, H. Geman, D.B. Madan, and M. Yor. Stochastic volatility for Lévy processes. *Mathematical Finance*, 13(3):345–382, 2003.

[36] P. Carr and R. Lee. Realized Volatility and Variance: Options via Swaps. available at http://math.uchicago.edu/ rogerlee/OVSwithAppendices.pdf, 2007.

[37] P. Carr and R. Lee. Volatility Derivatives. *Annual Review of Financial Economics*, 1(1):319–339, 2009.

[38] P. Carr and L. Wu. A tale of two indices. *The Journal of Derivatives*, 13(3):13–29, 2006.

[39] M. Chernov, A Ronald G., E. Ghysels, and G. Tauchen. Alternative models for stock price dynamics. *Journal of Econometrics*, 116(1):225–257, 2003.

[40] G. Choudhury, D.M. Lucantoni, and W. Whitt. Multidimensional transform inversion with application to the transient m/g/1 queue. *Ann. Appl. Prob.*, 4:719–740, 1994.

[41] A. M. Cohen. *Numerical methods for Laplace transform inversion*. Springer, 2007.

[42] R. Cont and T. Kokholm. A consistent pricing model for index options and volatility derivatives. *Mathematical Finance*, 23(2):248–274, 2013.

[43] J. Cox, J. Ingersoll, and S. Ross. A theory of the term structure of interest rates. *Econometrica*, 53(2):385–407, 1985.

[44] M. Craddock, D. Heath, and E. Platen. Numerical inversion of Laplace transforms: A survey of techniques with applications to derivative pricing. Research Paper Series 27, Quantitative Finance Research Centre, University of Technology, Sydney, 1999.

[45] C. Cuchiero, D. Filipović, E. Mayerhofer, and J. Teichmann. Affine processes on positive semidefinite matrices. *Ann. Appl. Probab.*, 21(2):397–463, 2011.

[46] J. Da Fonseca, M. Grasselli, and C. Tebaldi. Option pricing when correlations are stochastic: an analytical framework. *Review of Derivatives Research*, 10:151–180, 2007.

[47] J. Da Fonseca, M. Grasselli, and C. Tebaldi. A multifactor volatility Heston model. *Quantitative Finance*, 8(6):591–604, 2008.

[48] B. Davies and B. Martin. Numerical Inversion of the Laplace transform: a survey and comparison of methods. *Journal of Computational Physics*, 33(1), 1979.

[49] G. Di Graziano and L.C.G. Rogers. A dynamic approach to the modelling of correlation credit derivatives using Markov chains. *International Journal of Theoretical and Applied Finance*, 12:1–18, 2009.

[50] G. Doetsch. *Introduction to the Theory and Application of the Laplace Transformation*. Springer-Verlag, 1974.

[51] G.G. Drimus. Options on realized variance by transform methods: a non-affine stochastic volatility model. *Quantitative Finance*, 12(11):1679–1694, 2012.

[52] G.G. Drimus. Options on realized variance in Log-OU models. *Applied Mathematical Finance*, 19(5):477–494, 2012.

[53] D. Duffie, J. Pan, and K. Singleton. Transform analysis and asset pricing for affine jump-diffusions. *Econometrica*, 68(6):1343–1376, 2000.

[54] C. L. Epstein and J. Schotland. The Bad Truth about Laplace's Transform. *SIAM Review*, 50(3):504–520, 2008.

[55] B. Eraker. Do stock prices and volatility jump? Reconciling evidence from spot and option prices. *Journal of Finance*, 59(3):1367–1404, 2004.

[56] B. Eraker, M. Johannes, and N. Polson. The impact of jumps in volatility and returns. *Journal of Finance*, 58(3):1269–1300, 2003.

[57] L. Fatone, F. Mariani, M.C. Recchioni, and F. Zirilli. Pricing realized variance options using integrated stochastic variance options in the Heston stochastic volatility model. *Discrete and continuous dynamical systems supplement*, pages 354 – 363, 2007.

[58] W. Feller. *An Introduction to Probability Theory and Its Applications*, volume 2. John Wiley & Sons, 1974.

[59] M. C. Fu, D. B. Madan, and Wang T. Pricing continuous Asian options: a comparison of Monte Carlo and Laplace transform inversion methods. *Journal of Computational Finance*, 2:49–74, 1998.

[60] G. Fusai and A. Roncoroni. *Implementing models in Quantitative Finance: Methods and Cases*. Springer Finance, 2008.

[61] B. Gabutti and P. Lepora. The numerical performance of Tricomi's formula for inverting the Laplace transform. *Numerische Mathematik*, 51(3):369–380, 1987.

[62] J. Gatheral. *The Volatility Surface: A Practitioner's Guide*. Wiley, 2006.

[63] J. Gatheral. Consistent modelling of SPX and VIX options. Bachelier congress, London, 2008.

[64] D. P. Gaver. Observing stochastic processes and approximate transform inversion. *Operation Research*, 14:444–459, 1966.

[65] H. Geman and M. Yor. Pricing and hedging double barrier options: a probabilistic approach. *Mathematical Finance*, 6(4):365–378, 1996.

[66] G. Giunta, G. Laccetti, and M.R. Rizzardi. More on Weeks method for the numerical inversion of the Laplace transform. *Numerische Mathematik*, 54:193–200, 1988.

[67] P. Glasserman. *Monte Carlo methods in financial engineering*, volume 53 of *Applications of Mathematics (New York)*. Springer-Verlag, New York, 2004. Stochastic Modelling and Applied Probability.

[68] A. Gnoatto. The Wishart short rate model. *International Journal of Theoretical and Applied Finance*, 15(8):1250056, 24, 2012.

[69] C. Gourieroux. Continuous time Wishart process for stochastic risk. *Econometric Reviews*, 25(2):177–217, 2007.

[70] C. Gourieroux and R. Sufana. Discrete time Wishart term structure models. *Journal of Economic Dynamics & Control*, 35(6):815–824, 2011.

[71] A. Gulisashvili. Asymptotic Formulas with Error Estimates for Call Pricing Functions and the Implied Volatility at Extreme Strikes. *SIAM Journal on Financial Mathematics*, 1(1):609–641, January 2010.

[72] A. Gulisashvili. *Analytically Tractable Stochastic Stock Price Models*. Springer-Verlag, 2012.

[73] A. Gulisashvili. Asymptotic equivalence in Lee's moment formulas for the implied volatility, asset price models without moment explosions, and Piterbarg's conjecture. *International Journal of Theoretical and Applied Finance (IJTAF)*, 15(03):1250020–1–1, 2012.

[74] I. Gyöngy. Mimicking the one-dimensional marginal distributions of processes having an Itô differential. *Probability Theory and Related Fields*, 71(4):501–516, 1986.

[75] J.M. Harrison and D.M. Kreps. Martingales and arbitrage in multiperiod securities markets. *Journal of Economic Theory*, 20(3):381–408, 1979.

[76] J.M. Harrison and S.R. Pliska. Martingales and stochastic integrals in the theory of continuous trading. *Stochastic Processes and their Applications*, 11(3):215–260, 1981.

[77] S.L. Heston. A closed-form solution for options with stochastic volatility with applications to bond and currency options. *Review of Financial Studies*, 6(2):327–343, 1993.

[78] J. C. Hull. *Options, Futures and Other Derivatives*. Pearson, 2009.

[79] P. D. Iseger. Numerical transform inversion using Gaussian quadrature. *Probability in the Engineering and Informational Sciences*, 20(1):1–44, 2006.

[80] P. D. Iseger. Laplace transform inversion on the entire line, 2009. available on SSRN.

[81] C. Kahl and P. Jäckel. Not-so-complex logarithms in the Heston model. *Wilmott Magazine*, September, 2005.

[82] J. Kallsen, J. Muhle-Karbe, and M. Voß. Pricing options on variance in affine stochastic volatility models. *Mathematical Finance*, 21(4), 2010.

[83] D.G. Kendall. Some recent work and further problems in the theory of queues. *Theory of Probability and Its Applications*, 9(1):1–13, 1964.

[84] J. Korevaar. *Tauberian Theory: A Century of Developments*. Springer-Verlag, 2004.

[85] C. Labart and J. Lelong. Pricing double barrier parisian options using Laplace transforms. *International Journal of Theoretical and Applied Finance*, 12(01):19–44, 2009.

[86] D. Lamberton and B. Lapeyre. *Introduction to Stochastic Calculus applied to Finance*. Chapman & Hall, Berlin, Heidelberg, New York, 1996.

[87] A. Langnau. A dynamic model for correlation, 2010. Risk Magazine.

[88] B. Leblanc and Scaillet O. Path dependent options on yields in the affine term structure model. *Finance and Stochastics*, 2:349–367, 1998.

[89] R. W. Lee. The moment formula for implied volatility at extreme strikes. *Mathematical Finance*, 14(3):469–480, 2004.

[90] G. H. Lian and S. P. Zhu. Pricing VIX options with stochastic volatility and random jumps. *Decisions in Economics and Finance*, 36(1):71–88, 2011.

[91] R. Lord and C. Kahl. Why the rotation count algorithm works. Tinbergen Institute Discussion Paper No. 2006-065/2, 2006.

[92] R. Lord and C. Kahl. Complex logarithms in Heston-like models. *Mathematical Finance*, 20:671–694, 2010.

[93] R. Lord, R. Koekkoek, and D. van Dijk. A comparison of biased simulation schemes for stochastic volatility models. *Quantitative Finance*, 10(2):177–194, 2010.

[94] E. Nicolato and E. Venardos. Option pricing in stochastic volatility models of the Ornstein-Uhlenbeck type. *Mathematical Finance*, 13(4):445–466, 2003.

[95] S. Ninomiya and N. Victoir. Weak approximation of stochastic differential equations and application to derivative pricing. *Appl. Math. Finance*, pages 107–121, 2008.

[96] A. Papanicolaou. Extreme-strike comparisons and structural bounds for SPX and VIX options. *Available on SSRN*, 2014.

[97] A. Pelsser. Pricing double barrier options using Laplace transforms. *Finance and Stochastics*, 4:95–104, 2000.

[98] E. Platen and N. Bruti-Liberati. *Numerical Solution of Stochastic Differential Equations with Jumps in Finance*, volume 64. Springer Berlin Heidelberg, Berlin, Heidelberg, 2010.

[99] K. Sato. *Lévy Processes and Infinitely Divisible Distributions*. Cambridge University Press, 1999.

[100] A. Sepp. Pricing options on realized variance in the Heston model with jumps in returns and volatility. *Journal of Computational Finance*, 11(4):33–70, 2008.

[101] A. Sepp. VIX option pricing in a jump-diffusion model. *Risk Magazine*, pages 84–89, 2008.

[102] G. Smyth. *Numerical Integration in Encyclopedia of Biostatistics*. John Wiley and Sons, LTD, Chichester, 1998.

[103] H. Stehfest. Algorithm 368: Numerical inversion of Laplace transforms. *Communications of the ACM*, 13(1):47–49, 1970.

[104] E. M. Stein and G. L. Weiss. *Introduction to Fourier Analysis on Euclidean Spaces*. Princeton University Press, 1971.

[105] A. Talbot. The accurate inversion of Laplace transforms. *J. Inst. Maths. Applics.*, 23:97–120, 1979.

[106] F. Tricomi. Transformazione di Laplace e polinomi di Laguerre. *R.C. Accad. Nat. dei Lincei*, 21:232–239, 1935.

[107] W. Weeks. Numerical inversion of Laplace transforms using Laguerre functions. *J. ACM*, 13:419–426, 1966.

[108] D. V. Widder. An application of Laguerre plynomials. *Duke Math. J.*, 1:126–136, 1935.

DEPARTMENT OF ECONOMICS AND BUSINESS ECONOMICS

AARHUS UNIVERSITY
SCHOOL OF BUSINESS AND SOCIAL SCIENCES
www.econ.au.dk

PhD Theses since 1 July 2011

2011-4 Anders Bredahl Kock: Forecasting and Oracle Efficient Econometrics

2011-5 Christian Bach: The Game of Risk

2011-6 Stefan Holst Bache: Quantile Regression: Three Econometric Studies

2011:12 Bisheng Du: Essays on Advance Demand Information, Prioritization and Real Options in Inventory Management

2011:13 Christian Gormsen Schmidt: Exploring the Barriers to Globalization

2011:16 Dewi Fitriasari: Analyses of Social and Environmental Reporting as a Practice of Accountability to Stakeholders

2011:22 Sanne Hiller: Essays on International Trade and Migration: Firm Behavior, Networks and Barriers to Trade

2012-1 Johannes Tang Kristensen: From Determinants of Low Birthweight to Factor-Based Macroeconomic Forecasting

2012-2 Karina Hjortshøj Kjeldsen: Routing and Scheduling in Liner Shipping

2012-3 Soheil Abginehchi: Essays on Inventory Control in Presence of Multiple Sourcing

2012-4 Zhenjiang Qin: Essays on Heterogeneous Beliefs, Public Information, and Asset Pricing

2012-5 Lasse Frisgaard Gunnersen: Income Redistribution Policies

2012-6 Miriam Wüst: Essays on early investments in child health

2012-7 Yukai Yang: Modelling Nonlinear Vector Economic Time Series

2012-8 Lene Kjærsgaard: Empirical Essays of Active Labor Market Policy on Employment

2012-9 Henrik Nørholm: Structured Retail Products and Return Predictability

2012-10 Signe Frederiksen: Empirical Essays on Placements in Outside Home Care

2012-11 Mateusz P. Dziubinski: Essays on Financial Econometrics and Derivatives Pricing

2012-12 Jens Riis Andersen: Option Games under Incomplete Information

2012-13 Margit Malmmose: The Role of Management Accounting in New Public Management Reforms: Implications in a Socio-Political Health Care Context

2012-14 Laurent Callot: Large Panels and High-dimensional VAR

2012-15 Christian Rix-Nielsen: Strategic Investment

2013-1 Kenneth Lykke Sørensen: Essays on Wage Determination

2013-2 Tue Rauff Lind Christensen: Network Design Problems with Piecewise Linear Cost Functions

2013-3 Dominyka Sakalauskaite: A Challenge for Experts: Auditors, Forensic Specialists and the Detection of Fraud

2013-4 Rune Bysted: Essays on Innovative Work Behavior

2013-5 Mikkel Nørlem Hermansen: Longer Human Lifespan and the Retirement Decision

2013-6 Jannie H.G. Kristoffersen: Empirical Essays on Economics of Education

2013-7 Mark Strøm Kristoffersen: Essays on Economic Policies over the Business Cycle

2013-8 Philipp Meinen: Essays on Firms in International Trade

2013-9 Cédric Gorinas: Essays on Marginalization and Integration of Immigrants and Young Criminals – A Labour Economics Perspective

2013-10 Ina Charlotte Jäkel: Product Quality, Trade Policy, and Voter Preferences: Essays on International Trade

2013-11 Anna Gerstrøm: World Disruption - How Bankers Reconstruct the Financial Crisis: Essays on Interpretation

2013-12 Paola Andrea Barrientos Quiroga: Essays on Development Economics

2013-13 Peter Bodnar: Essays on Warehouse Operations

2013-14 Rune Vammen Lesner: Essays on Determinants of Inequality

2013-15 Peter Arendorf Bache: Firms and International Trade

2013-16 Anders Laugesen: On Complementarities, Heterogeneous Firms, and International Trade

2013-17	Anders Bruun Jonassen: Regression Discontinuity Analyses of the Disincentive Effects of Increasing Social Assistance
2014-1	David Sloth Pedersen: A Journey into the Dark Arts of Quantitative Finance
2014-2	Martin Schultz-Nielsen: Optimal Corporate Investments and Capital Structure
2014-3	Lukas Bach: Routing and Scheduling Problems - Optimization using Exact and Heuristic Methods
2014-4	Tanja Groth: Regulatory impacts in relation to a renewable fuel CHP technology: A financial and socioeconomic analysis
2014-5	Niels Strange Hansen: Forecasting Based on Unobserved Variables
2014-6	Ritwik Banerjee: Economics of Misbehavior
2014-7	Christina Annette Gravert: Giving and Taking – Essays in Experimental Economics
2014-8	Astrid Hanghøj: Papers in purchasing and supply management: A capability-based perspective
2014-9	Nima Nonejad: Essays in Applied Bayesian Particle and Markov Chain Monte Carlo Techniques in Time Series Econometrics
2014-10	Tine L. Mundbjerg Eriksen: Essays on Bullying: an Economist's Perspective
2014-11	Sashka Dimova: Essays on Job Search Assistance
2014-12	Rasmus Tangsgaard Varneskov: Econometric Analysis of Volatility in Financial Additive Noise Models
2015-1	Anne Floor Brix: Estimation of Continuous Time Models Driven by Lévy Processes
2015-2	Kasper Vinther Olesen: Realizing Conditional Distributions and Coherence Across Financial Asset Classes
2015-3	Manuel Sebastian Lukas: Estimation and Model Specification for Econometric Forecasting
2015-4	Sofie Theilade Nyland Brodersen: Essays on Job Search Assistance and Labor Market Outcomes
2015-5	Jesper Nydam Wulff: Empirical Research in Foreign Market Entry Mode

2015-6 Sanni Nørgaard Breining: The Sibling Relationship Dynamics and Spillovers

2015-7 Marie Herly: Empirical Studies of Earnings Quality

2015-8 Stine Ludvig Bech: The Relationship between Caseworkers and Unemployed Workers

2015-9 Kaleb Girma Abreha: Empirical Essays on Heterogeneous Firms and International Trade

2015-10 Jeanne Andersen: Modelling and Optimisation of Renewable Energy Systems

2015-11 Rasmus Landersø: Essays in the Economics of Crime

2015-12 Juan Carlos Parra-Alvarez: Solution Methods and Inference in Continuous-Time Dynamic Equilibrium Economies (with Applications in Asset Pricing and Income Fluctuation Models)

2015-13 Sakshi Girdhar: The Internationalization of Big Accounting Firms and the Implications on their Practices and Structures: An Institutional Analysis

2015-14 Wenjing Wang: Corporate Innovation, R&D Personnel and External Knowledge Utilization

2015-15 Lene Gilje Justesen: Empirical Banking

2015-16 Jonas Maibom: Structural and Empirical Analysis of the Labour Market

2015-17 Sylvanus Kwaku Afesorgbor: Essays on International Economics and Development

2015-18 Orimar Sauri: Lévy Semistationary Models with Applications in Energy Markets

2015-19 Kristine Vasiljeva: Essays on Immigration in a Generous Welfare State

2015-20 Jonas Nygaard Eriksen: Business Cycles and Expected Returns

2015-21 Simon Juul Hviid: Dynamic Models of the Housing Market

2016-1 Silvia Migali: Essays on International Migration: Institutions, Skill Recognition, and the Welfare State

2016-2 Lorenzo Boldrini: Essays on Forecasting with Linear State-Space Systems

2016-3 Palle Sørensen: Financial Frictions, Price Rigidities, and the Business Cycle

2016-4 Camilla Pisani: Volatility and Correlation in Financial Markets: Theoretical Developments and Numerical Analysis